Out-of-Autoclave Manufacturing of Complex Shape Composite Laminates

By

Mélanie Brillant

Department of Mechanical Engineering
McGill University
Montreal, Canada

A thesis submitted to
McGill University
in partial fulfillment of the requirements for the degree of
Master of Engineering

December 2010

ABSTRACT

Out-of-Autoclave (OOA) manufacturing answers the growing need of the aerospace industry to process components of larger sizes at reduced costs. Recent prepreg materials have been developed specifically for OOA manufacturing and feature increased in-plane permeability through the presence of dry-fibre paths for efficient evacuation of gases. However, the differences in impregnation and resin kinetics attributed to OOA prepregs with respect to autoclave prepregs may affect the compaction behaviour in complex shape laminates. This thesis presents the results of an investigation of important design and processing parameters on the quality of complex shape laminates manufactured by OOA methods.

L-shape composite laminates were manufactured by OOA methods, following the recommendations documented in the literature. The samples were tested for thickness variation at the corner and void content levels. The thickness variation at the corner was characterised based on the radius-to-thickness ratio for Cytec Cycom5320 PW and 8HS prepregs with concave and convex tools. The experimental study showed increased corner thickening with decreasing radius-to-thickness ratio for both tool shapes. The data can be used to determine the minimal radius-to-thickness ratio for acceptable thickness variation for each material and serve as a design guideline. An analytical model of the compaction of L-shape laminates was developed. The discrepancies between the experimental data and the model predictions for thickness variation at the corner highlight the importance of shearing mechanisms in the compaction of L-shape laminates.

Also, from the experimental investigation of various bagging arrangements, it is observed that the compaction at the corner is improved with the use of a pressure intensifier or pressure strip with proper corner radius. In addition, breather material should be placed under the pressure intensifier to allow efficient air removal and maintain a low void content level. A numerical analysis of the compaction of a laminate over a concave tool was performed and demonstrated that the material of the pressure intensifier or pressure strip should be of high stiffness for efficient laminate compaction.

RÉSUMÉ

L'industrie aérospatiale recherche davantage à fabriquer des pièces en matériaux composites de plus grandes dimensions. Ceci peut être accompli à plus faibles coûts par le procédé de fabrication hors-autoclave. Les matériaux pré-imprégnés utilisés pour ce procédé sont semi-imprégnés et donc, dotés d'une section de fibres sèches qui permet l'évacuation des bulles d'air et de gas avant la consolidation du laminé et la polymérisation de la résine. Cependant, le comportement en compaction de ces matériaux sur des moules complexes peut être très différent de celui des matériaux pré-imprégnés pour autoclave, vu le plus faible niveau d'imprégnation et une différente cinétique de réaction de la résine. Cet ouvrage présente les résultats de l'étude de la qualité de pièces complexes fabriquées par le procédé hors-autoclave. L'influence du rayon au coin, de l'épaisseur du laminé ainsi que de la configuration du sac à vide sur l'uniformité de l'épaisseur et le taux de porosité a été étudiée.

Des pièces en forme de « L » ont été fabriquées en suivant la méthodologie et les recommendations pour la fabrication hors-autoclave décrites dans la litérature. La variation de l'épaisseur au coin et le taux de porosité ont été mesurés pour chacun des échantillons. La variation de l'épaisseur a été caractérisée en fonction du rapport entre le rayon au coin et l'épaisseur du laminé (R/t), ceci pour deux pré-imprégnés et des moules convexe et concave. Les résutats démontrent une augmentation de la variation de l'épaisseur pour une diminution du rapport R/t. À partir des résultats, pour chaque matériau et pour des fins de conception, il est possible de déterminer le rapport R/t minimum pour une variation de l'épaisseur acceptable. Un modèle analytique de la compaction d'un laminé sur un moule de forme complexe a été dévelopé. La comparaison du modèle avec les résultats expérimentaux permet d'affirmer que les contraintes en cisaillement jouent un rôle important dans la compaction de laminés sur moules complexes.

Aussi, l'effet de la configuration du sac à vide et de l'utilisation d'un contre-moule de polymère sur la variation de l'épaisseur et du taux de vide ont été étudiés. Il est observé que le contre-moule augmente la compaction au coin et

réduit la variation de l'épaisseur. De plus, pour permettre l'évacuation efficace de l'air, il est important de placer du tissu de drainage sous le contre-moule. Également, l'analyse numérique de la compaction d'un laminé sur un moule convexe a démontré que l'épaisseur est plus uniforme pour un contre-moule de rigidité élevée.

ACKNOWLEDGMENTS

I would like to thank my supervisor, Dr. Pascal Hubert, for welcoming me into his research group and providing me with the opportunity to work in such close relationship with industry. He is an admirable person of great knowledge and experience and I am truly grateful for his guidance and support.

I would like to recognize the financial support that was awarded to me through the *Alexander Graham Bell Canada Graduate Scholarship* by the Natural Sciences and Engineering Research Council of Canada (NSERC). I would also like to thank McGill University for awarding me the *Provost's Graduate Fellowship*. Also, this research could not have been possible without the financial contribution and support from the following partners: Bombardier Aerospace, Bell Helicopter Textron Canada, Delastek Inc., the Centre for the Development of Composites of Québec (CDCQ), the Consortium for Research and Innovation in Aerospace in Québec (CRIAQ), the National Research Council of Canada (NRC), the Center for Applied Research on Polymers (CREPEC) and NSERC. Special recognition should be given to Bombardier and Bell Helicopter for donating the materials.

A special thank you goes to Philip Barsalou and his team at Bell Helicopter for their help and guidance in manufacturing and testing the experimental samples. I would like to thank David Wilson from Bombardier Aerospace for his input and suggestions in the development of the test plans.

I would like to express my gratitude to Jim Kratz and Timotei Centea for their help in using the equipment. I admire their work ethics and they have been great mentors. I wish to recognize the important help from Valentina Savona in the manufacturing of the samples. I would like to thank Dr. Lolei Khoun for her help in using ABAQUS and her sound input on my work. Also, I express sincere appreciation for the welcoming and dynamic work environment and special friendships built during my time at the Structures and Composites Laboratory.

Last, but not least, I would like to express my sincere gratitude to my family and friends for their generous encouragements throughout my studies. I would also like to thank Martin Drolet for his support, love and presence in my life.

TABLE OF CONTENTS

LIST OF TABLES

LIST OF FIGURES

NOMENCLATURE

c_1	Bulk factor
F_{eb}	Reaction force from edge breathing system
H	Height of tool
K	Fibre bed permeability
K_X	Fibre bed permeability in the x-direction
K_Y	Fibre bed permeability in the y-direction
k	Constant of linearity
L	Length
$L_{1, 2, 3 \text{ or } 4}$	Tool #1, 2, 3 or 4 length
P	Compaction pressure
$P_{avgtool}$	Reaction pressure at the tool side surface
$P_{autoclave}$	Autoclave pressure
P_R	Resin pressure
P_V	Vapour pressure
R	Tool corner radius
$R_{1, 2, 3 \text{ or } 4}$	Tool #1, 2, 3 or 4 corner radius
R_{Bag}	Final part inner corner radius
R_{in}	Desired part inner corner radius
R_{out}	Desired part outer corner radius
S_P	Arc surface exposed to the bag
S_T	Arc surface exposed to the tool
S_{void}	Total area occupied by voids
$S_{laminate}$	Total area of laminate surface
T	Tensile longitudinal stress
t	Desired laminate thickness
t_{avg}	Average thickness at flange for all specimen
$t_{avgflange}$	Average thickness at flange for a specimen
$t_{avgflange\ i}$	Average initial thickness at flange for a specimen
t_c	Final thickness at the corner
t_i	Initial thickness
$t_{i\ n}$	Initial thickness measurement at location “n”

t_m	Predicted thickness by analytical model
t_n	Thickness measurement at location "n"
$\overline{t_n}$	Average thickness measurement between corresponding locations "n" on surfaces of cut 01 and 02
$t_{rel\ n}$	Relative thickness measurement at location "n"
V	Resin velocity
vc	Void content
W	Width of part
X	Reference axis in absolute plane
x	Flange distance subjected to $P_{avgtool}$
Y	Reference axis in absolute plane
∂	Derivative operator
Δt	Thickness variation between corner and flange
Δx	Slippage distance between plies
ε_c	Strain at corner
ε_f	Strain at flange
ϕ	Instantaneous porosity
μ	Resin viscosity
σ	Applied stress
σ_{eb}	Reaction stress from edge breathing system
$\overline{\sigma}$	Fibre bed effective stress
τ	Shear stress

CHAPTER 1
Introduction

1.1 Composites in the Aerospace Industry

Advances in polymer research and the development of high-performance fibres have enabled composite materials to play a key role in the design of complex aircraft structures for modern programs. These materials are defined as a multiphase material engineered to provide a better combination of properties that cannot be achieved by each of its constituents on their own [1]. The significant reduction in weight without compromising mechanical strength that can be achieved by composite materials is the main driver for their increasing use in high-performance applications over conventional metal alloys [2, 3].

This weight reduction allows for better fuel efficiency, translating to increased range and payload or reduced operating costs, and improved manoeuvrability, which is especially important for military aircrafts. Also, composites may be formed into more complex shapes than metallic parts; assembly time and costs are thus greatly reduced with part integration and component performance is improved by reducing the use of fasteners and rivets that are source of stress concentration regions and crack initiation [3]. Composites also exhibit improved corrosion and fatigue resistance, which are key properties for aerospace applications given the hygrothermal and cyclic loading conditions.

Composite materials were initially limited to secondary structures such as movable wing components (rudder, flaps and spoilers). With developments in testing and inspection techniques, composite materials are now being used for primary structures, such as complete empennage, wings and fuselage, on many modern aircraft programs [4, 5]. Figure 1.1 presents typical aircraft components manufactured with composite materials.

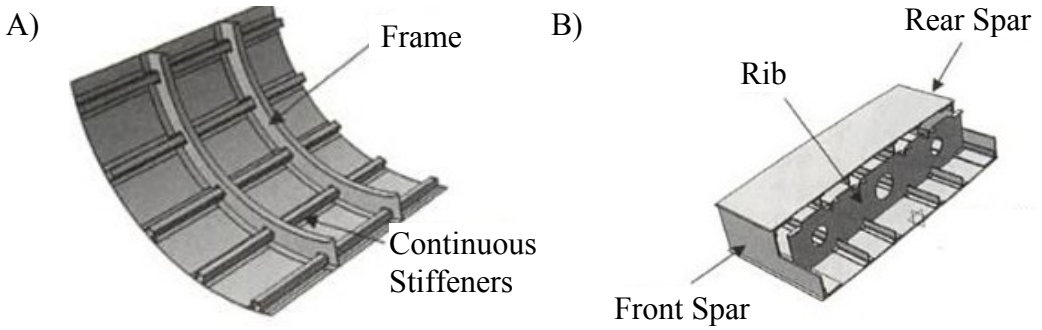

Figure 1.1: Typical aerospace components manufactured in composite materials. (A) Fuselage skin and frame and (B) Wing box [6]

1.2 Autoclave Manufacturing

Autoclave processing remains the process of choice for the manufacturing of most aerospace composite material components [7, 8]. High fibre volume fractions and very low porosity levels can be achieved with this manufacturing process, which explains its predominant use in high-performance applications [7]. The steps to autoclave processing are illustrated in Figure 1.2, and are separated in three main operations: laminate preparation, bagging and cure.

Figure 1.2: Autoclave processing block diagram

The tool must be treated with sealant and a releasing agent for proper tool protection and easy removal of parts after cure. In autoclave manufacturing, the laminate is made of a stack of prepreg plies: fibre plies pre-impregnated with partially cured resin by the supplier. Variability is greatly reduced with the use of prepreg, in comparison to injection processes or wet lay-up, since the resin content is tightly controlled at the time of impregnation by the supplier, plies are easy to cut and resin-hardener mixing errors are eliminated [9, 10]. The prepreg material must first be removed from the freezer and let thaw in its bag to room temperature to prevent moisture contamination [11]. The desired plies can then be cut from the prepreg and stacked on the tool per the lay-up design.

Once the laminate plies are stacked, the bagging operation is performed. A typical bagging sequence is illustrated in Figure 1.3. Dams are placed along the edges of the laminate to prevent resin flow. The laminate is covered with a release film or bleeder cloth when necessary. The bleeder cloth is used in bleed conditions, i.e. when excess resin must be evacuated from the top surface. Breather material is placed over the set-up for air and volatile evacuation. Bagging film is sealed around the tool and vacuum pressure is applied.

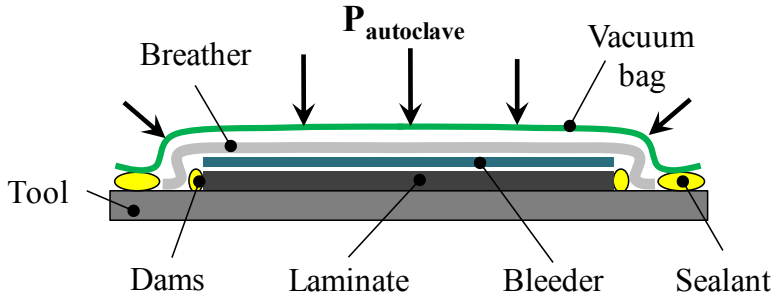

Figure 1.3: Typical bagging sequence for autoclave manufacturing (adapted from [8])

Finally, the set-up is placed in an autoclave for curing. The autoclave provides heat and additional pressure for resin cure and laminate consolidation. The cure cycle has a significant effect on the part quality by governing the impregnation of the fibre bed and the formation of voids, and must be chosen appropriately according to the material used. A typical cure cycle is illustrated in Figure 1.4. The cure cycle starts with a debulk operation; the set-up is under vacuum pressure only, at room temperature to evacuate entrapped air before resin flow starts. Resin flow starts during the first ramp and hold. As resin viscosity decreases, the fibre bed is impregnated and further compaction is achieved. During the second ramp and hold, the resin reaches gelation, and crosslinking due to polymerisation occurs. Structural strength is developed during this portion of the cure. However, any entrapped air bubbles that still remain will create voids. A post-cure operation may be done separately to further increase the degree of cure.

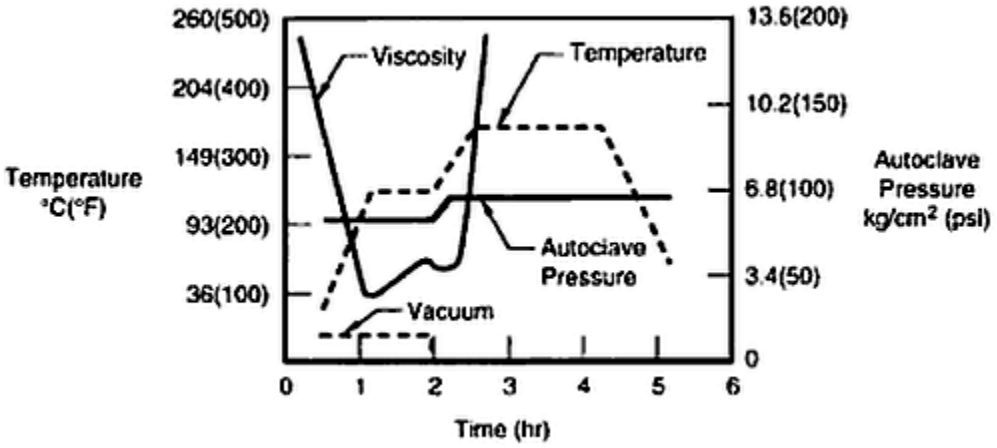

Figure 1.4: Typical autoclave processing cure cycle. Curves for temperature, pressure and resin viscosity evolution with time are presented [8]

1.3 Out-of-Autoclave Manufacturing

Although well established and offering excellent reliability and part quality, autoclave processing requires high capital investment and energy costs. In addition, part size is limited to the capacity of the autoclave, which in turn limits the possibility for part integration and maintains assembly requirements. Thus, industry is encouraging further research and development for manufacturing processes that do not make use of autoclaves. Special low-temperature curing prepregs have been recently designed for the manufacturing of aerospace-quality composite parts by Out-of-Autoclave (OOA) processing. This non-traditional method consists of vacuum bag-only curing in a conventional oven. OOA processing represents a great cost savings opportunity for the aerospace industry by eliminating the purchasing and service costs associated with large autoclaves and allowing the use of low-cost tooling due to the lower cure temperatures.

Out-of-Autoclave prepregs are different to most autoclave prepregs in that the fibre plies are semi-impregnated and the resin system is formulated for optimal cure at lower temperatures. The semi-impregnation is key to providing low porosity levels despite the lower compaction pressure. Figure 1.5 illustrates a schematic of a typical semi-impregnated OOA prepreg.

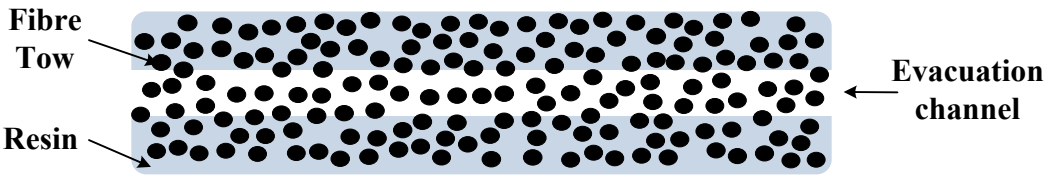

Figure 1.5: Typical OOA semi-impregnation. The dry fibre bed portion provides an evacuation path for entrapped air to be removed before resin flow starts (adapted from [12])

At the lower cure temperatures, porosity caused by dissolved volatiles is less problematic since the vapour pressure is lower. However, high porosity levels have been observed in fully impregnated OOA laminates due to entrapped air which cannot be collapsed by the lower compaction pressure [10]. The dry fibre path in semi-impregnated prepregs provides a means of evacuation for air before full resin impregnation of the fibre bed. Autoclave-comparable porosity levels have been demonstrated with such OOA prepregs [10].

1.4 Motivation and Thesis Organisation

Costs associated with autoclave manufacturing are becoming important inhibitors to the wider use of composite materials as the complexity and size of components increase. As a result, there is growing interest in OOA manufacturing. However, the absence of additional compaction pressure from an autoclave is of major concern. Especially for large and complex shape parts, the limited compaction pressure in OOA processing can yield higher void content levels and cause consolidation issues. Also, contrary to autoclave manufacturing, very few references exist on the manufacturing of complex shape composite laminates by OOA processing. Although void formation, flow and compaction theories and models developed for autoclave-cured laminates still apply, the extent to which the reduction in compaction pressure affects part quality and whether current vacuum bagging methods are appropriate for the specially designed OOA prepregs is still poorly understood.

This research was performed as part of a collaborative effort between academic, institutional and industrial partners to evaluate the possibility of manufacturing

autoclave-quality aerospace components using OOA methods. The general objective of this research was to evaluate the effect of important design and processing parameters on the quality of complex shape laminates manufactured by OOA methods. More specifically, the aim was to better understand the mechanisms that govern void formation and the compaction of complex shape laminates through (1) an experimental study of the effect of geometrical dimensions and bagging arrangements on the thickness variation and void content, (2) the development of an analytical model and (3) numerical work on the compaction of a laminate over a concave tool. Important deliverables were to provide design and manufacturing guidelines for OOA complex shape laminates.

Chapter 2 presents a review of the literature on flow and compaction theories, the results of experimental studies on the compaction of complex shapes, theories on void formation as well as recent research on Out-of-Autoclave manufacturing. Chapter 3 details the experimental procedure for the manufacturing of L-shape laminates by OOA methods. The methodology followed for testing of the samples is also described. Chapter 4 discusses the results for the experimental investigation of the thickness variation in L-shape laminates based on variations in geometrical dimensions. An analytical model of the compaction of complex shape laminates is developed and compared with the experimental results and possible mechanisms governing the compaction are discussed. In Chapter 5, various tool shapes and bagging arrangements are considered and their effect on part quality is investigated. Chapter 6 describes the numerical work performed to represent the compaction in complex shapes. Important conclusions of this research, recommendations and future work are discussed in Chapter 7.

CHAPTER 2

Literature Review

2.1 Flow and Compaction Theory

Vacuum-bag processing of composite laminates is a complex fabrication process that involves time-dependent heat and mass transfer combined with changes in material properties from the chemical reactions. Figure 2.1 illustrates the multiple factors that influence resin flow and laminate compaction behaviours, which in turn have a direct effect on void formation and laminate consolidation, as will be discussed in sections 2.2 and 2.3. An understanding of resin flow and laminate compaction during processing is thus key for the comprehension of the complex interaction between the process parameters and boundary conditions, and the resulting part quality.

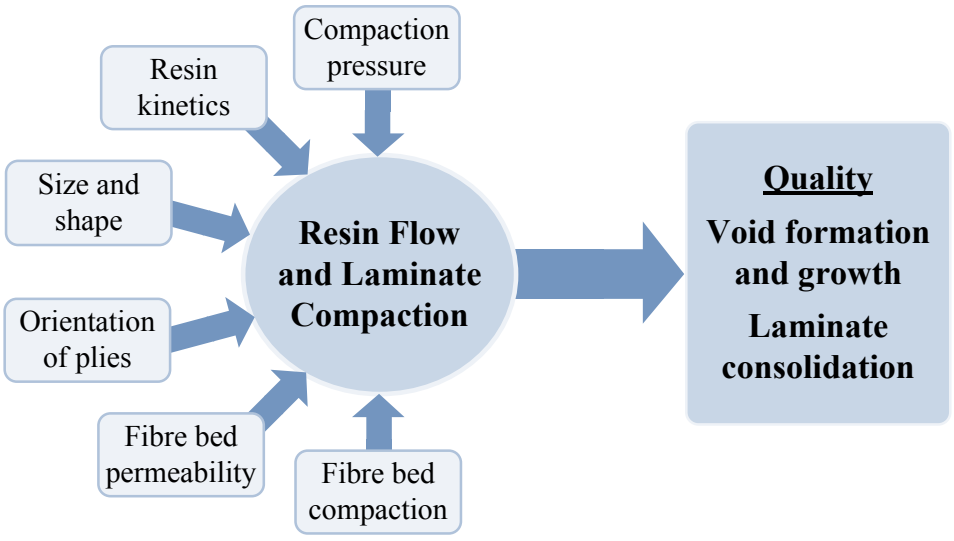

Figure 2.1: Process and laminate properties that affect part quality

Many flow and compaction models for laminates have been proposed in the past [13-16]. Good reviews of these models are provided by Hubert and Poursartip [17] and Kardos [18]. The two main flow mechanisms for composite laminates are, as illustrated in Figure 2.2, percolation flow, which describes the flow of

resin relative to the fibres, and shear flow, which characterizes interply and intraply shear deformation. Percolation flow is mostly applied to thermoset matrix composite processing. This mechanism is characterised based on viscous flow through a porous media (i.e. the fibre bed) following Darcy's law [Eq.(1)].

$$V = \frac{-K}{\mu}\frac{\Delta P_R}{L} \quad \textbf{(1)}$$

where V is the resin velocity, K is the fibre bed permeability, μ is the resin viscosity, and ΔP_R is the pressure gradient over the distance L. The impregnation of the fibre bed is a time-dependant phenomenon and is governed by the compaction pressure, resin kinetics and fibre bed permeability. Also, equation (1) leads to the two-dimensional continuity equation for axial and transverse resin flow described by Equation (2). The latter describes the resin mass loss due to resin flow out of the laminate (e.g. in bleed conditions) and has been verified experimentally by Loos and Springer [13]. Hence, resin flow is governed by the instantaneous porosity (Φ) and permeability (K_x, K_y) of the fibre bed, the viscosity (μ) of the resin, and the pressure gradient $\left({}^{\partial P_R}/_{\partial x, y}\right)$ that drives the flow.

$$\frac{\partial \phi}{\partial t} = \frac{-\phi}{\mu}\left[\frac{\partial}{\partial x}\left(K_x \frac{\partial P_R}{\partial x}\right) + \frac{\partial}{\partial y}\left(K_y \frac{\partial P_R}{\partial y}\right)\right] \quad \textbf{(2)}$$

A) Percolation B) Shear

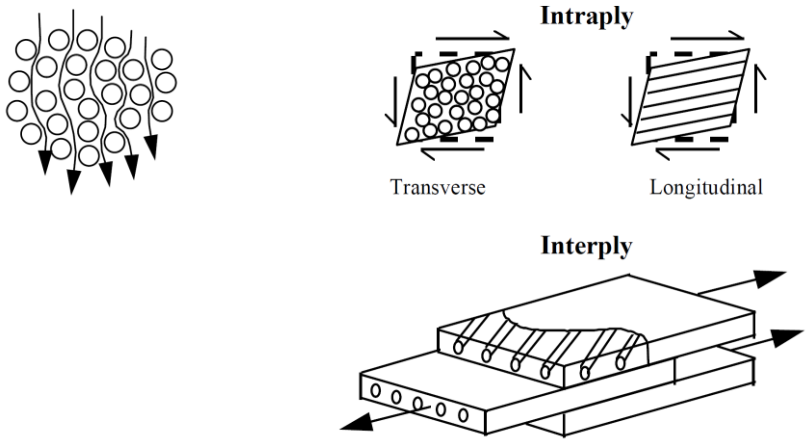

Figure 2.2: Percolation flow (A) and shear flow (B) mechanisms for composite laminates (adapted from [19])

The actual laminate consolidation during processing cannot be described only from the resin flow model; a combined approach for flow and laminate compaction is needed. One model for the laminate compaction is the effective stress formulation, which was first applied to the one-dimensional consolidation of composite laminates by Gutowski et al. [16], in conjunction with a three-dimensional resin flow model based on Darcy's law for flow through an anisotropic porous medium. The effective stress formulation is based on the following equation:

$$\sigma = \overline{\sigma} + P_R \quad \textbf{(3)}$$

where σ is the applied stress, $\overline{\sigma}$ is the fibre bed effective stress and P_R is the resin pressure.

This compaction model can be represented with a spring-piston analogy. Figure 2.3 to Figure 2.5 illustrate the interaction between the fibre bed, the resin and the compaction load through the representation of a spring, a liquid and a piston, respectively. Three cases are considered: no-bleed conditions on a fully impregnated prepreg (1), no-bleed conditions on a semi-impregnated prepreg (2) and general bleed conditions (3). The evolution of resin pressure (P_R) and the effective fibre bed stress ($\overline{\sigma}$) during compaction is also illustrated.

Let's examine case (1) first. At the initial state, no load is applied to the system and, thus the resin pressure and the fibre bed stress are zero. Once a compaction stress (σ) is applied, the resin pressure increases in reaction to the loading for case (1). No load is carried by the fibre bed since no deformation occurs. Such a case would only be found in very low fibre volume fraction laminates.

For case (2), the load causes the compaction of the fibre bed. Since no contact is made with the resin initially (2b), the fibre bed carries the entire load and the resin pressure remains zero. As compaction continues, the load is shared between the resin and the fibre bed (2c), as shown by Equation (3). The amount of load carried by the fibre bed is governed by its elastic response, similarly to a spring. The balance of the compaction load is carried by the resin pressure.

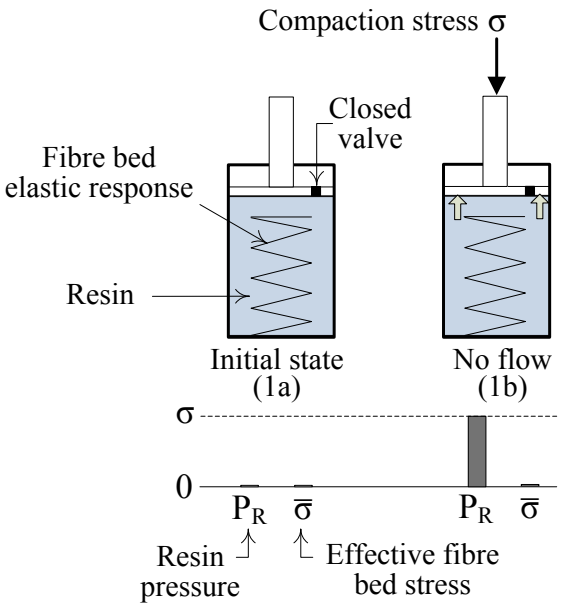

Figure 2.3: Case (1) Spring-piston analogy for the effective stress formulation of the compaction of a fully-impregnated laminate under no-bleed conditions

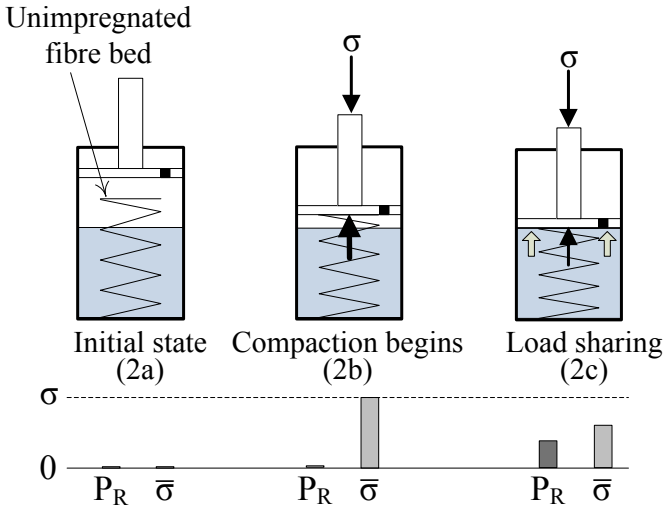

Figure 2.4: Case (2) Spring-piston analogy for the effective stress formulation of the compaction of a semi-impregnated laminate under no-bleed conditions

For case (3), once the compaction stress is applied, the resin carries the entire load (3b), similarly to case (1b). However, because bleeding is allowed, resin flow begins. From the evacuation of resin, the load reaches the fibre bed and causes its deformation (3c). In response, fibre bed stress develops and resin pressure decreases, per Equation (3). The larger the deformation, the higher the load

carried by the fibre bed and the lower the resin pressure (3c, d). At the same time, the rate of flow of resin decreases since the driving resin pressure decreases. Finally, if the valve is not closed (i.e. if bleeding is still allowed), resin flow and compaction of the laminate is stopped only once full compaction is reached (3e). At this point, equilibrium is found between the load and the fibre bed stress; the resin pressure has dropped to zero. Hence, from the effective stress formulation, final resin pressure is lower in bleed conditions.

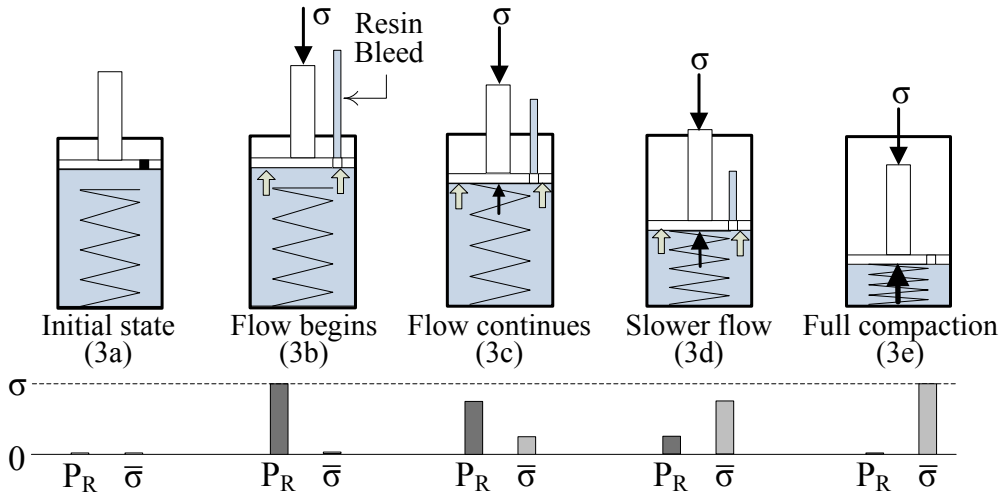

Figure 2.5: Case (3) Spring-piston analogy for the effective stress formulation of the compaction of a laminate under bleed conditions

In their work, Gutowski et al. [16] demonstrated that the fibre bed exhibits a non-linear elastic deformation behaviour and shares a portion of the applied load during processing, as represented in Equation (3). It is observed that the modeling of the load sharing function of the fibres is most important for high fibre volume fraction consolidation cases. Davé et al. [14] decoupled the resin flow and fibre bed compaction governing equations to obtain predicted final ply thicknesses of various one-dimensional laminate compaction cases by finite difference methods. The model made use of a fibre compaction curve that represented the fibre effective stress as a function of fibre bed deformation. Good agreement was found for both [14] and [16] modeling work.

2.2 Compaction of Complex Shape Laminates

A large amount of experimental and numerical work has been published on the compaction of autoclave-cured complex shape laminates, e.g. [20-25]. The effect of various process parameters, such as cure cycle, tool shape, corner radius, flange length, bagging configuration, ply orientation and resin system, on the quality of complex shape laminates, in terms of thickness variation and void content, were investigated. Common defects that were observed include resin accumulation at the corner and fibre wrinkling, as illustrated in Figure 2.6A and B. Resin accumulation was due to the formation of a low-pressure region at the corner from vacuum-bag bridging and was associated with parts manufactured over a concave tool. Fibre wrinkling resulted from the inability of the laminate plies to shear with the compaction or to eliminate wrinkles transferred from the consumable materials. Sensitivity to wrinkling was more dominant for lay-ups that included [90°] plies because of the low resistance of these plies to local pressure from wrinkles [20].

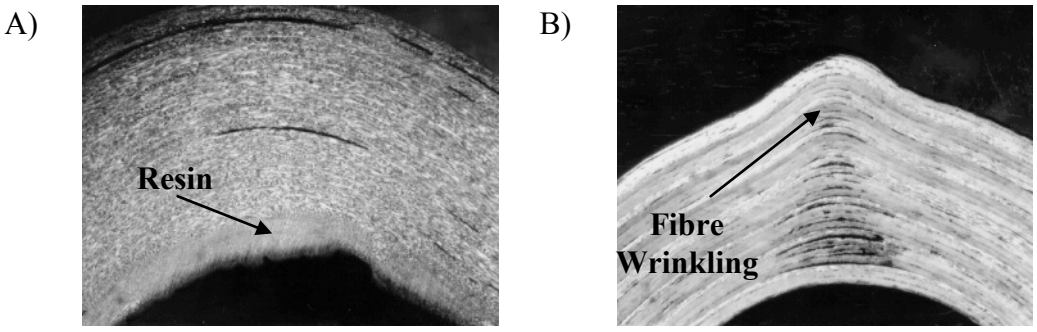

Figure 2.6: Common defects in complex shape laminates. Resin accumulation at the corner of a laminate manufactured over a concave tool (A) and fibre wrinkling from laminate compaction over a convex tool (B) [20]

Also, thickness variations were common issues in the compaction of complex shape laminates. It was found that the highest thickness gradient is localized at the corner [20-23, 25-30] and the compaction behaviour (i.e. thinning or thickening) is dependent on tool shape and fibre ply orientation, as summarized in Table 2.1.

Table 2.1: Corner compaction behaviour observed for different tool shapes and ply orientations

	Convex (male)	Concave (female)
[0°]	Thickening due to fibre wrinkling	Thickening due to reaction pressure difference causing resin flow
[90°]	Thinning due to reaction pressure difference causing resin flow	Thickening due to reaction pressure difference causing resin flow

In general, quasi-isotropic laminates exhibit a more uniform thickness profile than laminates with plies oriented in the [0°] or [90°] directions [20, 23]. Also, laminates manufactured over a concave (female) tool exhibited corner thickening while those processed over a convex (male) tool demonstrated corner thinning [20, 21, 23]. These thickness variations are caused by a difference in reaction stress at the corner between the surface of the laminate exposed to the tool and the surface exposed to the bag. Figure 2.7 illustrates the free body diagrams of an L-shape laminate subjected to a compaction pressure P over a concave tool (A) and the corner section with reduced compaction (B). S_T and S_P are the arc surfaces exposed to the tool and the bag, respectively. Stresses in the hoop direction that develop from the compaction are denoted as T.

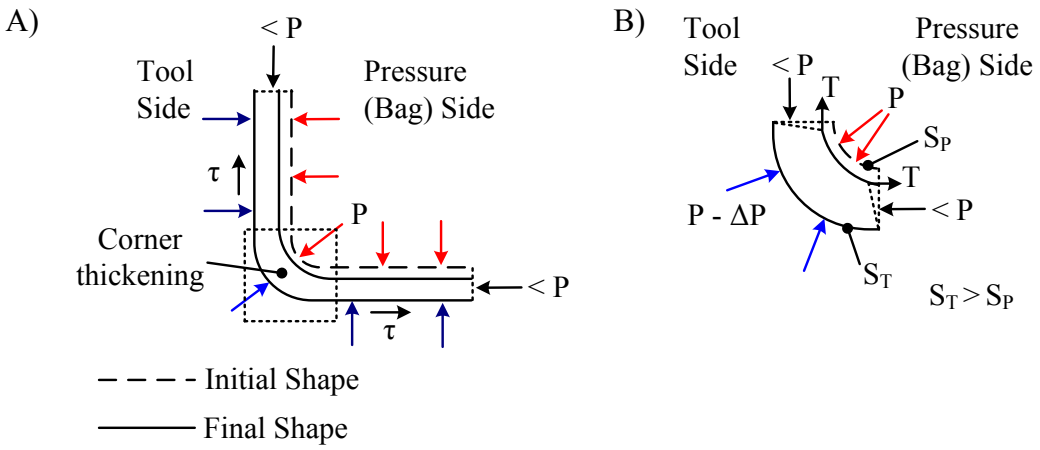

Figure 2.7: Free-body diagrams of an L-shape laminate processed over a concave tool (A) and detail of the corner section (B)

For equilibrium, the tool reaction stresses along the flanges (in dark blue) will be the same as the compaction pressure applied P. However, at the corner, the surface exposed to the pressure S_P is smaller than the contact surface at the tool side S_T. Therefore, for equilibrium, the reaction stresses at the tool side (in light blue) are then smaller than the compaction pressure applied on the bag side (in red). The laminate radial compressive stress is then lower at the corner in the case of a concave tool; corner thickening occurs due to this lower compaction and resin can migrate towards this region of lower pressure. Bag bridging also contributes to lower compressive stress at the corner. Figure 2.8 illustrates the free-body diagrams for the compaction of an L-shape laminate over a convex tool. For this case, at the corner, the surface at the tool side is smaller than that at the bag side. Higher laminate radial compressive stress develops and causes corner thinning because of higher compaction, and resin migration away from the corner.

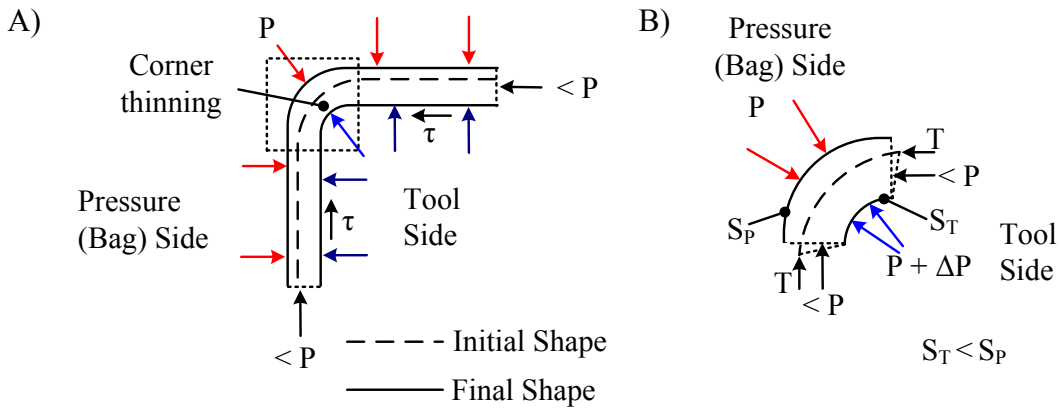

Figure 2.8: Free-body diagrams of an L-shape laminate processed over a convex tool (A) and detail of the corner section (B)

However, in the case of [0°] and quasi-isotropic laminates over a convex tool, if interply shearing is limited, the fibres in the hoop direction resist the compaction and may even wrinkle, resulting in corner thickening instead of thinning [20, 23, 27]. The influence of the ply orientation suggests that shear flow is also an important mechanism involved in the compaction of laminates of complex geometries. In fact, based on numerical work, Hubert [26] observed that the fibre bed shear behaviour is dominant in the compaction of complex shape laminates.

The extent of thickness variation at the corner is dependent on tool radius, part thickness and flange length. Better consolidation is observed for large tool radius and thin laminates [23, 24] since the difference in reaction stress is reduced and less axial deformation in the plies is required. Also, Li and Tucker [27] studied the effect of flange length on consolidation of angle laminates. They found that short parts exhibit less thickness variation at the corner. In fact, short flange lengths provide less resistance to interply shearing, thus allowing compaction to occur by fibre ply movement, which compensates for the resistance of the fibres to the axial deformation. Fernlund et al. [21] investigated the effect of caul-sheets on corner thinning of laminates manufactured over a convex tool. A caul-sheet may be used to modify the pressure distribution transferred to the laminate and thus, reduce thickness variations in cases where the pressure distribution is not uniform. Fernlund et al. found that a caul-sheet of intermediate stiffness improved the thickness uniformity of the laminate by limiting compaction pressure at the corner, where corner thinning usually occurs.

2.3 Theory on Void Formation and Growth

Voids are a type of defect consisting of small cavities in the composite part. These cavities vary in shape and size and are often found between laminate plies, in the resin or in fibre bundles. Figure 2.9A illustrates common locations for voids to form.

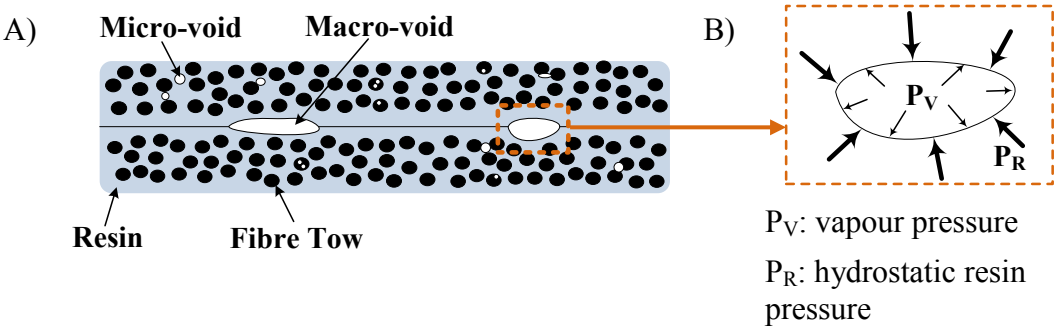

Figure 2.9: Voids from entrapped air between plies, in the resin and partially impregnated fibre bundles (A). Enlarged view of the pressure forces acting on the air or gas bubble surface (B)

Voids are detrimental to the mechanical performance of the part because they are source of stress concentration regions and may also cause contamination of the composite by moisture infiltration and accumulation. An understanding of the mechanisms that drive void formation is essential for the identification of the key manufacturing parameters, such as prepreg material, bagging sequence and cure cycle, which will minimize void content and optimize part quality.

Theories on void formation and growth phenomenon are discussed in [8, 13, 18, 31]. Voids may form in composite laminates from four mechanisms: (1) entrapped air during ply collation, (2) volatiles released from the curing process, (3) dissolved gases or moisture in the resin, and (4) internal stress build-up from resin cure shrinkage [13, 32]. Moisture content may be minimized by allowing the prepreg material to reach room temperature, after removing the roll from the freezer, before opening its protective bag for the ply cutting operation [11]. Entrapped air bubbles or volatile gases released during the curing process may be collapsed or dissolved before resin gelation if the hydrostatic resin pressure is higher than the local bubble pressure [13, 14, 18], as shown in Figure 2.9B. Otherwise, the bubble remains and a void is created in the composite once the resin gels. The bubble pressure is governed by the water vapour pressure and hence, increases with temperature. Thus, to minimize the local bubble pressure, low initial cure temperatures are ideal.

In addition, high hydrostatic resin pressure will contribute in minimizing void formation during processing because the resin has more potential in collapsing air bubbles and preventing dissolved gases from creating voids. Furthermore, high resin pressure is desired since it compensates for tensile stresses developed in the resin from cure shrinkage. If the resin pressure is too low, the internal stress state during densification may reach the critical condition for stress-initiated voids [32-34]. Therefore, as discussed in Section 2.1, high compaction pressure on the laminate and no-bleed conditions are ideal for maximizing resin pressure. Recall that bleed conditions are detrimental for void formation since, from compaction theory, the resin pressure is decreased in bleed conditions; as resin flows out of the laminate, the resin pressure decreases and full compaction is more likely to be

reached, yielding zero resin pressure. Hubert and Poursartip [20] confirmed experimentally that higher void contents are observed for bleed conditions as a result of lower resin pressure regions.

2.4 Out-of-Autoclave Manufacturing Research

Out-of-Autoclave manufacturing refers to vacuum-bag only curing of composite laminates. There has been interest in this process for many years since it represents great cost savings in comparison to autoclave manufacturing. First generation prepreg systems were developed for very low temperature curing (60°C-80°C) as they were targeted for low production parts and prototyping applications and permitted the use of economical tool materials, such as wood and foam [35]. However, early applications of OOA processing resulted in laminates of high void contents and low toughness, preventing this process from being used for high performance parts [12]. In fact, the absence of autoclave pressure for the compaction of the laminate decreased the potential of resin to collapse air bubbles or maintain dissolved gases and moisture into solution. Hence, the key challenge associated with OOA manufacturing was to develop methods to increase the permeability of the prepreg to allow evacuation of entrapped air and volatiles before resin gelation.

It was found that the method of impregnation of the prepreg had to be changed to improve the permeability; OOA prepregs should be semi-impregnated with resin, leaving dry-fibre paths as illustrated in Figure 2.10 [12, 35, 36]. Thus, entrapped air and volatiles can escape through the evacuation channels. It has been documented that standard prepregs used for autoclave manufacturing yield high void contents (above 3%) when processed by OOA methods, since the gases cannot escape and the vacuum pressure is too low to collapse the bubbles [12, 18, 35]. In comparison, semi-impregnated prepregs used for OOA manufacturing resulted in low void contents (below 1%).

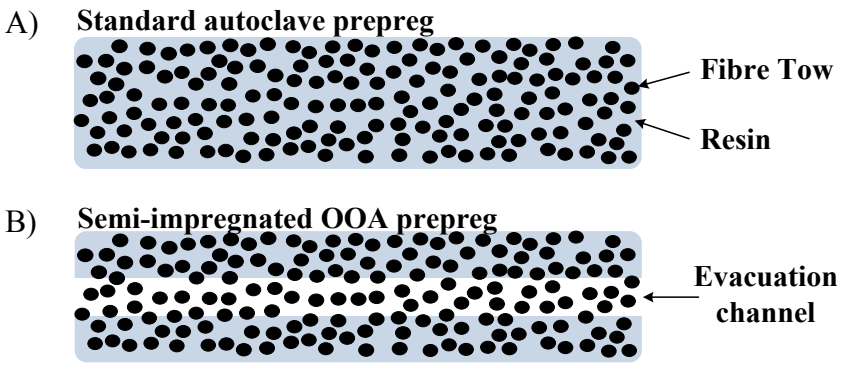

Figure 2.10: Schematic representation of the impregnation of standard autoclave prepreg (A) and semi-impregnated OOA prepreg (B)

With the development of new resin systems and fibre impregnation methods, new generations of prepregs were optimized specifically for OOA manufacturing, including Cytec's Cycom 5320 and the Advanced Composites Group's MTM45-1 and MTM46 prepregs. These new materials resulted in improved quality laminates with mechanical properties comparable to autoclave-cured laminates [12, 35-39].

An increasing number of references can be found on OOA manufacturing in the literature with growing interest in this process from the industry [12, 34-43]. Most of the literature discusses the latest improvements made to OOA prepreg systems [12, 34, 36-39]. Manufacturers develop various materials, each adapted for particular requirements for design and processing. Important characteristics sought include: high mechanical performance, long out-life, low cure temperature and high green strength. Compromises between these characteristics are inevitable, such as the tradeoff between toughness and low temperature cure, which explains the multitude of products being developed for various applications [35].

Out-life is defined as the allowable time for the prepreg to be removed from the freezer before final cure and is an important parameter in providing consistent results [12]. With time, the resin viscosity increases at room temperature which can prevent good laminate consolidation and affect void content. A long out-life is mostly important for the manufacturing of very large parts for which the lay-up

requires multiple days. If the resin viscosity changes through the lay-up operation, the final part quality could be non-uniform. However, this resin property comes at the expense of higher cure temperatures, thus reducing the cost advantage of the use of low-temperature tooling.

Green strength is defined as the ability of a composite part to be removed from the tool prior to complete cure and handled without deformation. This property determines the minimal degree of cure at which the composite developed enough green strength to be removed from the tool and undergo freestanding post-cure. This operation is commonly performed to increase production throughput; the cure temperatures are no longer limited by the tooling materials and thus complete cure can be reached at a faster rate.

Important contributions to the literature include a description of lessons learned for OOA manufacturing. References [12], [35] and [36] share important considerations for manufacturing void-free parts, as detailed below:

1. Edge breathing systems should be used to promote breathing of the laminate and create a passage for air and volatiles between the laminate plies and the breather material. Two common configurations of edge breathing are illustrated in Figure 2.11. In system (A), woven fibreglass fabric is wrapped around sealant tape and is in contact with the laminate and breather cloth. The fibreglass fabric provides a channel for the air to be evacuated through the breather cloth and into the vacuum line, whereas the sealant tape prevents any in-plane resin bleed. Each laminate ply must be in contact with the fibreglass fabric to ensure efficient breathing. In system (B), individual fibreglass tows are equally spaced around the laminate perimeter and overlap into the laminate thickness. The glass tows are in contact with the laminate and breather, creating the evacuation paths. Cork dams can be placed along the laminate edges. In both systems, the sealant tape and cork dams are used to prevent the vacuum bag from pinching the laminate edges and blocking the evacuation paths. Therefore,

the thickness of the sealant tape and cork dam must be equal or a bit higher than that of the laminate [12, 35].

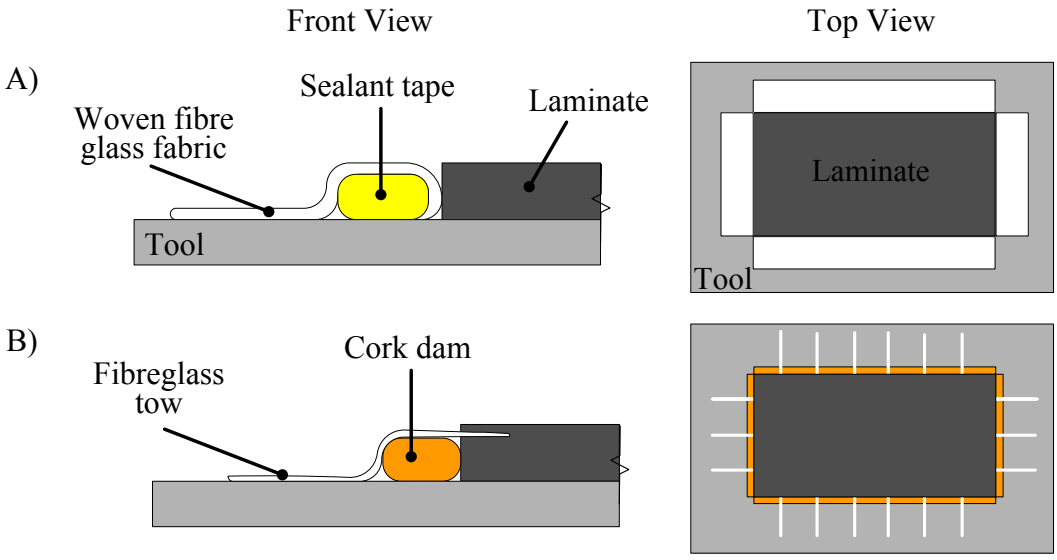

Figure 2.11: Schematic of edge breathing systems (A) and (B) (adapted from [42] and [35], respectively)

2. Vacuum bag leaks must be eliminated in order to maximize the compaction pressure as the available pressure is already limited.
3. Debulking is critical in providing low void contents. This operation consists in maintaining vacuum for a certain amount of time at room temperature. The majority of entrapped air from ply collation should be removed during this operation. A simple 1-D gas transport model was developed by Arafath et al. [44] to estimate the time required for debulk to evacuate the desired mass fraction of air based on the in-plane permeability of the laminate.
4. The cure cycle must be chosen such that it allows sufficient time for air and volatiles to escape before the resin viscosity decreases to a point where resin flow will cause impregnation of the evacuation paths. Also, the temperature at which the resin gels must be minimized to reduce the vapour pressure of dissolved volatiles and moisture in the resin.

Most of the literature on OOA manufacturing discusses the processing of flat laminates only. A limited number of references focused their studies on other

composite shapes. Recent work performed by The *Boeing Company* was published on the manufacturing of composite components featuring complex geometries and honeycomb core assemblies [43]. However, limited details are provided on the challenges related to these features and influencing processing parameters; the scope of the research documented remained general and the main objective was to share the success in manufacturing such components.

2.5 Literature Review Summary

A significant amount of work has been published on the compaction of autoclave-cured composite laminates. Resin percolation flow and laminate compaction theories have been developed to describe the consolidation of composite laminates of simple geometry and predict the thickness after cure.

Further studies have been performed on the compaction of laminates of complex geometry and have demonstrated the importance of shear flow in addition to percolation flow. Also, thickness variations were a common issue observed in the compaction of complex shape laminates and were associated with non-uniform pressure distributions particular to the complex geometry. The thickness variations were mostly localized at the corner and dependant on the corner radius and laminate thickness. Due to shear flow, the orientation of plies also had an important effect on the thickness variation.

Based on void formation theory, the main requirement for low void content is high resin pressure, such that entrapped air bubbles can be collapsed and dissolved volatiles be maintained into solution. However, for low-pressure applications, such as OOA manufacturing, the laminate quality depends rather on efficient air and volatile evacuation prior to resin flow and gelation. This is achieved with the presence of dry-fibre paths in the prepreg and edge breathing systems.

2.6 Problem statement

Given the potential cost savings associated with OOA manufacturing, there is growing interest in broadening the use of this process in the aerospace industry.

However, most of the literature focuses on the challenges related to the OOA manufacturing of simple geometries. Furthermore, the low impregnation level of typical OOA prepregs, in comparison to autoclave prepregs, for improved permeability, results in high bulk factors, which can cause bridging and wrinkling issues for the compaction of complex shape laminates. It would therefore be interesting to investigate the compaction behaviour of laminates of complex geometry, which align better with actual production components, under OOA conditions. In addition, no clear guideline for the design of complex shape laminates has been established in the literature. The combined effect of the geometrical parameters, such as the radius and the thickness, on the thickness variation has yet to be investigated thoroughly.

2.7 Research objectives

The present research addresses the problem stated above and the objective was to develop guidelines for the manufacturing of complex shape laminates using OOA materials. To achieve this, the following tasks were performed.

1. Develop an analytical model of the compaction of L-shape laminates to better understand the governing mechanisms.
2. Conduct an experimental study for the characterisation of thickness variations based on radius-to-thickness ratios of L-shape laminates.
3. Evaluate how to widen the processing range of L-shape laminates with changes in bagging arrangements, for improved thickness uniformity and void content, through an experimental study.
4. Perform a numerical analysis of the compaction of a laminate over a concave tool to investigate the effect of changes in bagging arrangements at a stress-level.

CHAPTER 3
Manufacturing of Complex Shape Laminates

The present chapter details the experimental procedure followed to manufacture L-shape composite laminates by Out-of-Autoclave (OOA) methods. This includes the main recommendations documented in the literature and summarized in Section 2.4. The experimental investigations discussed in the subsequent chapters will refer to the procedure detailed here.

Sections 3.1 and 3.2 provide details of typical materials used and details of the laminates under study. Section 3.3 describes the methodology for OOA manufacturing. The steps for preparing the specimens for testing and the measuring techniques employed are described in Section 3.4.

3.1 Materials

3.1.1 Prepreg

The composite laminates were made from epoxy resin pre-impregnated carbon fibre fabrics (prepregs). The prepregs were specially designed to help the evacuation of air and volatiles during debulk and cure under OOA processing conditions, similar to those presented in the introduction (Section 1.3). Specific details on the prepregs used will be given in the subsequent chapters.

3.1.2 Consumable materials

Various consumable materials are required for OOA bagging. These materials are made for one-time use and serve the purpose of evacuating air and volatiles while transferring the compaction pressure. The following table describes the types of consumable materials used and their function.

Table 3.1: Details of consumable materials

Consumable Material	Type	Function
Breather cloth	Airtech Ultraweave 606 Nylon breather	Provide passage for air and volatiles to evacuate from laminate to vacuum valve. Must not compact under vacuum pressure.
Non-perforated release film	Airtech A4000 Fluoropolymer	Prevent through-thickness resin bleed during cure and allow easy removal of the cured part.
Vacuum bag	Airtech Wrightlon 7400 Nylon vacuum film	Vacuum seal the laminate set-up and provide compaction pressure.
Sealant tape	Airtech GS213 sealant tape	Provide seal of vacuum bag. Prevent in-plane resin bleed and adjust thickness of edge breathing system.
Fibreglass	3 inch-wide plain weave fibreglass fabric	Used for edge breathing. Provide passage for air and volatiles from the laminate to the breather cloth.

3.1.3 Tools

Four tools were used to manufacture the L-shape laminates: two concave and two convex tools. These were made of extruded aluminum and are illustrated in Figure 3.1. The detailed dimensions are provided in Table 3.2.

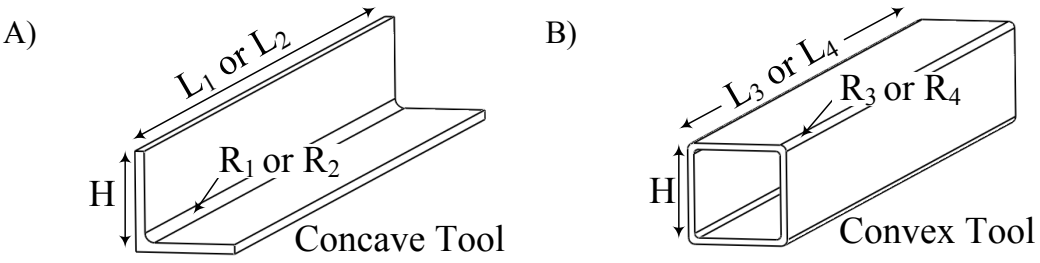

Figure 3.1: Schematic of the convex (A) and concave (B) tools

Table 3.2: Dimensions of the tools

Tool reference (n)	Shape	R_n (mm)	L_n (mm)	H (mm)
1	Concave	9.53	840	102
2	Concave	12.7	915	102
3	Convex	6.35	560	102
4	Convex	9.53	915	102

3.2 Laminate Details

An L-shape corner was selected as the complex shape for study as it is the simplest shape that includes a corner; feature of interest that commonly exhibits compaction issues. A schematic of a typical part with detailed dimensions is illustrated in Figure 3.2. R_{in} and R_{out} are the inner and outer part corner radii, respectively, and t is the thickness of the laminate.

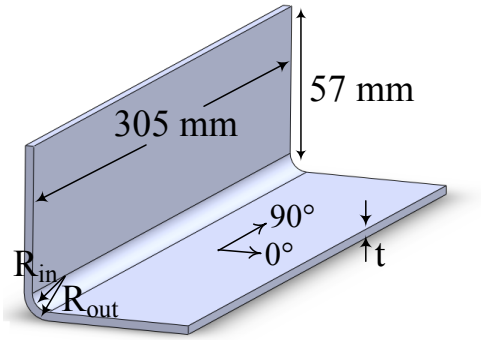

Figure 3.2: Detailed dimensions of a typical part

3.3 L-shape Parts Fabrication Method

3.3.1 Laminate preparation

The prepreg roll was removed from the freezer and placed horizontally over two blocks, to allow air to circulate under the roll, for a few hours, depending on the roll size. The sealed bag was opened only once the roll thawed to room temperature. The prepreg was cut in rectangular shapes of 305 mm in the weft

direction by 128 mm in the warp direction, which accounts for the final trimming of the edges.

Before the tools were used the first time, these were sanded with an electric or air-powered sander with 120, 320, 600 and 800-grit waterproof sandpaper. The tools could also be polished afterwards with polishing cream for a better surface finish. The tools were then cleaned with acetone and one coat of Zyvax's *Waterworks Fresh Start* cleaner was applied to remove the aluminum dust. The tools were treated with four coats of Zyvax's *Waterworks PreFlight* sealer or Zyvax's *Sealer GP*, waiting 15 minutes between each coat. Also, before each lay-up of the plies, the tools were treated with two coats of Zyvax's *EnviroShield* release agent for easy removal of the cured parts.

The plies were then stacked on the tool with a [0°] lay-up order (warp direction) for each part to be manufactured. The plies were stacked with the "backing paper" side facing the tool. A plastic spatula was used to apply pressure at the corner and help the plies conform to the shape of the tool. After every set of four plies, the laminate was debulked at room temperature: the set-up was placed in a vacuum bag and covered with breather cloth and perforated release film to prevent the laminate from sticking to the breather. The bag was then sealed under 90 kPa vacuum pressure for approximately 10 minutes. This operation was performed to compact the plies and remove most of the air bubbles between plies.

Each edge of the laminate was trimmed to a square edge with an exacto knife. However, when the blade of the knife was less sharp, the plies were bent before the cut was achieved. This can pinch the plies and close the air evacuation paths, which could have a detrimental effect on the void content. Therefore, the blade should be changed regularly and the cutting operation should be done with care.

3.3.2 Edge breathing set-up

As presented in section 2.3, special edge breathing systems were developed to promote air and volatile evacuation during debulk and cure of OOA composite

laminates. These systems are one the main features that differentiates the bagging arrangements for OOA and Autoclave manufacturing.

The edge breathing system that was used in the present study is illustrated in Figure 2.11A. The set-up consisted of woven fibreglass fabric wrapped around sealant tape and was placed along each edge of the laminate. In order to ensure efficient air removal, the fibreglass fabric must be in contact with all the plies of the laminate stack. This emphasizes the need for trimming of the edges after lay-up. The sealant tape is critical in preventing resin bleed which should be avoided since the prepreg was designed with net resin content.

3.3.3 Bagging arrangement

The reference convex and concave tool bagging arrangements are illustrated in Figure 3.3 (configuration #1). Following this configuration, the laminate stack was covered with a non-perforated release film, to prevent through-thickness resin bleed, followed by breather cloth. A vacuum bag was sealed around the tool-laminate set-up and vacuum pressure was applied through one vacuum connector.

Another configuration that will be used is illustrated in Figure 3.4 (configuration #2). The breather cloth was cut in two pieces of equal dimensions and placed over each flange section, leaving the corner exposed to the vacuum bag directly.

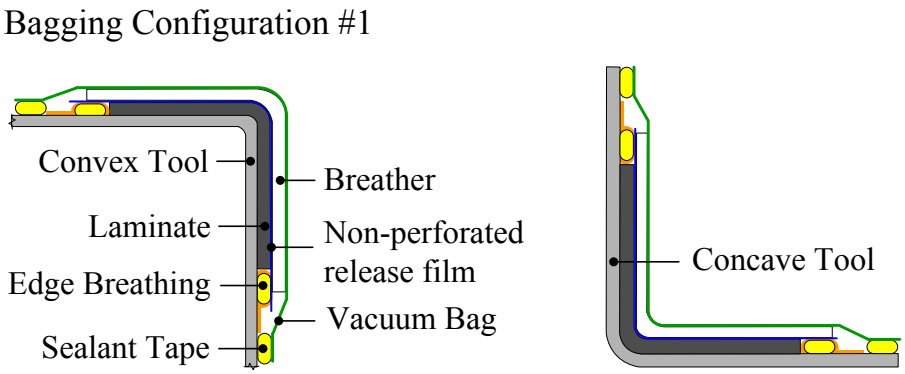

Figure 3.3: Schematic of Bagging Configuration #1. Convex tool (left) and concave tool configurations (right)

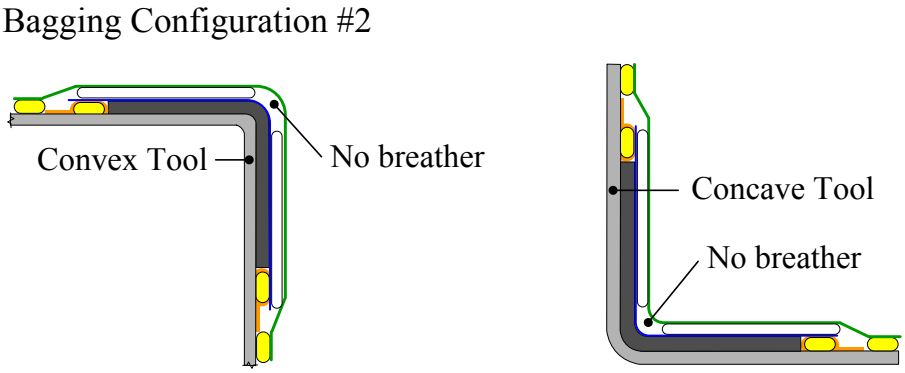

Figure 3.4: Schematic of Bagging Configuration #2. Convex tool (left) and concave tool configurations (right)

3.3.4 Cure cycle and instrumentation

The laminates were cured in a temperature controlled oven. The heating power is controlled to follow the target oven temperatures input to the oven controller. The cure cycle was comprised of four phases: 1) debulk at room temperature to allow entrapped air to evacuate before resin impregnation, 2) 1st ramp and dwell to a temperature that allows the resin viscosity to drop and impregnation of the fibre plies, 3) 2nd ramp and dwell to a higher temperature to undergo resin cure and 4) cool down to room temperature. The debulk time, ramp rates, dwell temperatures and dwell times were selected based on the prepreg system requirements for efficient air removal during debulk and full impregnation before resin cure. The cure cycle details for each study are provided in their respective chapters.

The oven and part temperatures were monitored during cure for each part. The part temperature was monitored with the use of one thermocouple placed between the middle plies at one edge of the laminate at the center of the curvature. To ensure there was no gradient in temperature along the width of the parts, a second thermocouple was placed similarly on the opposite edge for some laminates.

3.4 Specimen Measurements

3.4.1 Specimen preparation

After processing, each part was cut about 100 mm from the right and left edges to obtain a final specimen of 100 mm width, as illustrated in Figure 3.5. Each specimen exhibits two cut surfaces (01 and 02) which will be used for post-processing measurements.

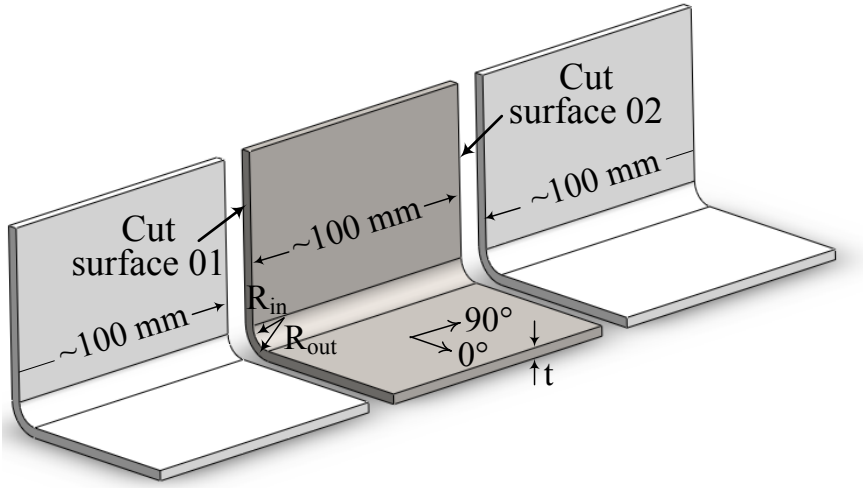

Figure 3.5: Typical cut sample. Final specimen used for post-processing measurements appears in dark gray

Both cut surfaces (01 and 02) were polished up to 600-grit silicone-carbide waterproof sandpaper and then scanned at a resolution of 1200 dpi on an Epson Perfection 2580 Photo scanner, giving images of about 4000 x 4000 pixels. A ruler was placed along one edge of the specimen during the scan for image calibration. For each image, using either *Image J* or *GIMP* imaging software, a line was traced over the ruler and the calibration was performed by assigning the length of the line in pixels to the corresponding length in mm. The techniques employed for measuring the thickness and void content are presented in the following sections.

3.4.2 Thickness measurements

The thickness was measured at 18 locations: 9 measurements per cut surface, as illustrated in Figure 3.6. The first 2-3 cm from the edges were not included in the measurements since they may be subjected to edge effects; where the compaction is influenced by vacuum bag bridging or resin accumulation. The measurements were performed by image analysis; a line was drawn between the top and bottom surfaces of the part at each measurement location, the software then estimated the length of the line in pixels. From calibration, as described in the previous section, the distance in pixels was converted to a distance in mm.

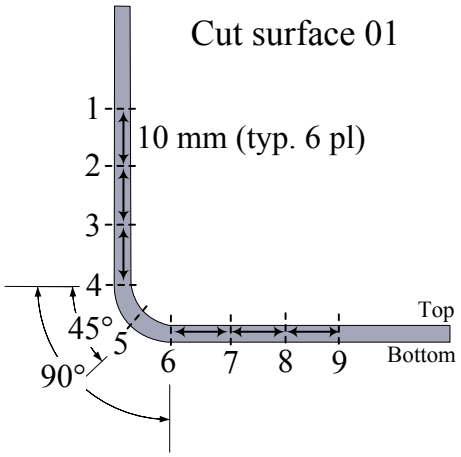

Figure 3.6: Thickness measurement locations #1 to 9 on cut surface 01. Similarly for measurement locations #10 to 18 on cut surface 02

3.4.2.1 Thickness variation calculation

From Figure 3.6 and defining t_n as the thickness measurement at location "n", the average flange thickness for each cut surface was calculated following Eq. (4). The average flange thickness for each specimen, $t_{avgflange}$, corresponded to the average of both cut surfaces, as shown by Eq. (5).

$$t_{avgflange_{01}} = \frac{t_1 + t_2 + t_3 + t_7 + t_8 + t_9}{6}$$
$$t_{avgflange_{02}} = \frac{t_{10} + t_{11} + t_{12} + t_{16} + t_{17} + t_{18}}{6} \quad \textbf{(4)}$$

$$t_{avgflange} = \frac{t_{avgflange_{01}} + t_{avgflange_{02}}}{2} \quad \textbf{(5)}$$

Also, the thickness at the corner t_c for each cut surface was given by Eq. (6). The thickness at the corner for each specimen was calculated as the average of both cut surfaces, as shown by Eq. (7).

$$t_{c_{01}} = t_5$$
$$t_{c_{02}} = t_{14} \quad \textbf{(6)}$$

$$t_c = \frac{t_{c_{01}} + t_{c_{02}}}{2} \quad \textbf{(7)}$$

The thickness variation Δt was defined as the difference in thickness between the corner and the flange, as described by Eq. (8), and was calculated for each cut surface. The thickness variation for each specimen was calculated from Eq. (9). The error was estimated following Eq.(10).

$$\Delta t_{01} = t_{c_{01}} - t_{\text{avgflange}_{01}}$$
$$\Delta t_{02} = t_{c_{02}} - t_{\text{avgflange}_{02}} \quad \textbf{(8)}$$

$$\Delta t = \frac{\Delta t_{01} + \Delta t_{02}}{2} \quad \textbf{(9)}$$

$$\text{error } \Delta t = |\Delta t - \Delta t_{01}| \quad \textbf{(10)}$$

3.4.2.2 Relative thickness calculation

The local thickness measurements were averaged between corresponding locations on surfaces 01 and 02 following Eq.(11).

$$\overline{t_1} = \frac{t_1 + t_{10}}{2}, \quad \overline{t_2} = \frac{t_2 + t_{11}}{2}, \quad \overline{t_3} = \frac{t_3 + t_{12}}{2}, \quad \overline{t_4} = \frac{t_4 + t_{13}}{2}, \quad \overline{t_5} = \frac{t_5 + t_{14}}{2},$$
$$\overline{t_6} = \frac{t_6 + t_{15}}{2}, \quad \overline{t_7} = \frac{t_7 + t_{16}}{2}, \quad \overline{t_8} = \frac{t_8 + t_{17}}{2}, \quad \overline{t_9} = \frac{t_9 + t_{18}}{2} \quad \textbf{(11)}$$

The relative thickness measurements, $t_{\text{rel n}}$, were calculated following Eq. (13) and corresponded to the average local thickness measurement normalized by the average flange thickness of all specimen, t_{avg}, given the specimens are of the same material and number of plies.

$$t_{avg} = \frac{\sum t_{\text{avgflange}}}{\text{number of specimen}} \quad \textbf{(12)}$$

$$t_{\text{rel n}} = \frac{\overline{t_n}}{t_{avg}} \quad \textbf{(13)}$$

3.4.2.3 Bulk factor calculation

The bulk factor of a material, c_1, is defined as the ratio of the initial thickness to the final flange thickness. To calculate the bulk factor of each material, thickness measurements were performed on sample laminates before cure, including a last debulk at room temperature for 10 minutes. Referring to Figure 3.6, the initial thickness, t_i, was measured with a calliper along the left edge at locations 1, 2, 3, 7, 8 and 9. The average initial flange thickness was calculated following Eq. (14). The bulk factor was calculated for each of the sample laminates per Eq. (15) and then averaged to determine the material bulk factor.

$$t_{avgflange\ i} = \frac{t_{i1} + t_{i2} + t_{i3} + t_{i7} + t_{i8} + t_{i9}}{6} \quad \textbf{(14)}$$

$$c_1 = \frac{t_{avgflange\ i}}{t_{avgflange}} \quad \textbf{(15)}$$

3.4.3 Void content measurements

The void content was estimated by image analysis of both cut surfaces for each part. Each image was first converted to a 32-bit greyscale picture using the *Image J* software. After adjusting the threshold to highlight each void, the image was converted to a binary image as shown in Figure 3.7.

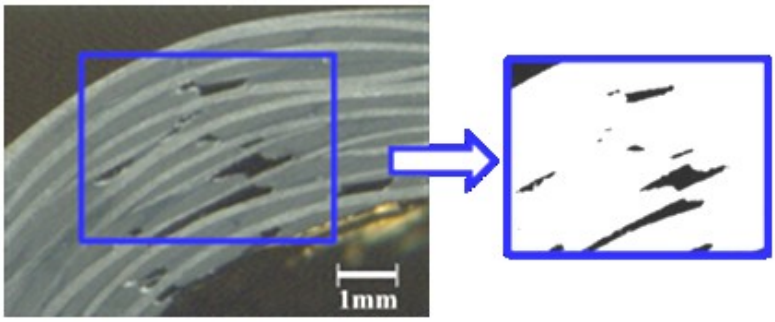

Figure 3.7: Conversion from greyscale to binary image of cut section with void contours for void content estimation

Using the tracing tool, the contour of each void was traced and the area was measured by the software. The total area occupied by voids, S_{void}, was calculated for each cut surface by adding all void areas. The threshold was then adjusted to

trace the contour of the laminate surface and estimate the total surface area, $S_{laminate}$.

The void content was calculated for each cut surface as the ratio of total area occupied by voids over the total laminate surface area, as described by Eq.(16). The final void content for each specimen was given as the average of the void contents calculated for each cut surface, as shown in Eq. (17). The error was defined as the difference between the average void content and that of each cut surface and was estimated following Eq. (18).

$$vc_{01} = \frac{S_{void_{01}}}{S_{laminate_{01}}} * 100 \text{ and } vc_{02} = \frac{S_{void_{02}}}{S_{laminate_{02}}} * 100 \quad \textbf{(16)}$$

$$vc = \frac{vc_{01} + vc_{02}}{2} \quad \textbf{(17)}$$

$$\text{error } vc = |vc - vc_{01}| \quad \textbf{(18)}$$

CHAPTER 4

Characterisation of Thickness Variations Based on Radius-to-Thickness Ratios

As discussed in Section 2.2, previous research has demonstrated the recurring issue of thickness variations in the manufacturing of complex shape laminates. In fact, it has been observed that the thickness gradient is localized at the corner and varies with the tool corner radius and the laminate thickness. Also, the thickness gradient has been explained as being the result of non-uniform pressure distributions along the complex geometry, as presented in Section 2.2.

However, the thickness variation at the corner of complex shape laminates has yet to be characterised based on the thickness and corner radius. Therefore, current design guidelines for these geometrical characteristics are still unclear and not optimized. In order to better understand the combined effect of the thickness and corner radius on the thickness variation, a more in-depth analytical study of the non-uniform pressure distributions and their effect on laminate compaction is necessary. Also, an elaborate experimental study for the characterisation of thickness variations based on radius-to-thickness ratios should be performed to develop a design guideline: the critical radius-to-thickness ratio for acceptable thickness variation.

The first section of this chapter presents the simplified analytical model developed for the compaction of an L-shape laminate and which correlates the radius and thickness of a laminate to the final thickness variation at the corner. Section 4.2 outlines the experimental procedure followed to characterise the thickness variations in L-shape composite laminates based on variations in radius-to-thickness ratios and to evaluate the compliance of the analytical model. Finally, a discussion of the results and their application for design purposes, as well as the limitations of the analytical model are provided in Sections 4.3 and 4.4.

4.1 Analytical Model

4.1.1 Assumptions

As proposed by Hubert et al. [26], an important mechanism behind thickness variations in complex shape laminates, lies in the differential in reaction stress between the corner and the flange. This mechanism constituted the basis of the analytical model that was developed through the refinement of the free-body diagram analysis presented in Section 2.2. The models were developed to predict the thickness variation attributed to the differential in reaction stress based on the corner radius and laminate thickness. The models required the following assumptions.

1. The deformation is symmetric with regards to the symmetry line of the geometry.
2. Stresses in the hoop direction, which develop due to the compaction, are neglected for simplification. This assumes no restriction to interply shearing of the laminate plies.
3. The reaction pressure at the tool side surface can be averaged as $P_{avgtool}$.
4. The overall compaction pressure acting on the laminate at the corner can be averaged as $P_{avgtool}$.
5. The compaction behaviour of the laminate approaches that of a purely elastic fibre bed. This neglects any viscous effects and the time-dependency of the compaction phenomenon.
6. The maximum compaction pressure applied is such that the fibre bed compaction stress vs strain curve can be approximated as linearly elastic.
7. The thickness before cure is uniform.

4.1.2 Concave tool model

4.1.2.1 Free-body diagram analysis

Consider the free-body diagram of the corner section of a typical laminate over a concave tool after compaction as illustrated in Figure 4.1. At the corner, the applied pressure P acts on surface S_P in red and the tool reaction pressure $P_{avgtool}$

acts on surface S_T in blue. The following geometrical dimensions are illustrated: t is the flange final thickness, t_c is the thickness at the corner, R is the tool corner radius, R_{bag} is the laminate final inner radius at the corner and x is the flange portion subjected to $P_{avgtool}$.

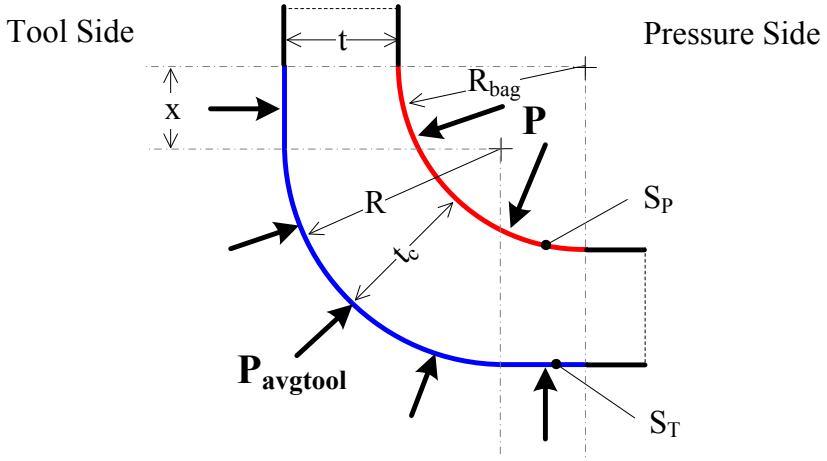

Figure 4.1: Free-body diagram of the corner section of a laminate over a concave tool after compaction. Geometrical dimensions t, t_c, R, R_{bag} and x are illustrated for reference

From equilibrium of forces at the corner, the pressure stresses at the tool side and the pressure side are related following Eq. (19).

$$\sum F_{bag} = \sum F_{tool}$$

$$P \cdot S_P = P_{avgtool} \cdot S_T \tag{19}$$

Surfaces S_P and S_T are given by the following relations.

$$S_P = \frac{1}{4}(2\pi R_{bag})W \quad \text{where W=width of the part} \tag{20}$$

$$S_T = \left[\frac{1}{4}(2\pi R) + 2x\right]W \tag{21}$$

From similar triangles and trigonometry, the following expressions can be determined for R_{bag} and x.

$$R_{bag} = (R - t) + (1 + \sqrt{2})\Delta t \quad \text{where } \Delta t = t_c - t \tag{22}$$

$$x = (1 + \sqrt{2})\Delta t \tag{23}$$

Substituting Eqs. (20) to (23) into Eq. (19) yields the following equilibrium of forces relation.

$$\frac{\pi}{2} P\left[(R - t) + \left(1 + \sqrt{2}\right)\Delta t\right] = P_{avgtool}\left[\frac{\pi}{2} R + (2 + 2\sqrt{2})\Delta t\right] \tag{24}$$

Dividing both sides by t and rearranging for the ratio of pressures gives Eq. (25).

$$\frac{P_{avgtool}}{P} = \frac{\frac{\pi}{2}\left[\left({}^{R}/_{t} - 1\right) + \left(1 + \sqrt{2}\right){}^{\Delta t}/_{t}\right]}{\frac{\pi}{2}{}^{R}/_{t} + (2 + 2\sqrt{2}){}^{\Delta t}/_{t}} \tag{25}$$

4.1.2.2 Compaction and deformation

The compaction behaviour of a typical laminate would be represented by a compaction curve similar to the one illustrated in Figure 4.2 [26]. Also, under out-of-autoclave pressure conditions (i.e. 100 kPa), the stress-strain relation can be approximated as linear and neglect the usual stiffening behaviour of the fibre bed observed for high stress loads.

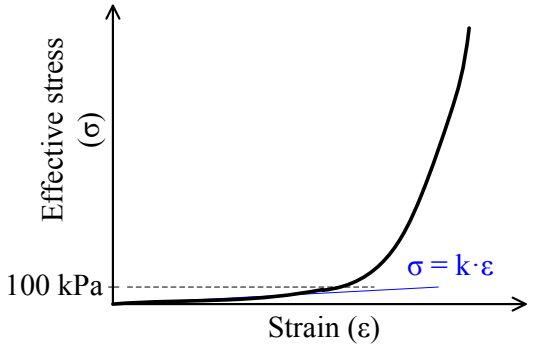

Figure 4.2: Typical compaction curve of a laminate with a purely elastic compaction behaviour

Given the above statements, the relations between the pressure stresses and the strains at the flange (ε_f) and corner (ε_c) can be expressed as follows:

$$P = k \cdot \varepsilon_f \tag{26}$$

$$P_{avgtool} = k \cdot \varepsilon_c \tag{27}$$

Therefore, the ratio between the pressure stresses is given by Eq. (28).

$$\frac{P_{avgtool}}{P} = \frac{\varepsilon_c}{\varepsilon_f} \quad \textbf{(28)}$$

By definition, the strains at the flange and at the corner are given by Eqs. (29) and (30) with t_i defined as the thickness before cure of the laminate.

$$\varepsilon_f = \frac{t_i - t}{t_i} \quad \textbf{(29)}$$

$$\varepsilon_c = \frac{t_i - t_c}{t_i} \quad \textbf{(30)}$$

The bulk factor c_1, specific property of the material, is defined as the ratio of the initial thickness t_i to the final flange thickness t. Equations (29) and (30) can then be re-written as follows:

$$\varepsilon_f = \frac{c_1 - 1}{c_1} \quad \textbf{(31)}$$

$$\varepsilon_c = \frac{c_1 - \left(\Delta t/t + 1\right)}{c_1} \quad \textbf{(32)}$$

The ratio of the strains at the flange and the corner is given by Eq. (33).

$$\frac{\varepsilon_c}{\varepsilon_f} = \frac{c_1 - \left(\Delta t/t + 1\right)}{c_1 - 1} \quad \textbf{(33)}$$

4.1.2.3 Model of the thickness variations in the case of a concave tool for various radius-to-thickness ratios

Combining Eqs. (25), (28) and (33) and rearranging for Δt, one obtains Eq. (34) giving the relation between the radius-to-thickness ratio (R/t), the laminate thickness (t) and the resulting thickness variation at the corner (Δt). The model of Eq. (34) suggests that the thickness variation Δt is a function of both the radius-to-thickness ratio and the thickness of the laminate.

$$\Delta t = t * \left\{ \frac{\left[\left(\frac{4}{\pi} - 1\right)A - R/t\right] + \sqrt{\left[\left(\frac{4}{\pi} - 1\right)A - R/t\right]^2 + \frac{16}{\pi}A}}{\frac{8}{\pi}\left(1 + \sqrt{2}\right)} \right\} \quad \textbf{(34)}$$

$$\text{where } A = (c_1 - 1) * \left(1 + \sqrt{2}\right)$$

Figure 4.3 illustrates a map of the predicted thickness variation for various radius-to-thickness ratios obtained by solving Eq. (34). The bulk factor c_1 was assumed a

value of 1.2, which corresponds to the average calculated value of parts manufactured for the experimental study detailed in Section 4.2, see Table A.1. The predicted thickness variations are plotted for the constant radius curves of 5, 10 and 15 mm. The thin black lines represent the constant thickness curves of 2, 3 and 4 mm. Positive values for Δt represent corner thickening.

The independent effect of laminate thickness and corner radius on the thickness variation at the corner has been documented in the literature. However, the model illustrated in Figure 4.3 is the first, to the author's knowledge, to demonstrate the combined effect of laminate thickness and corner radius. The model suggests that the effect of the corner radius on the thickness variation is more significant with increasing laminate thickness. Similarly, the thickness variation is more sensitive to laminate thickness with decreasing corner radius.

With the model of Eq. (34), a designer can build a map similar to Figure 4.3 with typical standard corner radius curves and determine, for a given acceptable amount of thickness variation, the corresponding critical radius-to-thickness ratios for design.

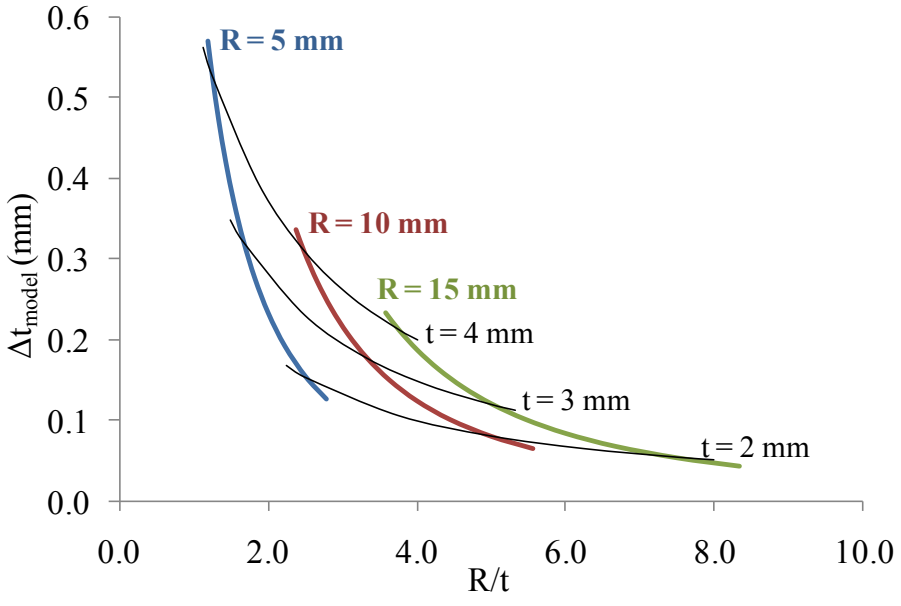

Figure 4.3: Constant radius curves of the predicted thickness variations for various radius-to-thickness ratios for compaction over a concave tool

4.1.3 Convex tool model

4.1.3.1 Free-body diagram analysis

Similarly to the previous section, a relation for the thickness variation at the corner as a function of the geometrical parameters of a laminate over a convex tool can be developed. Consider the free-body diagram of the corner section of a typical laminate over a convex tool after compaction as illustrated in Figure 4.4. The applied pressure P acts on surface S_P in red and the tool reaction pressure $P_{avgtool}$ acts on surface S_T in blue. The geometrical dimensions t, t_c, R, R_{bag} and x are as illustrated.

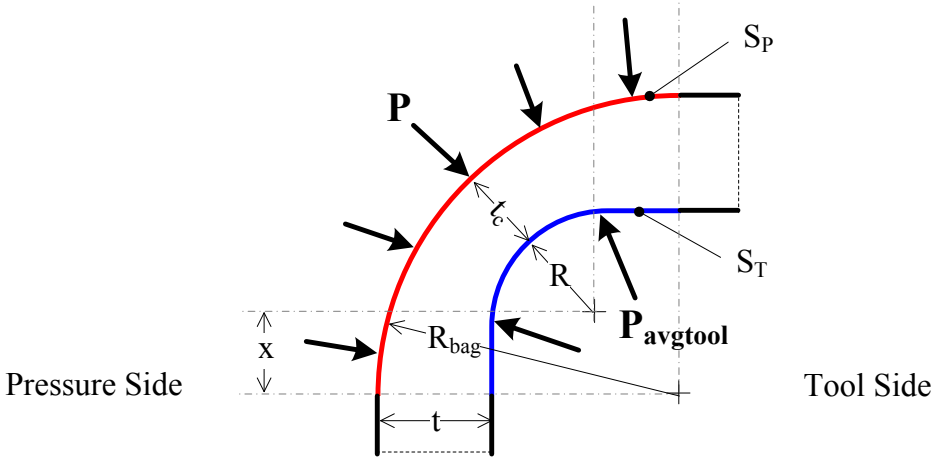

Figure 4.4: Free-body diagram of the corner section of a laminate over a convex tool after compaction, neglecting longitudinal stresses. Geometrical dimensions t, t_c, R, R_{bag} and x are illustrated for reference

Following the same steps as the analysis for the concave tool, the relations for R_{bag} (Eq. (22)) and x (Eq. (23)) become:

$$R_{bag} = (R + t) - \left(1 + \sqrt{2}\right)\Delta t \qquad \text{where } \Delta t = t_c - t \tag{35}$$

$$x = -(1 + \sqrt{2})\Delta t \tag{36}$$

The equilibrium of forces relation becomes:

$$\frac{\pi}{2} P\left[(R + t) - \left(1 + \sqrt{2}\right)\Delta t\right] = P_{avgtool}\left[\frac{\pi}{2} R - (2 + 2\sqrt{2})\Delta t\right] \tag{37}$$

Dividing both sides by t and rearranging for the ratio of pressures gives Eq. (38).

$$\frac{P_{avgtool}}{P} = \frac{\frac{\pi}{2}\left[\left({}^{R}/_{t} + 1\right) - \left(1 + \sqrt{2}\right){}^{\Delta t}/_{t}\right]}{\frac{\pi}{2}{}^{R}/_{t} - (2 + 2\sqrt{2}){}^{\Delta t}/_{t}} \quad \textbf{(38)}$$

4.1.3.2 Compaction and deformation

The compaction analysis is the same for the convex tool. The ratio of the pressure stresses is related to the bulk factor and the thickness variation as follows:

$$\frac{P_{avgtool}}{P} = \frac{c_1 - \left({}^{\Delta t}/_{t} + 1\right)}{c_1 - 1} \quad \textbf{(39)}$$

4.1.3.3 Model of the thickness variations in the case of a convex tool for various radius-to-thickness ratios

Equation (40) gives the relation between the radius-to-thickness ratio (R/t), the laminate thickness (t) and the resulting thickness variation at the corner (Δt) for a laminate over a convex tool. The latter was obtained by combining Eqs. (38) and (39) and rearranging for Δt.

$$\Delta t = t * \left\{ \frac{\left[\left(\frac{4}{\pi} - 1\right)A + {}^{R}/_{t}\right] - \sqrt{\left[\left(\frac{4}{\pi} - 1\right)A + {}^{R}/_{t}\right]^{2} + \frac{16}{\pi}A}}{\frac{8}{\pi}\left(1 + \sqrt{2}\right)} \right\} \quad \textbf{(40)}$$

$$\text{where } A = (c_1 - 1) * \left(1 + \sqrt{2}\right)$$

For various values of radius-to-thickness ratio and laminate thickness, the thickness variation at the corner can be calculated by solving Eq. (40), with c_1=1.2 again. Figure 4.5 illustrates the predicted thickness variation for the 5, 10 and 15 mm constant radius curves and the 2, 3 and 4 mm constant thickness curves. Corner thinning is predicted since the thickness variations are negative. Also, similarly to the model for the concave tool, with increasing thickness, the effect of decreasing the corner radius is more significant.

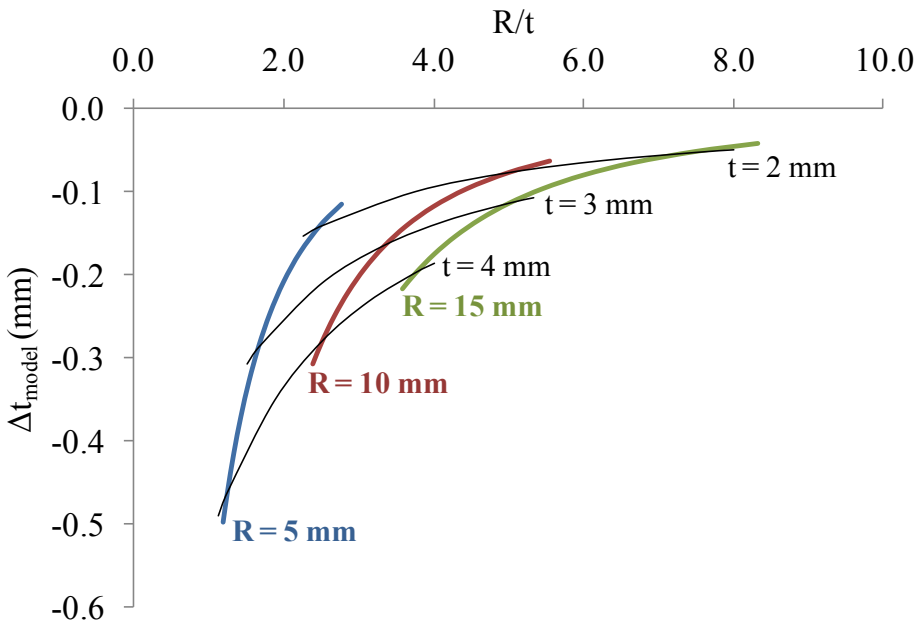

Figure 4.5: Constant radius curves of the predicted thickness variations for various radius-to-thickness ratios for compaction over a convex tool

4.2 Experimental Investigation

4.2.1 Objectives and test plan

An elaborate experimental study was conducted to characterise the thickness variation in complex shape laminates based on the radius-to-thickness ratios for two materials and use the data to formulate design guidelines. The thickness variation predictions obtained from the models presented in Section 4.1 will be compared with the experimental data.

The study consisted in the manufacturing of 40 L-shape composite laminates of various R/t, following the test plan detailed in Table 4.1 and Table 4.2. Standard tool corner radii were selected due to tool availability. The laminate thicknesses were adjusted to cover a wide range of R/t values, similar to that observed in the numerical models of Section 4.1. The highest and lowest R/t ratios were chosen based on reasonable laminate thickness observed in industry. The smallest R/t ratio for laminates over a concave tool is above 1.0; below this value, zero thickness variation would be geometrically impossible. More laminates were

manufactured with a low R/t ratio; at which thickness variations are more pronounced. For each tool shape, two R/t ratios were repeated at both tool radii. The tests were performed for two materials.

Table 4.1: Specimen identifications for material, tool shape, tool corner radius, number of plies and resultant radius-to-thickness ratio (R/t) – Cytec Cycom 5320 8-harness satin (8HS) laminates

Laminate number	Material	Tool shape	Tool radius (mm)	Number of plies	R/t
1	8HS	Concave	9.53	5	5.14
2	8HS	Concave	9.53	6	4.28
3	8HS	Concave	9.53	9	2.85
4	8HS	Concave	9.53	12	2.14
5	8HS	Concave	9.53	16	1.61
6	8HS	Concave	9.53	18	1.43
7	8HS	Concave	12.7	5	6.85
8	8HS	Concave	12.7	8	4.28
9	8HS	Concave	12.7	10	3.42
10	8HS	Concave	12.7	12	2.85
11	8HS	Convex	6.35	5	3.42
12	8HS	Convex	6.35	8	2.14
13	8HS	Convex	6.35	12	1.43
14	8HS	Convex	6.35	14	1.22
15	8HS	Convex	6.35	16	1.07
16	8HS	Convex	6.35	20	0.86
17	8HS	Convex	9.53	9	2.85
18	8HS	Convex	9.53	12	2.14
19	8HS	Convex	9.53	16	1.61
20	8HS	Convex	9.53	18	1.43

Table 4.2: Specimen identifications for material, tool shape, tool corner radius, number of plies and resultant radius-to-thickness ratio (R/t) – Cytec Cycom 5320 plain weave (PW) laminates

Laminate number	Material	Tool shape	Tool radius (mm)	Number of plies	R/t
21	PW	Concave	9.53	7	6.96
22	PW	Concave	9.53	12	4.06
23	PW	Concave	9.53	18	2.71
24	PW	Concave	9.53	24	2.03
25	PW	Concave	9.53	30	1.62
26	PW	Concave	9.53	33	1.48
27	PW	Concave	12.7	12	5.41
28	PW	Concave	12.7	16	4.06
29	PW	Concave	12.7	20	3.25
30	PW	Concave	12.7	24	2.71
31	PW	Convex	6.35	10	3.25
32	PW	Convex	6.35	16	2.03
33	PW	Convex	6.35	22	1.48
34	PW	Convex	6.35	27	1.20
35	PW	Convex	6.35	30	1.08
36	PW	Convex	6.35	38	0.85
37	PW	Convex	9.53	18	2.71
38	PW	Convex	9.53	24	2.03
39	PW	Convex	9.53	30	1.62
40	PW	Convex	9.53	33	1.48

The laminates were manufactured following the procedure detailed in Chapter 3. The cure cycle was the same for all laminates and is presented in Section 4.2.2.2. The dimensions of the parts were as presented in Figure 3.2. After manufacturing, the parts were prepared for testing as described in Section 3.4.1 and the thickness variation calculations were performed for each laminate, as described in Section 3.4.2.

4.2.2 Details of manufacturing

4.2.2.1 Material, tools and bagging arrangement

The materials used for the present study were Cycom 5320 OOA prepreg provided in two forms: 3K PW and 3K 8HS woven pre-impregnated carbon fibre fabrics. The prepregs were supplied by Cytec Industries. Both systems feature Cycom 5320 OOA toughened epoxy resin. Any effect of the material on the measurements was then attributed to the weave style and fibre aerial density. Figure 4.6 illustrates the differences in the weave styles. Plain weave fabrics usually demonstrate a looser weave and are more difficult to drape than harness satin fabrics [45]. However, the 5320 PW prepreg had a lower fibre aerial density (195g/m^2 [46]) in comparison with the 8HS prepreg (370g/m^2 [46]), making it easier to drape. The cured ply thicknesses were also different for the two materials, with the 8HS being twice the thickness of the PW.

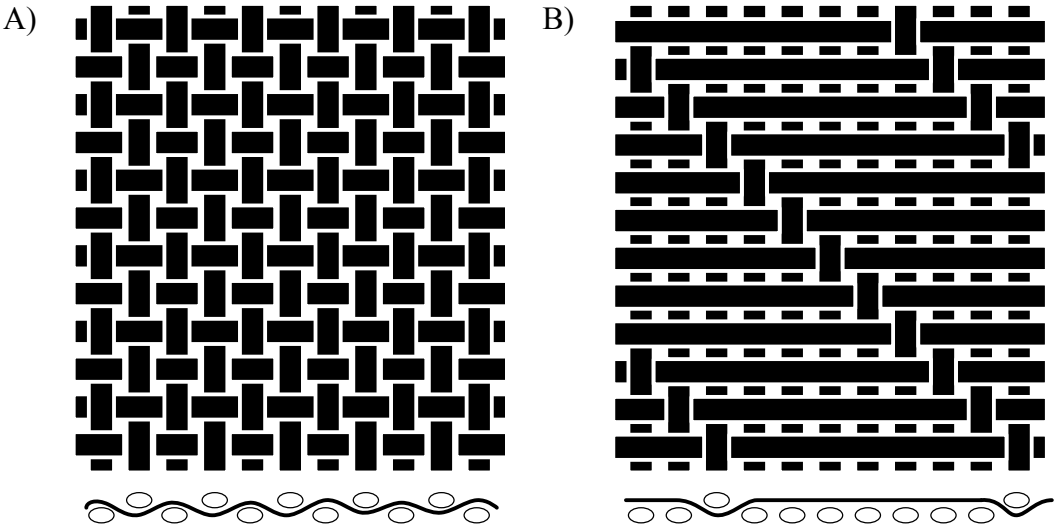

Figure 4.6: Plain weave (A) and 8-harness satin (B) fabric architectures

The four tools presented in Section 3.1.3 were used to manufacture the laminates in order to investigate the effect of the tool shape and provide the desired radius-to-thickness ratios.

The consumable materials were placed following bagging configuration #2 presented in Section 3.3.3 (see Figure 3.4).

4.2.2.2 Cure cycle

The oven temperature cycle was set for a 2-hour debulk at room temperature followed by a ramp at 2.8°C/min to a first dwell cure temperature of 93°C, to be maintained for 2:45 hours. A second ramp at 1.7°C/min follows up to a dwell cure temperature of 143°C, to be maintained for 2:25 hours. The dwell times were adjusted to account for the lag in temperature of the laminate; the laminate temperature dwell times were then around 2 hours, as required. The part is removed from the oven once it reaches a temperature below 75°C. Typical part and oven temperatures are plotted in Figure 4.7.

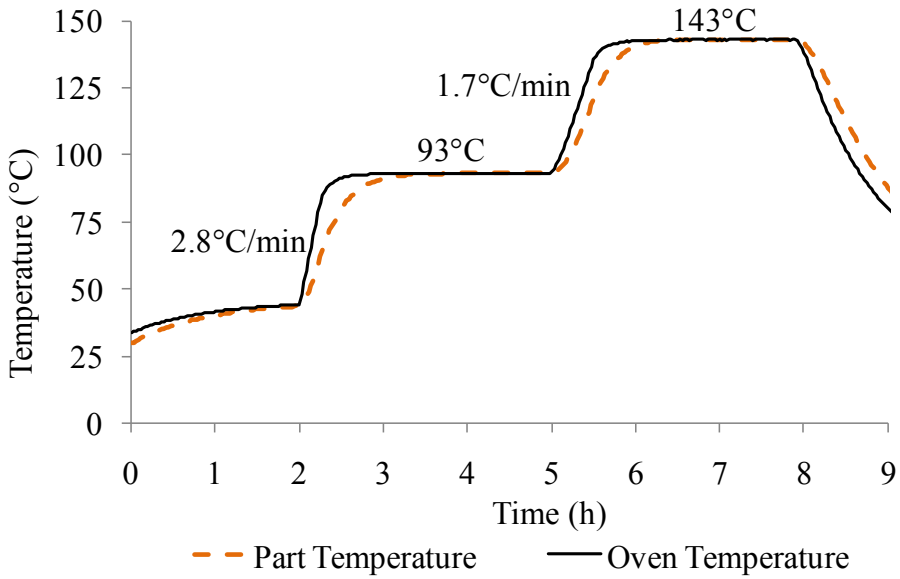

Figure 4.7: Typical part and oven temperature evolution with time

4.3 Results and Discussion

The thickness measurements and the thickness variation calculations are provided in Table A.2 and Table A.3 of Appendix A. Figure 4.8 to Figure 4.11 illustrate the average thickness variation for each laminate as a function of their respective radius-to-thickness ratio (R/t). The results are grouped for constant tool shape and material. An error bar is illustrated for each laminate and corresponds to the maximum and minimum distribution of thickness variation calculated for both surfaces (01 and 02). The variability within the results was considered small enough to permit adequate observations.

The predicted thickness variations from the analytical model are also presented on the figures for each corner radius. These were obtained by solving Eqs. (34) and (40) for Δt, based on the combinations of R/t and thickness of each experimental laminate. The bulk factor was calculated following Eq. (15) for sample laminates of each material. The detailed thickness measurements before cure and calculations are provided in Table A.1. The bulk factor was similar for both materials; thus, an average value of 1.21 was taken for all the model predictions.

4.3.1 Laminates manufactured with a concave tool

The experimental results for the laminates manufactured over the concave tool (see Figure 4.8 and Figure 4.9) confirm the observations found in the literature: with increasing laminate thickness and decreasing tool corner radius, the thickness variation is increased. Also, as R/t approaches a value of 1, the thickness variation increases more prominently. Although both materials demonstrate the same trends, the material had a clear effect on the magnitude of the thickness variations. The 8HS prepreg demonstrated almost twice as much thickness variation as the PW prepreg.

The analytical model described by Eq. (34) correlates well with the experimental results for the PW laminates. Thus, Figure 4.3, based on Eq. (34), could be used to determine the minimal design radius-to-thickness ratio allowable for acceptable thickness variation of PW laminates based either on a design thickness or design corner radius. Also, the agreement between the model predictions and the experimental results indicates that the differential in reaction stress is a dominant mechanism behind the thickness variation and that the assumption for free laminate shear holds for PW laminates. For the 8HS laminates, the model underestimates the thickness variation. A fitting factor of about 2 is required to adjust the model to the experimental data. Therefore, another mechanism that is not considered in the proposed analytical model decreases the ability of the 8HS prepreg to compact at the corner. This observation will be discussed in further detail in Section 4.4.

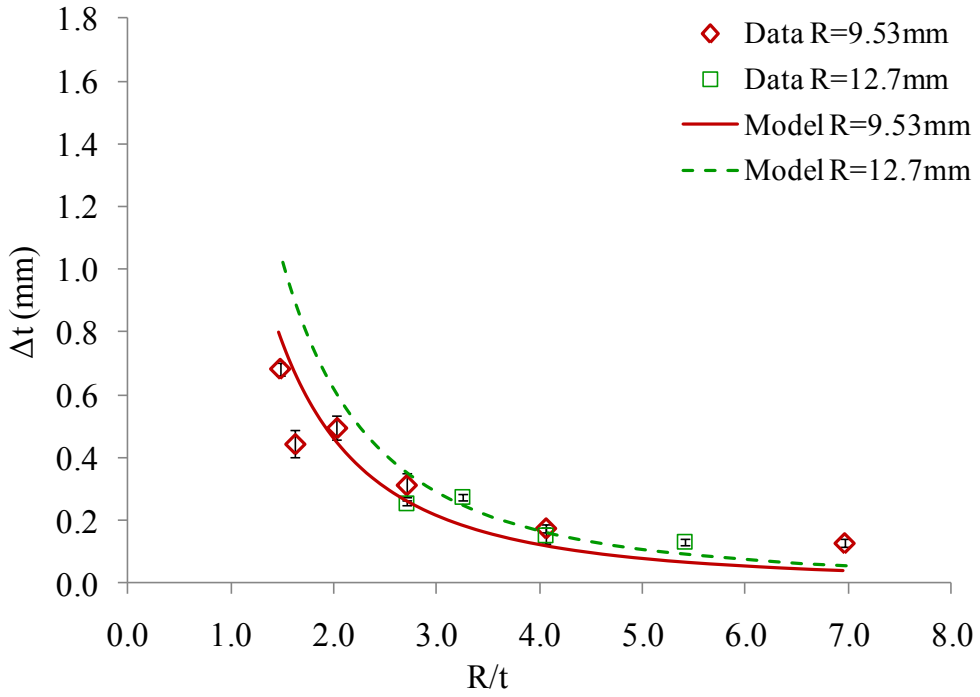

Figure 4.8: Experimental thickness variation (mm) and analytical model predictions (mm) as a function of R/t for concave PW laminates

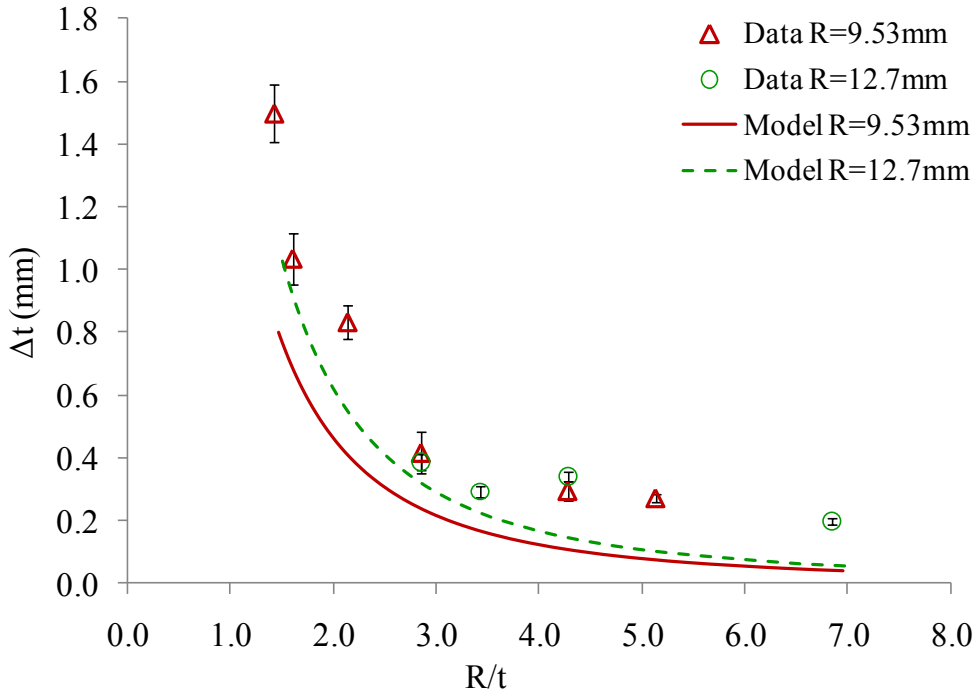

Figure 4.9: Experimental thickness variation (mm) and analytical model predictions (mm) as a function of R/t for concave 8HS laminates

4.3.2 Laminates manufactured with a convex tool

The experimental results for the laminates manufactured over the convex tool (see Figure 4.10 and Figure 4.11) demonstrated corner thickening as opposed to corner thinning observed in the literature. Also, with decreasing R/t, the thickness variation increases, similarly to the laminates manufactured over the concave tool. However, the magnitudes of the thickness variations were lower than those for the concave tool and were similar for both materials.

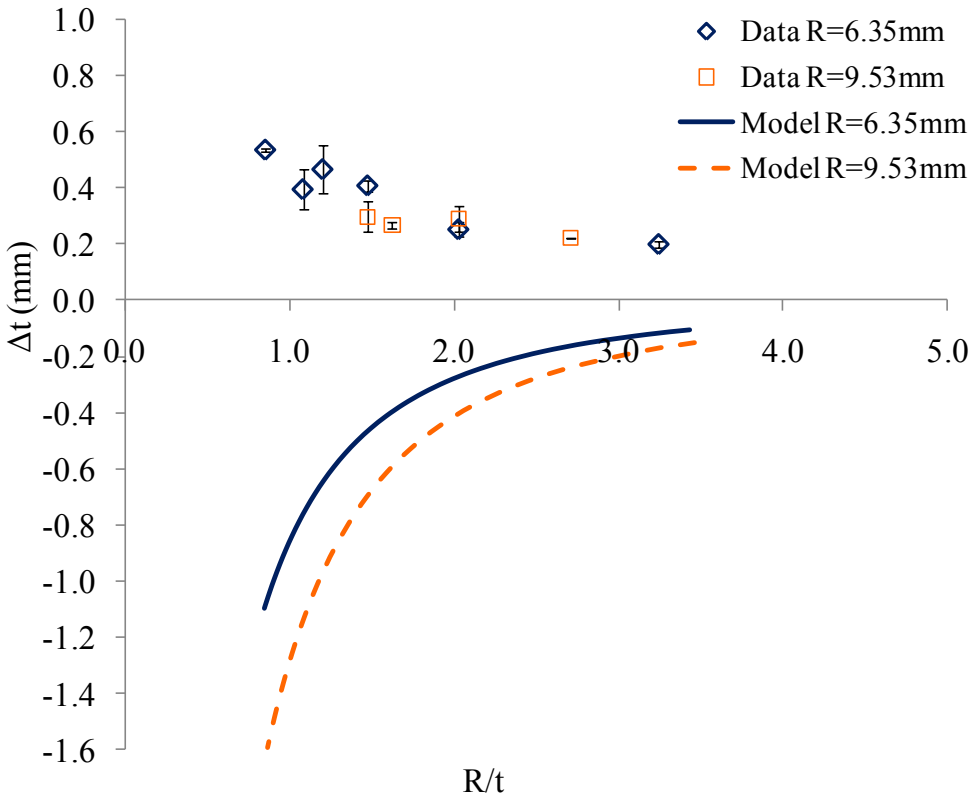

Figure 4.10: Experimental thickness variation (mm) and analytical model predictions (mm) as a function of R/t for convex PW laminates

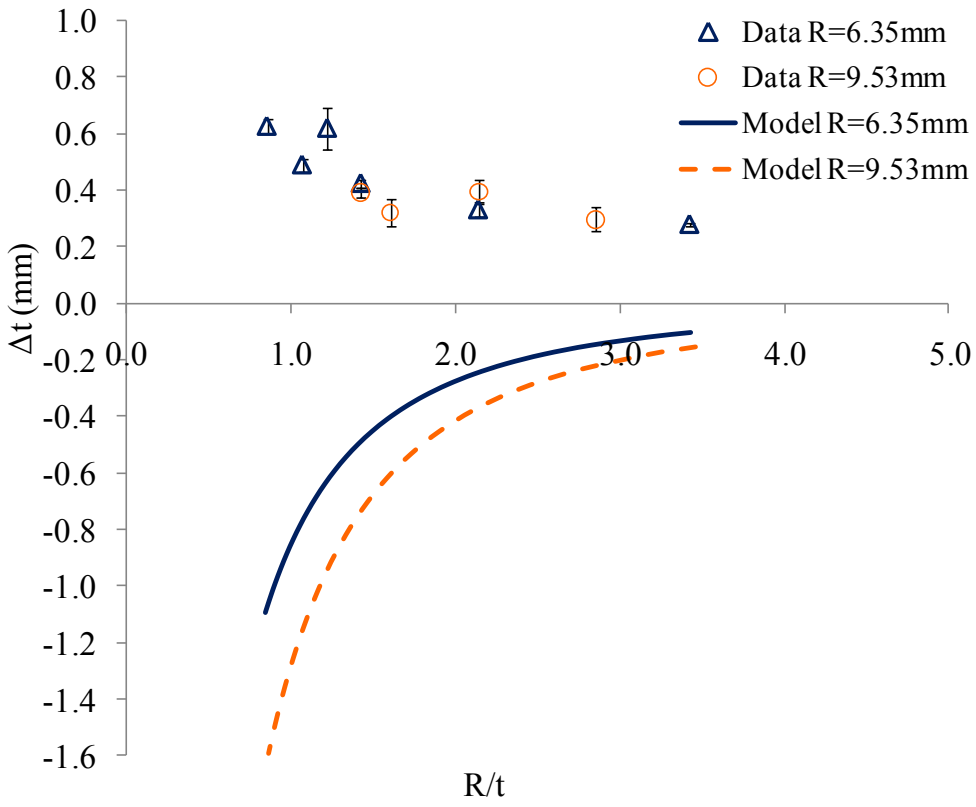

Figure 4.11: Experimental thickness variation (mm) and analytical model predictions (mm) as a function of R/t for convex 8HS laminates

Since the model predicted corner thinning, a large error exists between the predicted thickness variations and the experimental data, for both materials. Hence, for the laminates under investigation, the compaction at the corner was affected by an additional mechanism to the one considered in the analytical model. Figure 4.5, based on Eq. (40), cannot be used for predicting the thickness variation of laminates manufactured over the convex tool.

4.4 Model Limitations

The observations discussed in the previous sections (4.3.1 and 4.3.2) highlight the hypothesis that two other mechanisms, in addition to the differential in reaction stress considered in the analytical model, govern the results; one dominant for laminates manufactured over the concave tool and dependant on the material, and another dominant for laminates manufactured over the convex tool and causing

corner thickening. The analytical model assumed the laminate plies were free to slide relative to each other and stresses in the hoop direction could be neglected. However, this assumption may not hold for laminates of high thickness per ply and high bulk factor.

The following sub-sections discuss the possible mechanisms that would explain the differences between the experimental results and the model predictions. With further analysis of these mechanisms, the proposed analytical model could be complemented and better represent the compaction of complex shape laminates.

4.4.1 Laminates manufactured with a concave tool

The model underestimated the thickness variation for the 8HS material. Therefore, an additional mechanism inhibits the ability of the 8HS prepreg to compact at the corner.

In fact, laminate shear is required to accommodate the compaction at the corner. This is mostly obtained through intraply shear, or interply slip, when high stiffness fibres are oriented in the hoop direction. Interply slip has been studied in depth in the forming of thermoplastic laminates of complex geometries and was often associated with fibre wrinkling, buckling and thickness variation issues [47-49]. The amount of interply slippage determines the resulting additional thickness variation at the corner; free slippage allows the laminate to compact fully under the compaction pressure at the corner $P_{avgtool}$, whereas low slippage will restrain the compaction at the corner and cause corner thickening.

Also, the amount of slippage per ply is governed by the interply shear stresses that develop in reaction to the compaction at the corner. These shear stresses are function of the resin properties and compaction pressure [47]. Therefore, the total amount of slippage for the laminate would be function of the interply shear capabilities per ply and the number of ply interfaces. As illustrated in Figure 4.12, for two laminates of the same total thickness, the total amount of slippage of the laminate (Δx) will be greater for a higher number of plies due to the presence of a

higher number of interfaces for shear, given the resin system and compaction pressure are the same for both laminates.

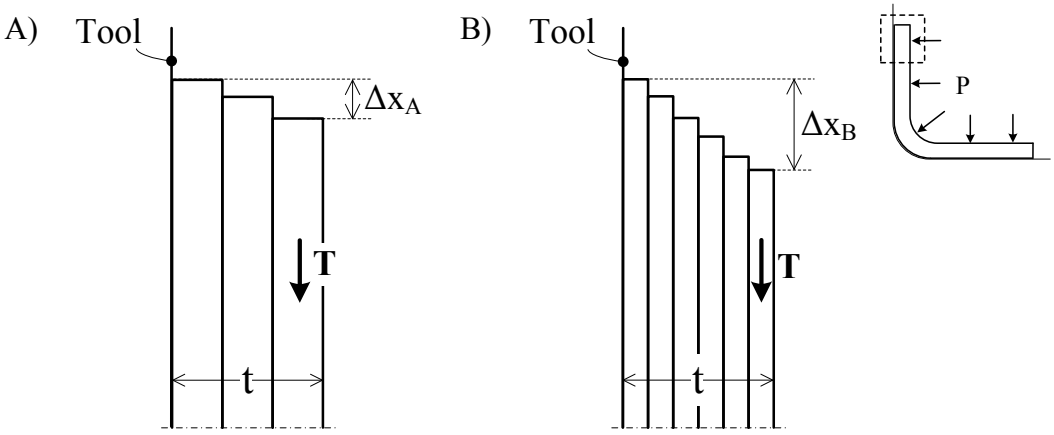

Figure 4.12: Schematic of interply slippage noticed at the ends due to longitudinal tensile stresses (T) for two different materials. The thickness per ply of material (A) is larger than that of material (B), resulting in lower total laminate slippage

Consequently, since the thickness per ply of the 8HS prepreg is twice that of the PW, half the number of plies were used to manufacture laminates of the same thickness. The 8HS had less potential in providing the amount of slippage required for deformation. In addition, this could explain why, for laminates of the same material and same R/t, the experimental data demonstrated a lower thickness variation for a higher thickness, hence a higher number of plies, whereas the model predicted a higher thickness variation for the laminate of larger thickness. The effect of ply thickness on the ability of the laminate to undergo laminate shear has not yet been documented in the literature.

4.4.2 Laminates manufactured with a convex tool

From the analytical model, the higher reaction stress at the corner should cause corner thinning of laminates manufactured with the convex tool. However, another mechanism restrained the ability of the laminate to shear and caused corner thickening.

Consider Figure 4.13 which illustrates the compaction of a laminate over a convex tool from the application of a pressure P. The dashed line represents the initial shape of the laminate. The dotted line represents the final shape considered by the analytical model, with corner thickness t_m. The full line illustrates the actual final shape of the laminate, with corner thickness t_c.

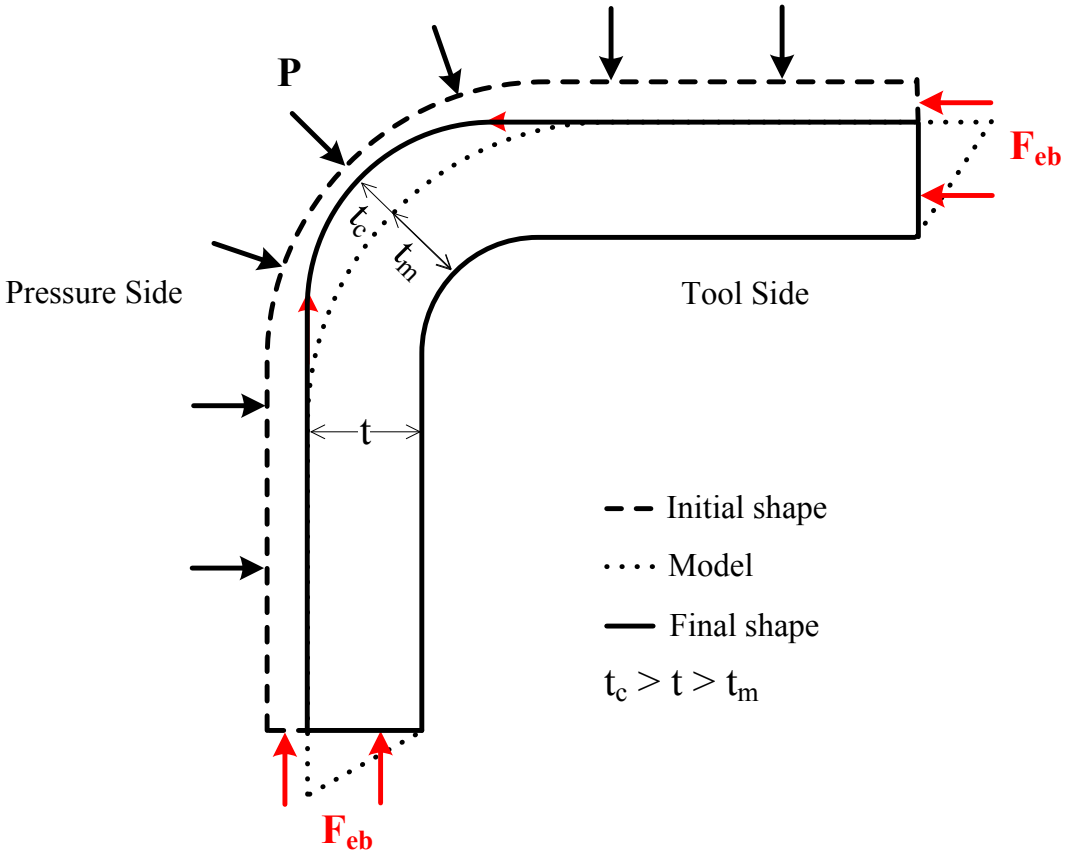

Figure 4.13: Schematic of the corner thickening resulting from the longitudinal stresses, F_{eb}, in a laminate manufactured over a convex tool with restrained ends

The compaction pressure induces laminate shear which opposes deformation. The analytical model assumed no resistance to laminate shear for simplification and to isolate the effect of the differential in reaction stress mechanism. Thus, the model predicted corner thinning (see dotted shape). However, experimentally, the edge breathing system around the laminate edges prevented the ends from shearing. A reaction force F_{eb} was then applied to the laminate causing longitudinal stresses in

the fibres. These intraply stresses counteracted the compaction pressure at the corner and thus reduced the amount of compaction at that region.

Also, these longitudinal stresses should increase with the magnitude of the deformation. Thus, for laminates of large thickness and materials of high bulk factor, the effect of the longitudinal stresses should dominate over the effect of the increased reaction stress at the corner. In fact, in the case where the laminate thickness was large, the shear stresses from the compaction caused the plies to move upwards, above the edge breathing set-up. This is observed in Figure 4.14. In addition, similarly to the concave laminates, interply shear stresses could have contributed to the resistance of the laminate to compaction. Thus, stresses in the hoop direction cannot be neglected in the model for convex laminates.

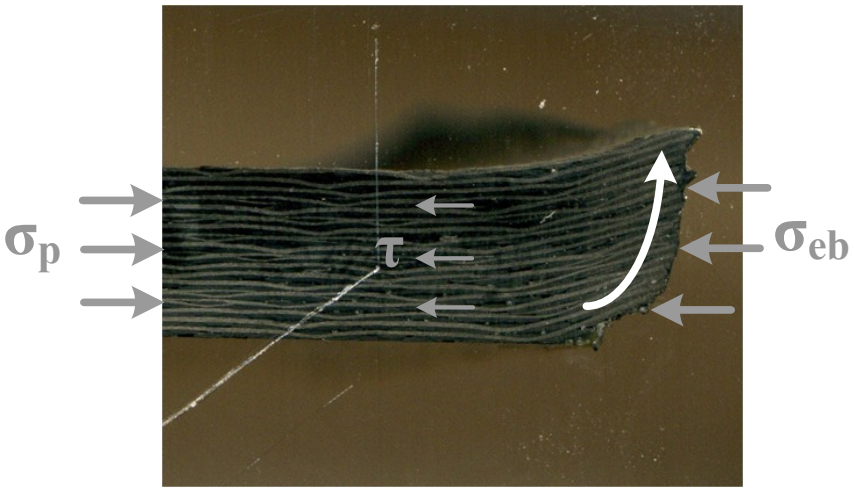

Figure 4.14: Close view of the end of laminate 20, where the plies moved upwards in reaction to the opposing compaction stresses (σ_p) with the resistance stresses (σ_{eb}) from the edge breathing set-up and the interply shear stresses (τ)

CHAPTER 5
Effect of Bagging Arrangement on Part Quality

The compaction behaviour of L-shape laminates was investigated in Chapter 4. In fact, the effect of tool shape (convex and concave), material and geometrical parameters on the thickness variation at the corner was evaluated. It was determined that, for the materials under study and within OOA conditions, the compaction was governed by different mechanisms depending on the tool shape. Also, the material had an effect on the thickness variation in the case of laminates manufactured over the concave tool. For both tool shapes, the laminates demonstrated corner thickening. More importantly, the magnitude of corner thickening was highly driven by the geometrical parameters (laminate corner radius and thickness); large thickness variations were observed for small radius-to-thickness ratios.

Still, for certain design applications, small radius-to-thickness ratios are required and consequently, their resulting thickness variations are unacceptable. Such cases are mostly found when manufacturing with concave tools. In order to improve the processing range of such laminates, the pressure distribution must be altered by providing increased pressure at the corner. This could be accomplished by varying the bagging arrangement. However, changes in bagging arrangement may also affect other aspects of part quality, such as the void content.

The present chapter details the experimental procedure followed to study the effect of the bagging arrangement on the thickness variation and void content in L-shape laminates manufactured by OOA methods. Section 5.1 describes the test plan for the study. The details relative to the manufacturing of the laminates are provided in Section 5.2. Section 5.3 illustrates the results for thickness and void content measurements. Finally, a summary of the results and important observations are provided in Section 5.4.

5.1 Objectives and Test Plan

The objective was to evaluate the effect of the bagging arrangement on the quality of complex shape composite laminates manufactured with convex and concave tools, in terms of thickness variation and void content. Seven L-shape laminates were manufactured. The dimensions of the parts were as presented in Figure 3.2, with R_{in} = 6.35 mm and R_{out} = 9.53 mm. All laminates were made of 8 plies of the same material, for which the details are provided in Section 5.2.1. To investigate the effect of the bagging arrangement, five different configurations were used and are presented in detail in Section 5.2.2. Some configurations (#3, 4 and 5) feature the use of a rubber pressure intensifier to promote compaction at the corner of laminates manufactured over the concave tool. Table 5.1 lists the tool shape and bagging configuration for each part.

Table 5.1: Characteristics of test samples

Part #	Tool Shape	Bagging Config. #	Pressure Intensifier	Comment
A	Convex (male)	1	N/A	Reference configuration for convex tool
B	Convex	1	N/A	Care in placement of consumable materials when applying vacuum pressure
C	Concave (female)	1	No	Reference configuration for concave tool
D	Concave	2	No	No breather cloth over the corner
E	Concave	3	Yes	Breather cloth only over pressure intensifier
F	Concave	4	Yes	Additional breather under pressure intensifier
G	Concave	5	Yes	Use of a smaller pressure intensifier

The laminates were manufactured following the procedure detailed in Chapter 3. The cure cycle was the same for all laminates and is presented in Section 5.2.3. After manufacturing, the parts were cut and polished; measurements for thickness and void content were performed, as described in Section 3.4.

5.2 Details of Manufacturing

5.2.1 Material and tools

The material used for the present study was MTM45-1 OOA prepreg supplied by the Advanced Composites Group. This material was chosen based on availability. The system consisted of MTM45-1 toughened epoxy resin pre-impregnated 5HS woven 6K carbon fibre fabric. The concave tool #1 and convex tool #3, presented in Section 3.1.3, were used to manufacture the laminates.

5.2.2 Bagging arrangement

For Parts A, B, and C, the bagging arrangement corresponded to configuration #1. This configuration represents the reference convex/concave tool bagging procedure and was illustrated in Figure 3.3. For Part B, the vacuum pressure was applied gradually and any wrinkles formed in the consumable materials were removed carefully. For Part D, the bagging arrangement corresponded to configuration #2, presented in Figure 3.4 for the concave tool.

For parts E and F, a pressure intensifier was used to increase the compaction pressure at the corner. The pressure intensifier was formed from Airtech *Pressure Strip* uncured 1-inch synthetic rubber tape stacks that were then cured at a minimum temperature of 120°C for at least 3 hours. The pressure intensifier for part E was directly moulded over the concave tool, giving a corner radius of R_1, which was larger than the desired final part inner radius (R_{in}). This will be taken into account in the discussion of the results. The pressure intensifier for Part F was moulded properly with a corner radius equal to the desired final part inner radius (R_{in}). The difference between the bagging arrangement of Parts E and F is the location of the breather cloth. Part E follows configuration #3 where the pressure intensifier is placed over the release film and covered in breather cloth. In the case of Part F, additional breather cloth was placed under the pressure intensifier above the flange sections of the laminate, giving configuration #4. Configurations #3 and 4 are illustrated in Figure 5.1 and Figure 5.2, respectively.

To isolate the effect of the breather cloth arrangement, another Part F (Part F_E) was manufactured with the pressure intensifier used for Part E.

Bagging Configuration #3

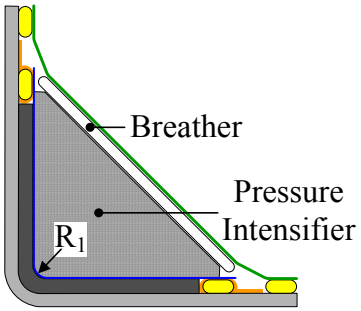

Part E

Figure 5.1: Schematic of Bagging Configuration #3, for Part E

Bagging Configuration #4

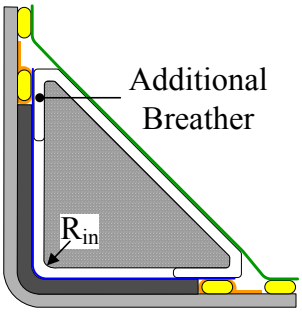

Part F

Figure 5.2: Schematic of Bagging Configuration #4, for Part F

For Part G, a smaller version of the pressure intensifier, which will be referred to as a pressure strip, was used to promote compaction at the corner. The pressure strip was formed of uncured synthetic rubber in the same manner as the pressure intensifier. The corner radius of the pressure strip corresponded to the desired final part inner radius (R_{in}). The pressure strip was placed over the release film and the set-up was covered in breather cloth as illustrated in Figure 5.3.

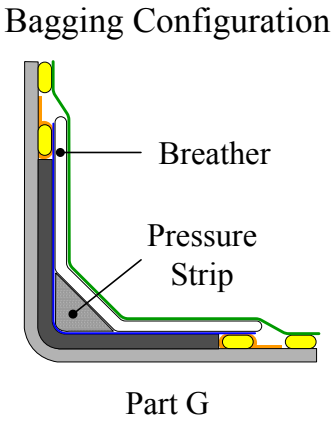

Figure 5.3: Schematic of Bagging Configuration #5, for Part G

5.2.3 Cure cycle

The oven temperature cycle was set for a 1-hour debulk at room temperature followed by a ramp at 2°C/min to a first dwell temperature of 80°C, to be maintained for 2 hours. A second ramp at 2°C/min follows up to a dwell temperature of 120°C, to be maintained for 4 hours. The part was removed from the oven once it reached a temperature below 75°C. Typical part and oven temperatures are plotted in Figure 5.4.

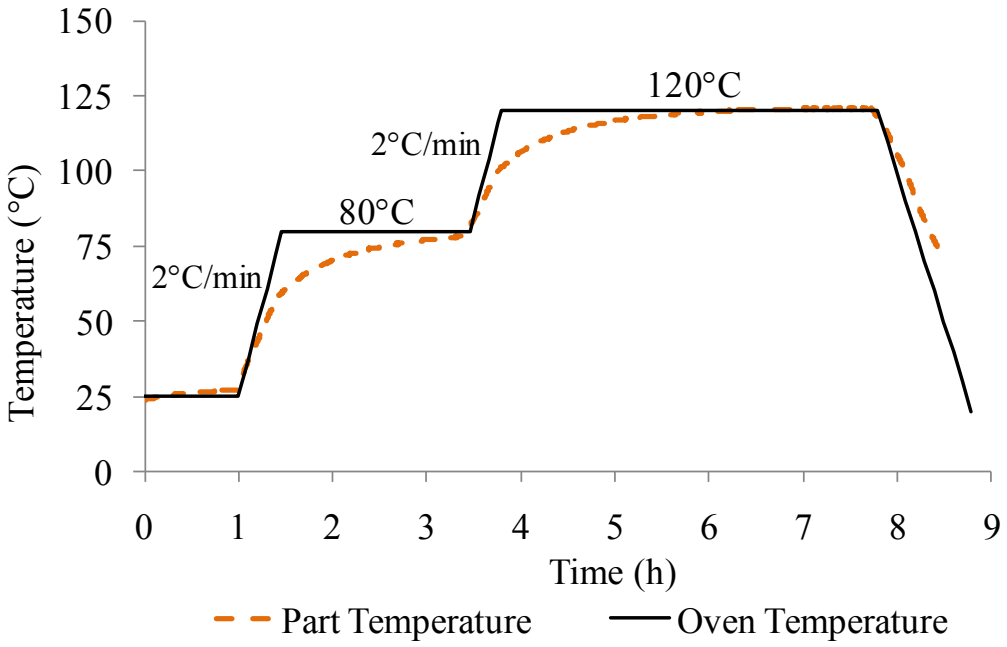

Figure 5.4: Typical part and oven temperature evolution with time

5.3 Results and Discussion

5.3.1 General defects

The defects and compaction issues were located at the corner region and are listed in Table 5.2. Voids were also observed in all laminates and will be characterised and discussed in section 5.3.4.

Table 5.2: Summary of defects observed for Parts A to G

Part #	Wrinkling	Resin accumulation	Thickening	Comment
A	X			Wrinkles in breather were transferred to laminate
B				
C		X	X	Thickening due to resin accumulation
D			X	
E			X	Pressure intensifier had a corner radius too large
F				Very little thickening
G		X		Resin mark-off along edge of pressure strip

5.3.2 Wrinkling

The wrinkling observed for Part A is illustrated in Figure 5.5A. During processing, as the resin becomes soft, any wrinkles in the consumable materials will transfer to the laminate. Such large wrinkles are due to the thick breather cloth that cannot provide a smooth surface. The operation of removing the wrinkles in the breather cloth by hand while applying vacuum pressure progressively for Part B resulted in a smooth corner, as shown in Figure 5.5B. This solution is, however, operator-dependant and highly sensitive to the care with which the task was accomplished. This reduces the robustness of the process to producing quality parts. An alternative solution would be to follow bagging configuration #2 (see Figure 3.4), where the breather cloth is separated in two pieces and the corner edge is exposed to the vacuum bag directly.

A) 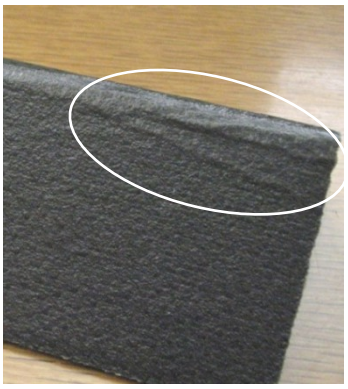 B) 

Figure 5.5: (A) Photograph of Part A: wrinkles formed along the corner due to the consumable materials. (B) Photograph of Part B: no wrinkling

5.3.2.1 Resin accumulation

The resin accumulation observed along the corner of Part C is illustrated in Figure 5.6A. The thick breather cloth did not follow a smooth line and formed wrinkles during the compaction, creating gaps where resin migrated. For Part D, the compaction pressure at the corner was directly transferred to the laminate plies without an intermediate breather cloth. No resin accumulated at the corner, as illustrated in Figure 5.6B. Parts E to G did not show resin accumulation at the corner; the smooth corner radius of the pressure intensifier and pressure strip allows for full contact with the laminate plies and prevents the formation of gaps where resin can migrate.

A) 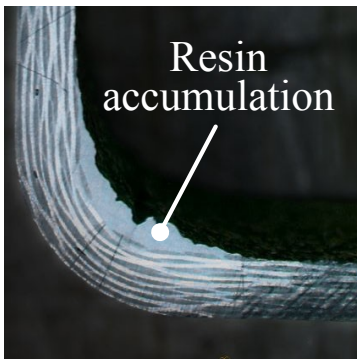

B) 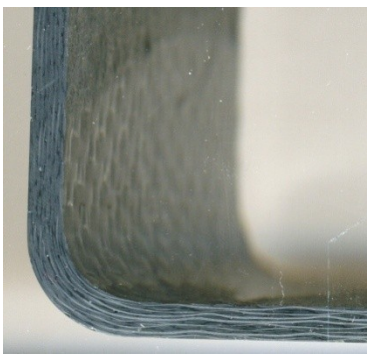

Figure 5.6: (A) Image of the cut surface at the corner of Part C where resin accumulated. (B) Image of the cut surface at the corner of Part D where no resin accumulated

Particular to Part G, small lines of resin mark-off were observed on the flanges delimiting the end edges of the pressure strip as shown in Figure 5.7. The breather cloth and vacuum bag could not conform perfectly around the slightly blunt edges of the pressure strip, creating a gap under the consumables where resin migrated.

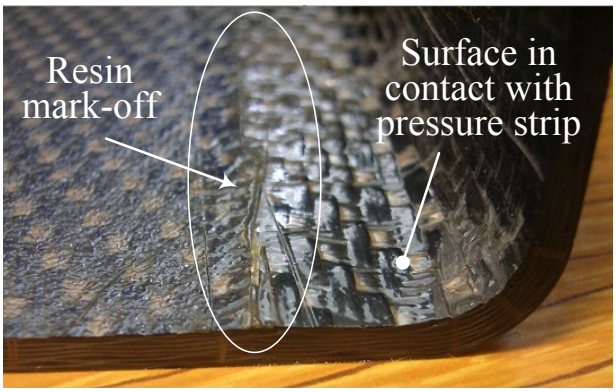

Figure 5.7: Photograph of the line of resin accumulated along the edges of the pressure strip

5.3.2.2 Thickening

The previous defects discussed are common and mostly related to difficulties with the bagging materials; they can thus be prevented with changes in the bagging scheme. However, variations in thickness at the corner are a problem particular to complex shapes as it is attributed to the geometry, as was shown in Chapter 4. Corner thickening was noticeable in most parts manufactured with the concave tool. This highlights the lower pressure that was applied to the corner, which resulted in lower compaction at that region. Such variations in thickness are undesirable as they indicate process variability and may cause assembly difficulties. A more detailed and quantitative analysis of these variations in thickness will be discussed in section 5.3.3.

5.3.3 Thickness measurements

The thickness measurements were performed following the procedure detailed in Section 3.4.2 and are given in the following sub-sections in terms of relative thickness. The detailed measurements are provided in Table A.4. All laminates demonstrated uniform thickness measurements along the flanges. Large thickness

gradients were localised at the corner region and their amplitude varied according to the tool shape and bagging configuration, as discussed below.

5.3.3.1 Effect of tool

Figure 5.8 illustrates the relative thickness measurements for Parts A and B, manufactured over the convex tool, and Parts C and D, manufactured over the concave tool. The results illustrate the defects discussed in section 5.3.1; wrinkling along the corner edge of Part A resulted in sharp thickness variations between locations 4 and 6 and a large increase in thickness is observed for Part C due to the resin accumulation at the corner.

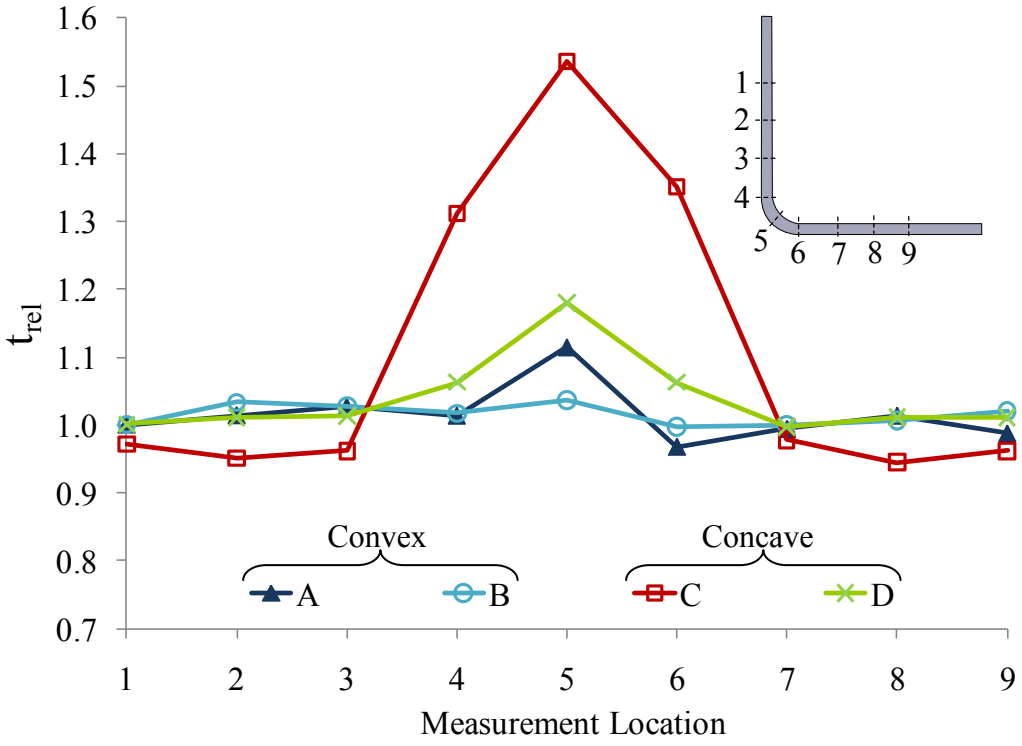

Figure 5.8: Relative thickness measurements after cure for Parts A to D

Minimal thickness variations were obtained for Part B by eliminating the wrinkles in the breather cloth prior to curing. The removal of local breather material at the corner in Part D prevented resin accumulation, and thus decreased the thickness gradient at the corner, in comparison with Part C. However, corner thickening was still observed. Therefore, for the current laminate design and processing conditions, a part of uniform thickness can be obtained when manufactured over

the convex tool, whereas a part manufactured over the concave tool will demonstrate corner thickening.

5.3.3.2 Effect of bagging

Figure 5.9 illustrates the relative thickness measurements for Parts C to G, all manufactured over the concave tool with different bagging arrangements.

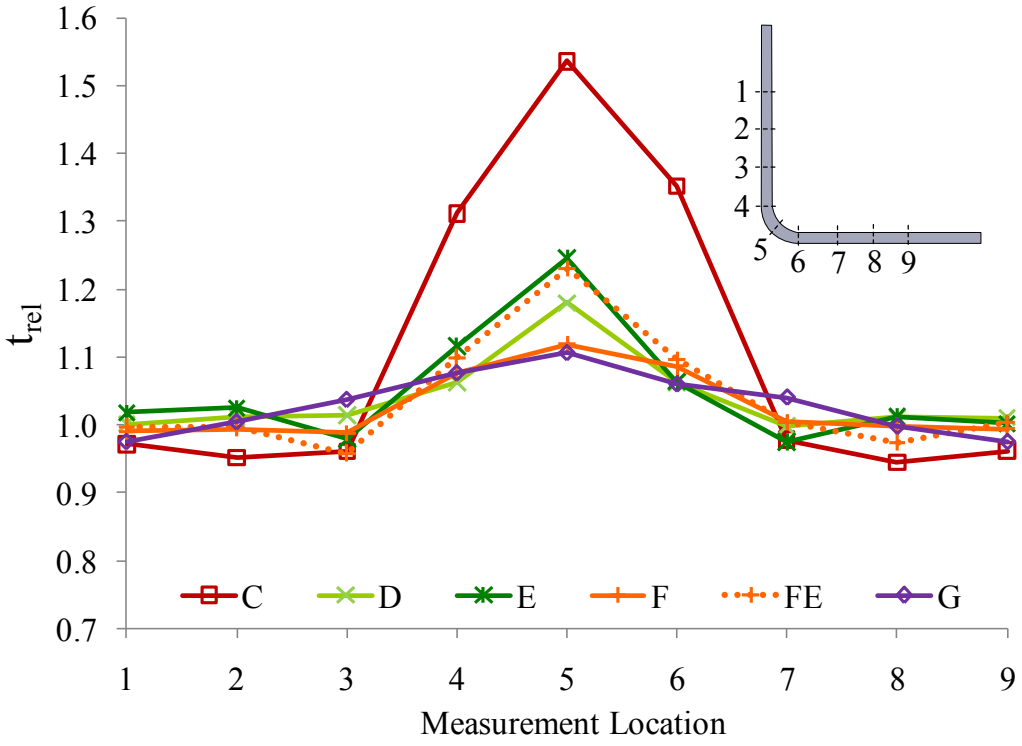

Figure 5.9: Relative thickness measurements after cure for parts manufactured over the concave tool (Parts C to G)

All pressure intensifiers and the pressure strip prevented resin accumulation and thus, Parts E to G demonstrated less thickening at the corner than Part C. However, the pressure intensifier for Part E had a corner radius (R_1) larger than the desired final part inner radius (R_{in}) and thus worsened corner thickening in comparison to Part D. Improved compaction was achieved for Part F with the pressure intensifier of proper corner radius.

The same improvement in compaction at the corner was achieved with the pressure strip (Part G). The corner radius of the pressure intensifier and pressure

strip is therefore an important parameter to control as it governs the final part inner radius and consequently the thickness at the corner. If the corner radius of the pressure intensifier/strip is not of proper dimension, corner thickening could be worsened.

Another Part F (Part F_E, results plotted in a dashed line in Figure 5.9) was manufactured following the same breather arrangement (bagging configuration #4) but the pressure intensifier of Part E was used to isolate the effect of the change in location of breather on the compaction of the laminate. As expected, the placement of breather cloth under the edges of the pressure intensifier in Part F_E did not have an effect on the thickness measurements compared to Part E.

5.3.4 Void content measurements

The void contents were calculated following Eq. (17) of Section 3.4.2.3 and are presented in Figure 5.10.

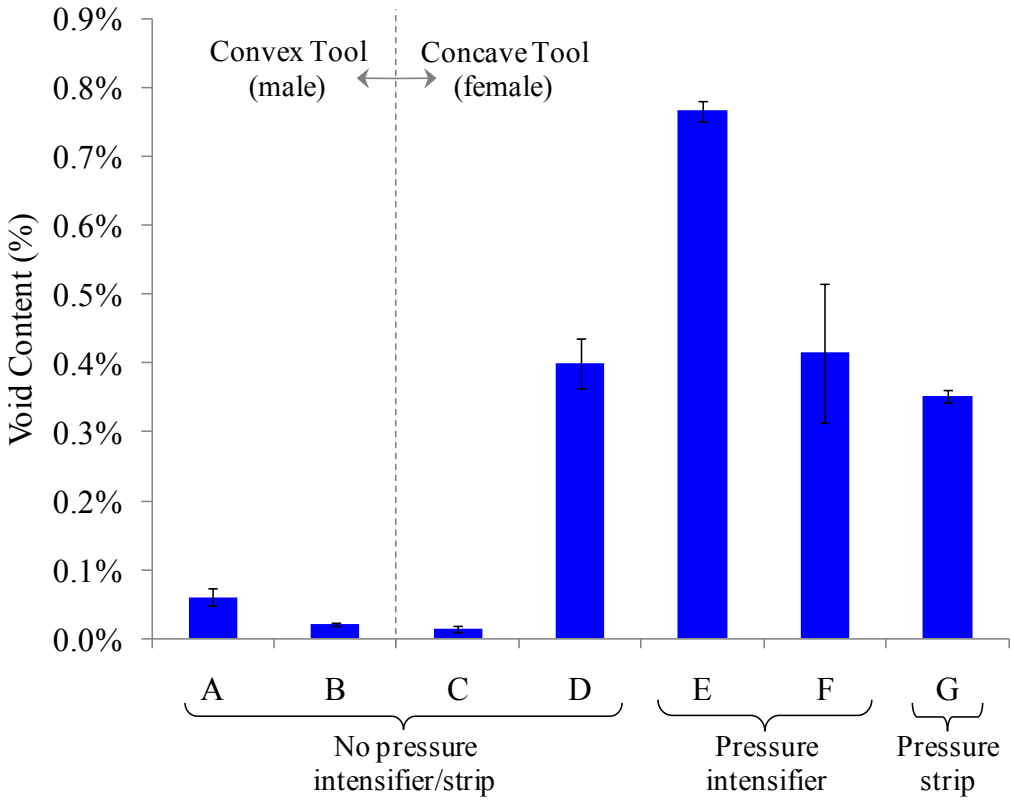

Figure 5.10: Void content (%) measurements

5.3.4.1 Effect of tool

For the same bagging arrangement, no considerable difference in void measurement is observed for parts manufactured over different tools (Parts A, B and C). Also, the removal of wrinkles in the consumable materials prior to curing for Part B shows little effect on the void content compared to Part A.

5.3.4.2 Effect of bagging

The bagging arrangement had an important effect on the void content. In fact, the amount and location of breather material directly affected the ability of the system to evacuate air from the laminate. The use of a pressure intensifier for Part E considerably increased the void content with regards to Part C. The pressure intensifier limited the contact between the edge breathing set-up and the breather material. Also, more voids were observed between the first 2-3 plies under the pressure intensifier, as shown in Figure 5.11. This suggests that the edges of the pressure intensifier may have deformed with the applied pressure and pinched the laminate plies, blocking some of the air evacuation paths. If the debulk is not long enough for the air to travel a further distance to another edge or if the corner is already impregnated with resin, any air bubbles present remains trapped.

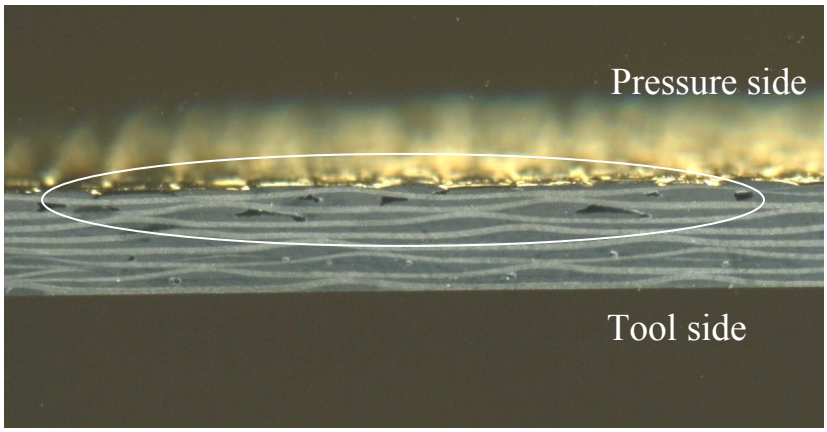

Figure 5.11: Image of a section of the flange of Part E showing the presence of voids between the first plies

The presence of additional breather material under the pressure intensifier for Part F significantly improved the void content. The additional breather prevents the pressure intensifier from pinching laminate plies and ensures full contact with the

edge breathing set-up. Similarly, the use of a pressure strip for Part G improved the void content with regards to Part E; the smaller size of the pressure strip does not restrain the breathing system.

Figure 5.10 shows an increase in void content for Part D compared with Part C. This suggests that the local removal of breather material at the corner decreased the ability of the system to evacuate air from the laminate. This could be due to the fact that the laminate is more exposed to the heat given the absence of breather at the corner and only one layer of breather was placed over the flanges, compared to two for Part C. From this, the laminate temperature could have been higher at any given time and thus, the air had less time to evacuate before resin flow started. A longer debulk might have prevented the higher void content. However, this should be confirmed with further tests and thermocouple measurements.

5.4 Summary

For both tools, the breather cloth at the corner was source of defects. The corner should therefore be clear of breather to (1) prevent the formation of wrinkles and therefore eliminate operator-dependency and decrease the variability in the results and (2) to prevent resin accumulation at the corner. However, the absence of breather at the corner has shown an increase in void content. The length of debulk at room temperature before cure should be adjusted to allow more time for air to evacuate.

For the manufacturing of complex shapes over a concave tool, the laminate will demonstrate corner thickening which can be reduced with the use of a pressure intensifier or a pressure strip. The corner radius of the pressure intensifier and pressure strip has a great effect on the final thickness profile of the laminate: the shape of the outer surface of the intensifier or strip is transferred to the laminate inner surface. The shape should thus be tightly controlled when forming the pressure intensifier or pressure strip.

Although corner thickening is reduced with the use of a pressure intensifier or pressure strip, these inserts bring on extra material and tooling costs to form and obtain a precise shape, and longer lay-up times. Also, the void contents are highly sensitive to the placement of breather material as discussed in the previous section. Therefore, in some cases, the use of a pressure intensifier or pressure strip may not be profitable even at the expense of some corner thickening.

CHAPTER 6
Numerical Modelling

A numerical analysis of the manufacturing of a composite laminate over a concave tool was performed to study the laminate deformation at a stress-level and explain the experimental results discussed in Chapter 5. Sections 6.1 and 6.2 describe the objectives and limitations of the study as well as the modelling details. Section 6.3 presents the numerical results for thickness predictions as well as the effect of the pressure intensifier on the stress contours and resulting laminate deformation.

6.1 Objective and Limitations

The objectives of the modelling exercise were three-fold:

1. Represent the deformation and compaction of a composite laminate similar to those discussed in Chapter 5 over a concave tool under the application of vacuum pressure.
2. Investigate the stress distribution within the laminate to better understand the effect of the pressure intensifier and pressure strip on the laminate deformation.
3. Study the effect of the pressure intensifier and pressure strip stiffness on the laminate deformation.

However, the objectives were not to accurately reproduce the experimental values but rather indicate the same trends. This analysis was performed through the creation of a two-dimensional simplified numerical model using ABAQUS v6.8.3 software.

Resin flow and curing, fibre impregnation and ply movement are important phenomenon in the manufacturing of thermoset composite prepreg laminates that make modelling the compaction and curing processes a complex and challenging

task. Many finite-element based formulations and codes to model changes in mechanical properties, flow and laminate compaction during autoclave processing can be found in the literature [21, 23, 27, 29]. These are used in conjunction with other finite-element codes to obtain deformations and states of stresses and strains. However, resin cure kinetics models, fibre bed compaction curves and other material properties are required for such finite-element models and ask for numerous material characterisation operations and testing. For this reason, the model for the laminate presented in this work was simplified to a two-dimensional uniform part with no distinction between fibres and matrix and changes in material properties associated with the curing process were not considered. The numerical results will be analysed qualitatively and no importance should be made to the magnitude of the results since these depend on the accuracy of the material and elastic properties.

6.2 Details of Models

6.2.1 Assumptions

The following lists the main assumptions for the modelling work.

1. Two-dimensional plane stress analysis.
2. Static analysis.
3. The entire deformation occurs during a short period when the resin viscosity is lowest.
4. No time-dependency of the material properties; given the assumption of point 3, equilibrium should be reached before any changes in material properties occur.
5. Stiffness of the laminate is very low; given the assumption of point 3, at low resin viscosity.
6. Isotropic material properties for simplification; given the assumption of point 3, at low resin viscosity, little stresses are transferred to the fibres since they may move relative to the resin. This limits the stiffness

contribution from the fibres in the longitudinal [0°] direction and thus reduces the anisotropic behaviour during compaction.

7. Frictionless contact between components, i.e. between the laminate and the tool and between the laminate and the pressure intensifier or strip.
8. Neglect effect of breather cloth and release film for simplification.

6.2.2 Models and boundary conditions

Three models were created as illustrated in Figure 6.1: (A) a laminate manufactured over a concave tool with the vacuum bag only, (B) with a pressure intensifier and (C) with a pressure strip.

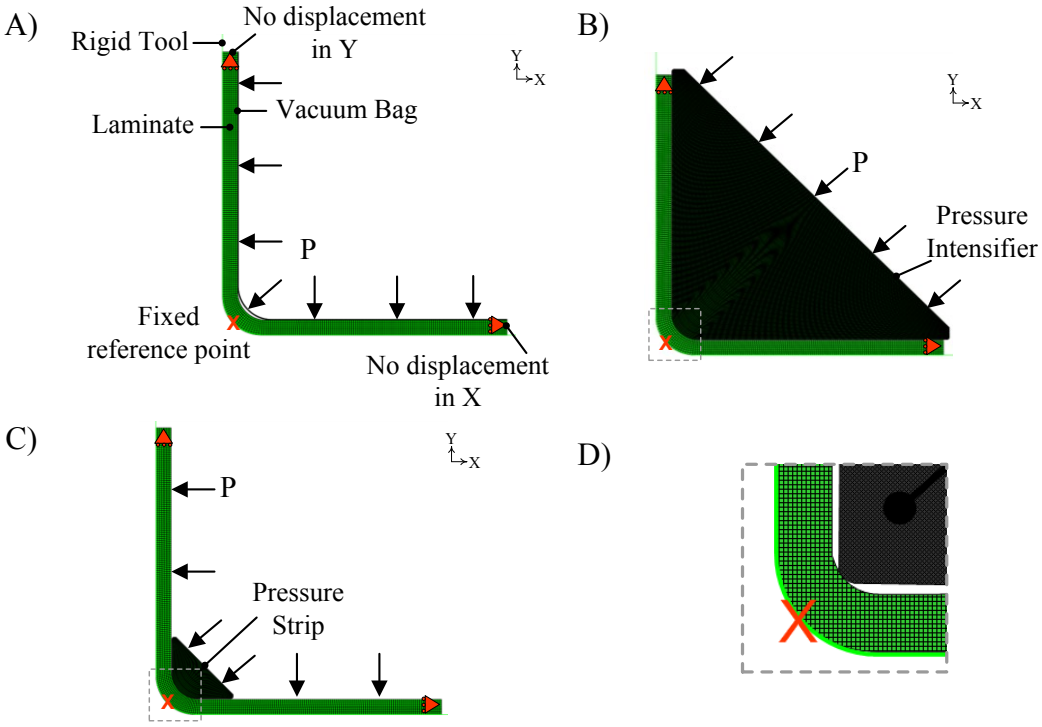

Figure 6.1: Schematics of the numerical model assemblies, loads and boundary conditions for models with (A) the vacuum bag only, (B) a pressure intensifier and (C) a pressure strip. (D) Schematic of the close-up view of the contact between the laminate and the pressure intensifier or pressure strip.

The laminate had the same dimensions as those presented in Figure 3.2 and the initial thickness corresponded to the average thickness before cure of the experimental samples discussed in Chapter 5. The corner radius for the pressure

intensifier and the pressure strip were set to provide the desired part inner corner radius (R_{in}).

The aluminum tool was modeled as a rigid body with a fixed reference point, represented as the orange "X" in Figure 6.1. As represented in Figure 6.1A, B and C, the ends of the laminate and the vacuum bag (for Model A) allowed for movement only in the thickness direction through sliding conditions. This boundary condition represents the restriction in the longitudinal direction by the edge breathing set-up and sealant tape. A uniform vacuum pressure of 91.4 kPa was applied as illustrated in Figure 6.1A, B and C.

The material properties used for the analysis are presented in Table 6.1. For isotropic material properties, only the stiffness and Poisson's ratio must be inputted. The laminate stiffness was obtained by trial-and-error to provide similar bulk factor as the experiments discussed in Chapter 5. The stiffness of the vacuum bag corresponded to common film grade nylon [50]. The stiffness of the pressure intensifier and pressure strip were varied between typical values for cured silicone rubbers [51] to investigate the effect of this property on the compaction of the laminate. A higher Poisson's ratio could have been used for the pressure intensifier to represent the incompressible nature of typical rubbers. This was not considered at the time the numerical work was performed. However, the numerical results show little difference with changes in Poisson's ratio for the pressure intensifier.

Table 6.1: Important material properties for numerical analysis

Laminate		Vacuum bag			Pressure intensifier and pressure strip	
Stiffness [MPa]	Poisson's ratio	Stiffness [GPa]	Poisson's ratio	Thickness [mm]	Stiffness [GPa]	Poisson's ratio
0.65	0.2	0.8	0.2	0.05	0.005-0.100	0.2

The mesh for the laminate part comprised in 2484 linear quadrilateral elements of type CPS4R, i.e. 4-node bilinear, reduced integration with hourglass control. The

vacuum bag, pressure intensifier and pressure strip meshes were formed with 644, 28000 and 1391 elements, respectively, of the same type.

6.3 Numerical Results

6.3.1 Relative thickness predictions

The relative thickness prediction values for all three models are plotted in Figure 6.2. The values are from the models with a pressure intensifier and pressure strip with stiffness of 0.010GPa. The values correspond to the predicted thickness normalised by the average flange thickness of the experimental samples discussed in Chapter 5. Locations 3.5 and 6.5 correspond to the location of the edges of the pressure strip.

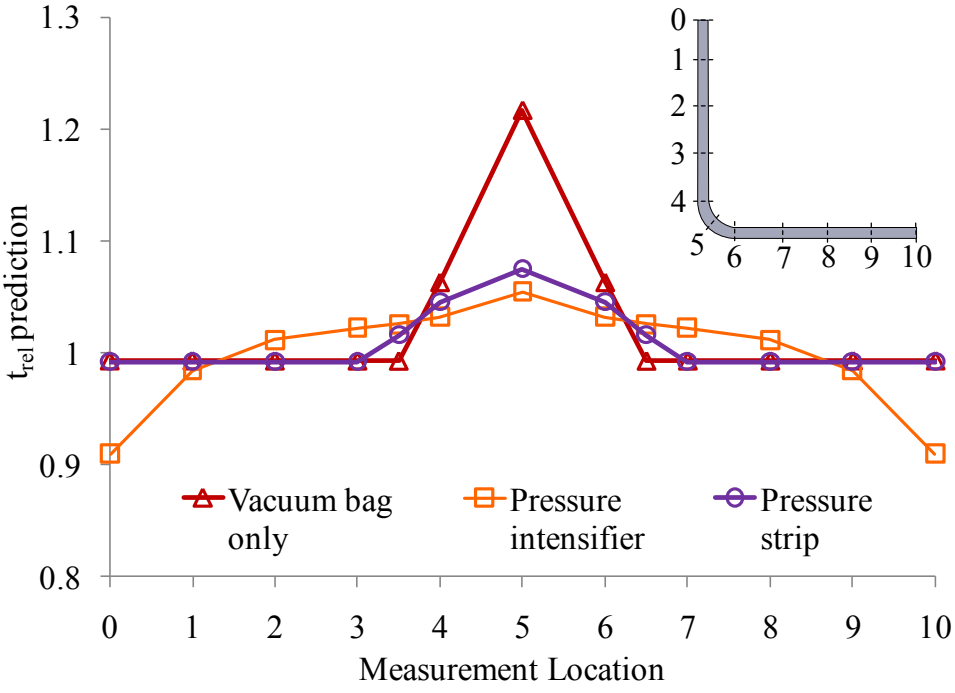

Figure 6.2: Relative thickness prediction values for the three models

The model with the vacuum bag only (see Figure 6.1A) clearly demonstrated corner thickening similar to its corresponding Part D (see Figure 5.8) of the experiments. Also, both the model with the pressure intensifier and the model with the pressure strip (see Figure 6.1B and C, respectively) illustrated better compaction at the corner and reduced corner thickening, as observed in the

experiments (see Figure 5.8, Parts F and G). However, for the model with the pressure intensifier, thinning was observed at the ends of the laminate. Also, for the model with the pressure strip, the thickness values for the region under the pressure strip (locations 3.5 to 6.5) were higher than at the flanges. These observations will be discussed in the following section.

6.3.2 Stress results

6.3.2.1 Model with vacuum-bag only (see Figure 6.1A)

Numerical contour plots of the radial stresses in the laminate and longitudinal stresses in the vacuum bag are illustrated in Figure 6.3. The radial laminate stress plot (Figure 6.3A) shows lower compressive laminate stresses (in blue) at the corner. Such stress conditions translated to lower laminate compaction which resulted in the corner thickening that was observed in Figure 6.2.

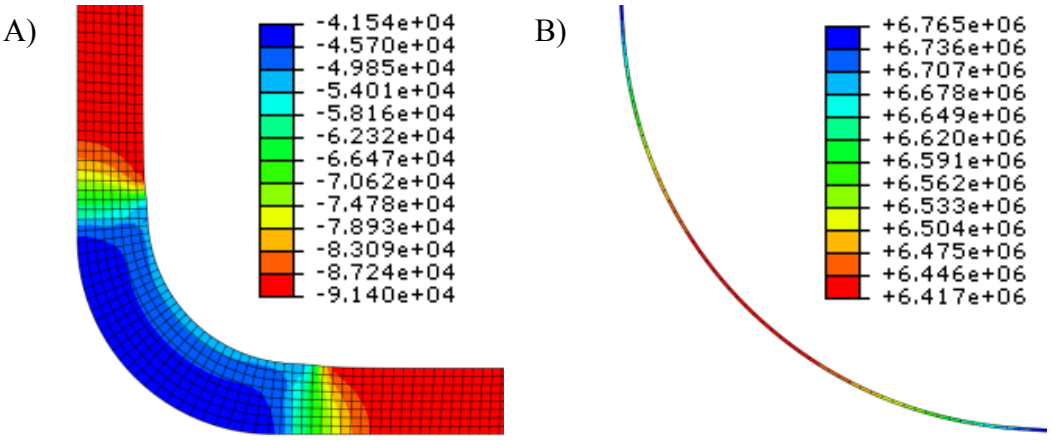

Figure 6.3: Numerical contour plots of stresses (Pa) for the model with vacuum bag only: (A) radial stresses in the laminate, (B) longitudinal stresses in the vacuum bag. (A) and (B) are not to same scale

The lower compressive stresses at the corner were caused by vacuum bag bridging. With the application of pressure, the laminate compacted and the vacuum bag stretched. This caused longitudinal tensile stresses to develop in the vacuum bag, as illustrated in red in Figure 6.3B. A state of equilibrium with the applied pressure was reached and stopped the compaction at the corner.

The lower laminate compressive stresses at the corner can also have been caused by the lower compressive reaction stresses at the tool due to the geometry as was presented in section 2.2. The free-body diagram of the corner section is presented again in Figure 6.4 and demonstrates the higher pressure at the bag side and the lower pressure at the tool side. This translates to higher radial compressive stresses in the laminate (light blue) at the bag side and lower radial compressive stresses (dark blue) at the tool side, as shown in Figure 6.3A.

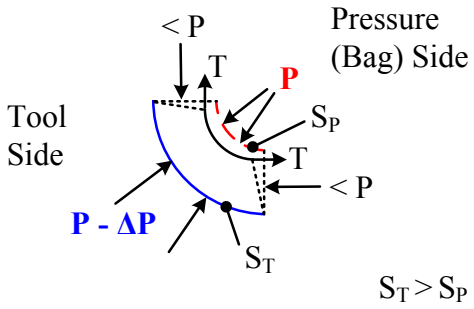

Figure 6.4: Free-body diagram of the corner section of a laminate over a concave tool under a compaction pressure P

With the compaction of the laminate, tensile stresses developed at the corner as illustrated in the free-body diagram (Figure 6.4). Concurrently, the sliding condition at the laminate ends restricted the elongation of the flanges during compaction and caused compressive longitudinal stresses to develop in the laminate. As illustrated in Figure 6.5, the resulting longitudinal stresses were higher in compression at the flanges and at the tool side of the corner than at the bag side of the corner where tensile stresses also acted.

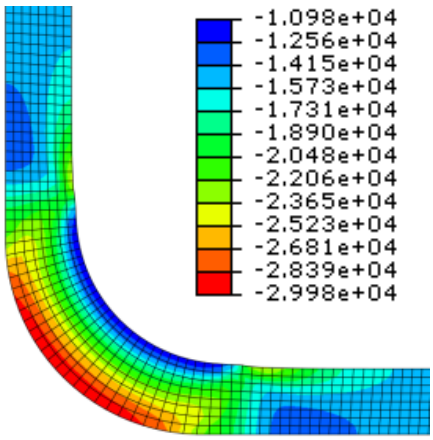

Figure 6.5: Numerical contour plot of the longitudinal stresses (Pa) in the laminate for the model with vacuum bag only

6.3.2.2 Model with pressure intensifier (see Figure 6.1B)

The effect of using a pressure intensifier on the deformation of the laminate is discussed in the present section. The initial contact surface between the pressure intensifier and the laminate is illustrated in Figure 6.6. The numerical contour plots for the radial and longitudinal stresses in the laminate are illustrated in Figure 6.7A and B.

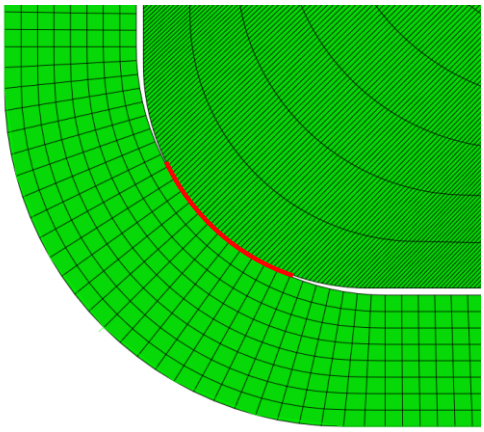

Figure 6.6: Initial contact surface between the pressure intensifier and the laminate

Since the corner radius of the pressure intensifier was smaller than the initial laminate inner corner radius, the initial contact surface between the components was very small. The vacuum pressure was transferred to the laminate through this

small local contact surface. This forced the laminate to compact at the corner before the flanges and to conform to the shape of the intensifier. This increased the compaction at the corner with regards to the model with the vacuum bag only and caused larger compressive radial stresses to develop, as shown in red in Figure 6.7A. Also, from the larger deformation and following the free-body diagram of Figure 6.4, larger tensile longitudinal stresses developed at the bag side of the corner, shown in blue in Figure 6.7B.

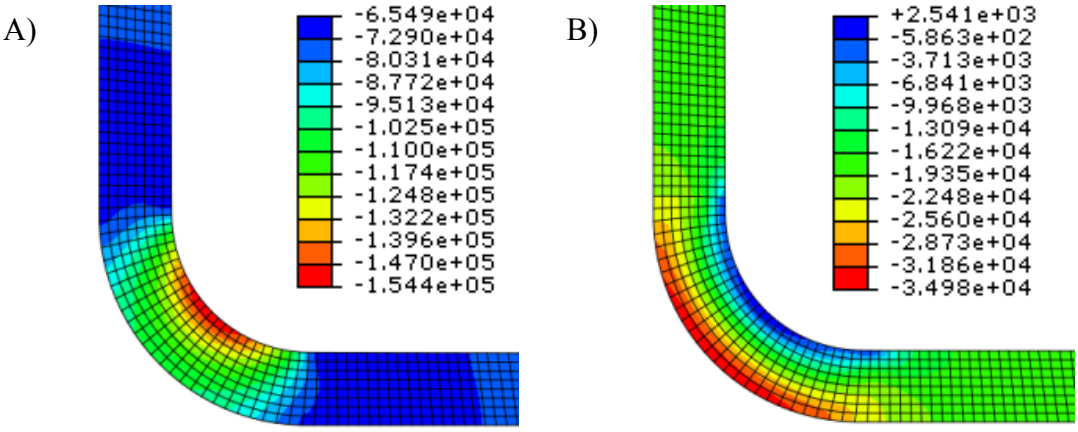

Figure 6.7: Numerical contour plot of the radial stresses (in Pa) in the laminate (A) and the longitudinal stresses (B) for the model with the pressure intensifier with a stiffness of 0.010GPa

Since the ends of the pressure intensifier are thin, and in the case of an intensifier of low stiffness, the latter can deform and cause thinning at the laminate ends, as shown in Figure 6.8. This was observed in the predicted thickness values shown in Figure 6.2. Such thinning was not observed in the experimental results of Chapter 5 for parts manufactured with a pressure intensifier because the ends of the intensifier were supported by the edge breathing set-up along the laminate edges. It is important to prevent the intensifier from deforming, not only to avoid thinning of the laminate, but also to prevent it from pinching the laminate plies and blocking the air from evacuating, which would result in a higher void content.

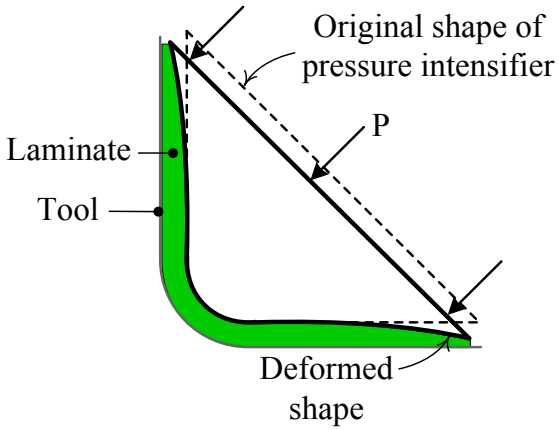

Figure 6.8: Deformation of a soft pressure intensifier under vacuum pressure, causing thinning of the laminate toward the ends

6.3.2.3 Model with pressure strip (see Figure 6.1C)

The effect of using a pressure strip on the deformation of the laminate is discussed in the present section. The numerical contour plots for the radial and longitudinal stresses of the deformed laminate are illustrated in Figure 6.9A and B. The contour plots are given for the case with a pressure strip stiffness of 0.010GPa. The pressure strip is shown in light gray to illustrate the thickness and stress discontinuities between the flange and the region under the pressure strip.

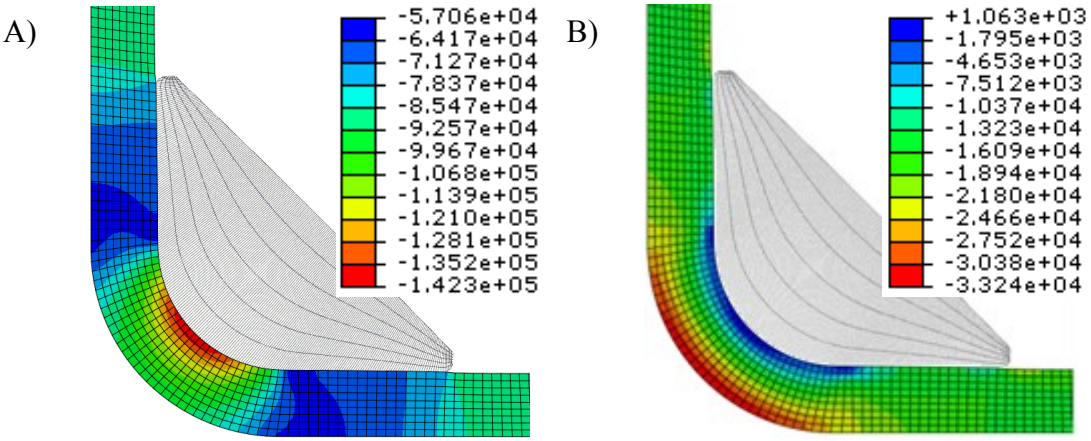

Figure 6.9: Numerical contour plot of the radial stresses (in Pa) in the laminate (A) and the longitudinal stresses (B) for the model with the pressure strip with a stiffness of 0.010GPa

Similarly to the model with the pressure intensifier, the compaction pressure at the corner was initially transferred to a small local contact surface. This increased the compressive radial stresses (shown in red in Figure 6.9A) at the corner with respect to the model with the vacuum bag only.

A distinctive result for the model with the pressure strip was the discontinuity in thickness located at the ends of the pressure strip. The thickness was larger for the laminate region under the pressure strip and smaller for the remaining flanges. This discontinuity was translated by the lower compressive radial stresses for the flange region under the pressure strip, shown in blue in Figure 6.9A. This suggests that the compaction continued at the flanges while it was stopped for the region under the pressure strip. In fact, as schematised in Figure 6.4, with compaction, tensile longitudinal stresses developed at the corner. These tensile stresses reached a state of equilibrium with the applied pressure on the pressure strip and stopped the compaction of the laminate for that region. However, since the pressure strip did not cover the part entirely, as did the pressure intensifier, the compaction may continue at the flanges from the direct applied pressure.

6.3.3 Effect of pressure intensifier stiffness

In section 6.3.2.2, it was observed that a soft pressure intensifier will cause laminate thinning at the ends since it deforms under vacuum pressure. It is therefore expected that the stiffness of the pressure intensifier would have an important effect on the integrity of its shape and consequently on the uniformity of thickness of the laminate. Thus, the models presented in the previous sections were repeated for various stiffnesses of pressure intensifier and pressure strip. The predicted relative thickness profiles for the model with the pressure intensifier and the model with the pressure strip are presented in Figure 6.10 and Figure 6.11 respectively. The values were normalised by the average flange thickness of the experimental samples discussed in Chapter 5.

The stiffness of the pressure intensifier and pressure strip plays an important role on the thickness uniformity and potential defects. In fact, with increasing stiffness, the pressure intensifier maintains its shape better and causes less

thinning at the laminate ends (see locations 0 and 10 in Figure 6.10). The same observation was made for the model with the pressure strip; where a more uniform thickness was obtained for the region under the pressure strip (locations 3.5 to 6.5) for the case of high stiffness.

Also, with increasing stiffness, the compaction of the laminate is increased; a rigid pressure intensifier and pressure strip absorbs less compaction energy and transfers this energy to the laminate more efficiently. Hence, the final thickness of the laminate is closer to the design thickness. This effect is better observed for the model with the pressure intensifier of Figure 6.10 since the latter covers a larger portion of the laminate. While the compaction of the laminate was decreased in the case of softer pressure intensifiers, the resulting final thickness of the laminate was then larger than the design thickness and thus, the pressure intensifier corner radius was no longer of the proper dimension. This resulted in corner thickening (locations 4 to 6) in both models.

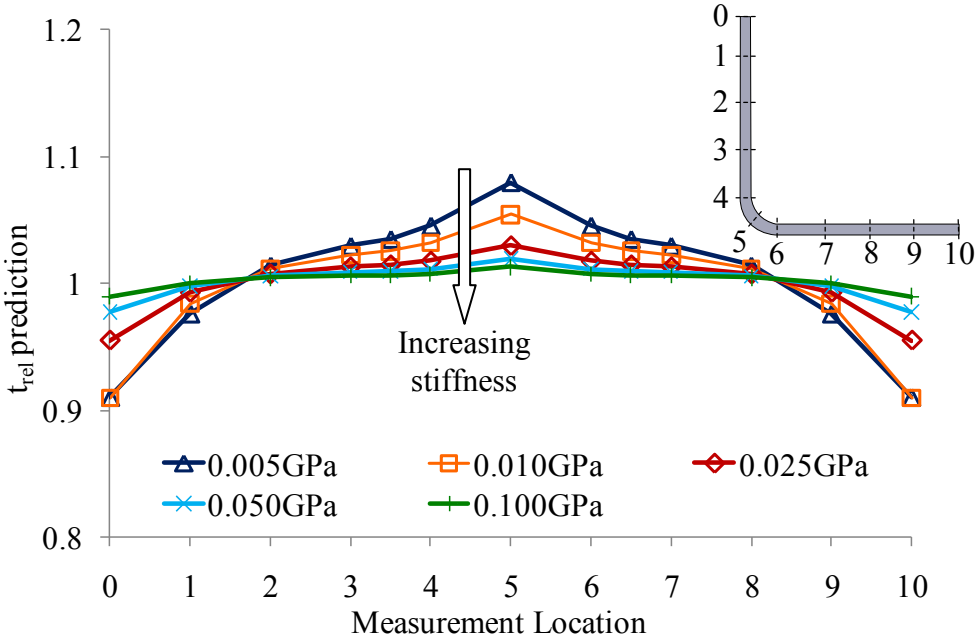

Figure 6.10: Relative thickness prediction values for the model with a pressure intensifier of stiffness varying between 0.005GPa and 0.100GPa

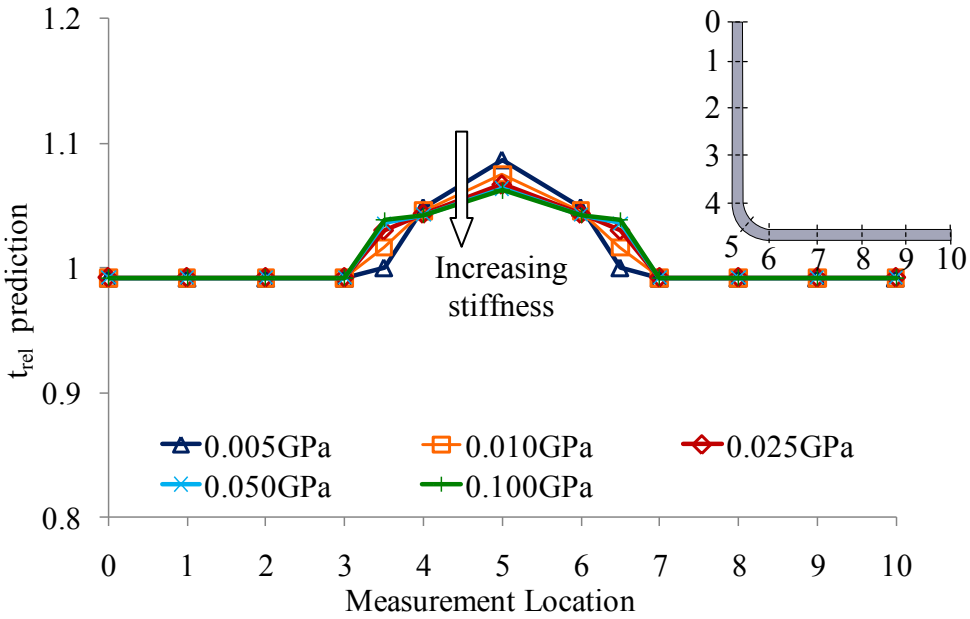

Figure 6.11: Relative thickness prediction values for the model with a pressure strip of stiffness varying between 0.005GPa and 0.100GPa

CHAPTER 7
Conclusion

7.1 Summary and Conclusions

The present research addressed the following problem: most of the literature related to OOA manufacturing was focused on the compaction of flat laminates. Also, research performed on autoclave-cured complex shape laminates may not directly apply to OOA manufacturing given the differences in impregnation level and resin kinetics of OOA prepregs relative to autoclave prepregs. Hence, the objective of this work was to investigate the compaction behaviour of complex shape laminates processed under OOA conditions. The main conclusions drawn from this investigation are described below.

1. **A critical radius-to-thickness ratio for acceptable thickness variation at the corner can be determined and serve as a guideline for the design of L-shape laminates**

   The thickness variation of OOA L-shape composite laminates was characterised for two materials based on radius-to-thickness ratios. The resulting graphs can be used to determine the critical ratio that provides acceptable thickness variation for the design of Cytec Cycom 5320 8HS and PW L-shape laminates. Also, it was observed that concave and convex laminates exhibited corner thickening. With decreasing radius-to-thickness ratio, the thickness variation increased. The material has a significant effect on the magnitude of the thickness variation; 8HS laminates demonstrated almost twice as much thickening as the PW laminates.

2. **The shearing capability of the laminate plays an important role on the thickness variation at the corner and varies with laminate ply thickness**

An analytical model for the compaction of L-shape laminates was developed. The model states that the thickness variation at the corner is a function of the radius-to-thickness ratio and laminate thickness. The model predicts corner thickening for concave laminates and thinning for convex laminates. The model for concave laminates predicted well the thickness variation for PW laminates. Longitudinal stresses from shear effects cannot be neglected for the 8HS material and the compaction over the convex tool. The thickness per ply could have an effect on the potential for interply slippage and explain the effect of material on the thickness variation at the corner.

3. **A pressure intensifier or pressure strip can be used to increase compaction at the corner**

   An experimental study of the effect of variations in bagging arrangement and the use of a pressure intensifier or pressure strip on the thickness variation and void content was performed. The compaction at the corner was improved with the use of the pressure intensifier and pressure strip. The corner radius of the pressure intensifier and pressure strip must be equal to the desired final part inner radius. Otherwise, the thickness variation can worsen. Breather cloth under the pressure intensifier significantly improved the void content.

4. **The material stiffness of the pressure intensifier and pressure strip should be maximised**

   A simplified numerical analysis of the compaction of a laminate over a concave tool was performed to investigate the effect of using a pressure intensifier and pressure strip at the stress-level. The compaction at the corner is improved with the use of a pressure intensifier because the pressure is initially transferred to the laminate through a small contact surface, concentrating the pressure at the corner. However, to avoid deformation of the laminate, the pressure intensifier material should be of high stiffness.

7.2 Future Work

Further improvements should be made to the analytical model by including the shear mechanisms that affect the compaction at the corner. This would require the development of an experimental method for the investigation and characterisation of interply shear displacement as a function of compaction, thickness per ply, resin properties and shear force. Such analysis could be performed with flat laminates.

Also, it was found that corner thickening could result in the compaction of a laminate over a convex tool due to the restriction in longitudinal deformation. This effect could be considered in the analytical model by describing the corner thickening as a function of laminate thickness, radius-to-thickness ratio and bulk factor through a geometrical relation only, assuming no longitudinal deformation due to the high stiffness of the fibres. The overall compaction could be described by the additive thickening effect of the longitudinal stresses and thinning effect of the non-uniform pressure distribution considered in the original model.

The characterisation of the thickness variation as a function of radius-to-thickness ratio for different materials and tool shapes was found useful in establishing design guidelines for L-shape laminates. However, the experimental work required to build the graphs was very laborious, costly and time consuming. It is therefore of interest to improve the numerical model developed with the inclusion of anisotropic material properties and interply shear behaviour. With the proper modeling of the mechanisms governing the compaction of L-shape laminates, the thickness variation could be characterised for multiple materials more easily and eliminate the need for elaborate experimental work. However, further investigation should be attributed to the description and measurement of the shearing properties of composite laminates.

Finally, the experimental characterisation of the thickness variation in L-shape laminates could be repeated for other laminate parameters, such as lay-up and flange length, to determine if these parameters significantly affect the compaction and, in such case, specific graphs and design guidelines should be built.

LIST OF REFERENCES

1. Callister, W. "Composites." *Materials Science and Engineering, An Introduction*. 6th Edition. Hoboken, NJ: John Wiley & Sons, (2003): 527-569
2. Lowe, J. "Aerospace Applications." *Design and Manufacture of Textile Composites*. Ed. Long, A. C. Cambridge, UK: Woodhead Publishing Ltd, (2005): 405-423
3. Quilter, A. "Composites in Aerospace Applications." IHS White Paper. 28 Mar. 2010. <http://uk.ihs.com/products/white-papers/index.htm>
4. "Taking the lead: the A350 XWB." Airbus A350 presentation at Paris Airshow 2007. 28 Mar. 2010. <http://www.eads.com/xml/content/OF00000000400004/7/19/41508197.pdf>
5. "Unrivaled Passenger Experience." B787 Design highlights. 28 Mar. 2010. <http://www.newairplane.com/787/design_highlights/>
6. Kelly, D. W., Scott, M. L. & Thomson, R. S. "Composite Aircraft Structures." *Modeling Complex Engineering Structures*. Ed. Robert E. Melchers. Reston, VA: American Society of Civil Engineers, (2007): 247-274
7. Advani, S. G. & Sozer, E. M. "Processing Advanced Thermoset Fiber Composites." *Process Modeling in Composites Manufacturing*. New York: CRC Press, (2003): 339-408
8. Mallow, Andrew R. & Campbell, Flake C. "Autoclave Processing." *Processing of Composites*. Ed. Raju S. Davé and Alfred C. Loos. Vol.1. Munich: Hanser, (2000): 295-316
9. Dominy, J. & Rudd, C. "Manufacturing with Thermosets." *Design and Manufacture of Textile Composites*. Ed. Long, A. C. Cambridge, UK: Woodhead Publishing Ltd, (2005): 181-196
10. Campbell, Flake C. "Commercial Composite Processes." *Manufacturing Processes for Advanced Composites*. Oxford, UK: Elsevier, (2004): p.400-438
11. Strong, Brent A. "Manufacturing Methods." *Fundamentals of Composites Manufacturing: materials, methods, and applications*. 1st edition. Dearborn, Mich: Society of Manufacturing Engineers, Publications Development Dept., Reference Publications Division, (1989): 107-159
12. Repecka, L. & Boyd, J. "Vacuum-Bag-Only-Curable Prepregs That Produce Void-Free Parts." *47th International SAMPE Symposium and Exhibition* Long Beach, CA May 12-16 (2002): 1862-1874
13. Loos, A. C. & Springer, G. S. "Curing of Epoxy Matrix Composites." *Journal of Composite Materials* 17 (1983): 135-169
14. Dave, R., Kardos, J. L. & Dudukovic, M. P. "A Model for Resin Flow During Composite Processing .2. Numerical-Analysis for Unidirectional Graphite Epoxy Laminates." *Polymer Composites* 8 (1987): 123-132

15. Dave, R., Kardos, J. L. & Dudukovic, M. P. "A Model for Resin Flow During Composite Processing .1. General Mathematical Development." *Polymer Composites* 8 (1987): 29-38

16. Gutowski, T. G., Morigaki, T. & Cai, Z. "The Consolidation of Laminate Composites." *Journal of Composite Materials* 21 (1987): 172-188

17. Hubert, P. & Poursartip, A. "A review of flow and compaction modelling relevant to thermoset matrix laminate processing." *Journal of Reinforced Plastics and Composites* 17 (1998): 286-318

18. Kardos, J. L. "Void Growth and Dissolution." *Processing of Composites*. Ed. Raju S. Davé and Alfred C. Loos. Vol.1. Munich: Hanser, (2000): 182-207.

19. ÓBrádaigh, C. M., McGuinness, G. B. & Pipes, R. B., "Numerical Analysis of Stresses and Deformations in Composite Materials Sheet Forming: Central Indentation of a Circular Sheet." *Composites Manufacturing* 4 (1993): 67-83

20. Hubert, P. & Poursartip, A."Aspects of the compaction of composite angle laminates: An experimental investigation." *Journal of Composite Materials* 35 (2001): 2-26

21. Fernlund, G., Griffith, J., Courdji, R. & Poursartip, A."Experimental and numerical study of the effect of caul-sheets on corner thinning of composite laminates." *Composites Part a-Applied Science and Manufacturing* 33 (2002): 411-426

22. Naji, M. I. & Hoa, S. V. "Curing of thick angle-bend thermoset composite part: Curing process modification for uniform thickness and uniform fiber volume fraction distribution." *Journal of Composite Materials* 34 (2000): 1710-1755

23. Li, Y. X., Li, M., Gu, Y. Z. & Zhang, Z. G. "Numerical and Experimental Study on the Effect of Lay-Up Type and Structural Elements on Thickness Uniformity of L-Shaped Laminates." *Applied Composite Materials* 16 (2009): 101-115

24. Wang, X., Zhang, Z., Xie, F., Li, M., Dai, D. & Wang, F. "Correlated Rules between Complex Structure of Composite Components and Manufacturing Defects in Autoclave Molding Technology." *Journal of Reinforced Plastics and Composites* 28 (2009): 2791-2803

25. Li, M. "Optimal Curing of Thermoset Composites: Thermochemical and Consolidation Considerations." PhD. Thesis, University of Illinois at Urbana-Champaign (2001)

26. Hubert, P. "Aspects of Flow and Compaction of Laminated Composite Shapes During Cure." PhD. Thesis, University of British Columbia (1996)

27. Li, M. & Tucker, C. L. "Modeling and simulation of two-dimensional consolidation for thermoset matrix composites." *Composites Part a-Applied Science and Manufacturing* 33 (2002): 877-892

28. Li, Y. X., Li, M., Zhang, Z. G. & Gu, Y. Z. "Numerical Analysis of Parametric Effects on Consolidation of Angle-Bended Composite Laminates." *Polymer Composites* 30 (2009): 1510-1516

29. Hubert, P., Vaziri, R. & Poursartip, A. "A two-dimensional flow model for the process simulation of complex shape composite laminates." *International Journal for Numerical Methods in Engineering* 44 (1999): 1-26

30. Naji, M. I. & Hoa, S. V. "Curing of thick angle-bend thermoset composite part: Curing Cycle Effect on Thickness Variation and Fiber Volume Fraction." *Journal of Reinforced Plastics and Composites* 18 (1999): 702-723

31. Kardos, J. L., Dudukivić, M. P. & Dave, R. "Void Growth and Resin Transport During Processing of Thermosetting – Matrix Composites." *Advances in Polymer Science* 80 (1980):101-123

32. Eom, Y., Boogh, L., Michaud, V. & Manson, J.-A. "A Structure and Property Based Process Window for Void Free Thermoset Composites." *Polymer Composites* 22 (2001): 22-31

33. Eom, Y., Boogh, L., Michaud, V., Sunderland, P. & Manson, J.-A. "Stress-initiated void formation during cure of three-dimensionally constrained thermoset resin." *Polymer Engineering Science* 41 (2001): 492-503

34. Michaud, V., Tavares, S. S., Sigg, A., Lavanchy, S. & Manson, J.-A. "Low Pressure Processing of High Fiber Content Composites." *8th International Conference on Flow Processes in Composite Materials (FPCM8)* Douai, France, July 11-13 (2006)

35. Ridgard, C. "Out of Autoclave Composite Technology for Aerospace, Defense, and Space Structures." *53th International SAMPE Symposium and Exhibition* Baltimore, MD, May 18-21 (2009)

36. Bond, G. G., Griffith, J. M. & Hahn, G. "A Study of Non-Autoclave Prepreg Manufacturing Technology" *SAMPE Journal* 45 (2009): 6-19

37. Mitani, K., Wakabayashi, K. & Shigetsugu, H. "A new low temperature curing prepreg." *46th International SAMPE Symposium and Exhibition* Long Beach, CA, May 6-10 (2001): 2293-2302

38. Jackson, K. "Low temperature curing materials: the next generation." *SAMPE Journal* 34 (1998): 23-31

39. Ridgard, C. "Advances in low temperature curing prepregs for aerospace structures." *45th International SAMPE Symposium and Exhibition* Long Beach, CA, May 21-25 (2000)

40. Bond, G. G. & Luner, J. L. "Design of Experiments Evaluation of Processing Parameters for Non-Autoclave Composite Prepreg." *53th International SAMPE Symposium and Exhibition* Baltimore, MD, May 18-21 (2009)

41. Louis, B. M., Hsiao, K. & Fernlund, G. "Gas Permeability Measurements of Out of Autoclave Prepreg MTM45-1/CF2426A." *54th International SAMPE Symposium and Exhibition*, Seattle, WA, May 17-20 (2010)

42. Brillant, M. & Hubert, P. "Out-of-Autoclave Processing of Complex Shape Laminates." *54th International SAMPE Symposium and Exhibition* Seattle, WA, May 17-20 (2010)

43. Bernetich, K. "Evaluation of Detail Part Fabrication using Out-of-Autoclave Prepreg." *54th International SAMPE Symposium and Exhibition* Seattle, WA, May 17-20 (2010)

44. Arafath, A.R.A., Fernlund, G. & Poursartip, A. "Gas Transport in Prepregs: Model and Permeability Experiments." *17th International Conference on Composite Materials (ICCM-17)* Edinburgh, Scotland, July 27-21 (2009)

45. Woven Fabrics. NetComposites, Reinforcements. 17 Oct. 2010. <http://www.netcomposites.com/education.asp?sequence=41>

46. CYCOM® 5320 Toughened Epoxy for Structural Applications Out-of-Autoclave Manufacturing. Cytec Industries Inc., Product Information. 24 Aug. 2010. <http://www.cytec.com/engineered-materials/Products/CYCOM%205320.htm>

47. Hou, M., Friedrich, K. & Scherer, R. "Optimization of Stamp Forming of Thermoplastic Composite Bends." *Composite Structures* 27 (1994): 157-167

48. Morris, S. R. & Sun, C. T. "Analysis of Forming Loads for Thermoplastic Composite Laminates." *Composites Part A* 27A (1996): 633-640

49. Cogswell, F. N. "Continuous Fibre Systems." *Flow and Rheology in Polymer Composites Manufacturing*. Ed. Suresh G. Advani. Amsterdam, Netherlands: Elsevier, Composite Materials Series Vol. 10 (1994): 127-144

50. Overview of Nylon 6, Film Grade. MatWeb, Material Property Data. 20 Jan. 2010. <http://www.matweb.com/search/DataSheet.aspx?MatGUID=6532b02c347d446b8241390cc04a3e66&ckck=1>

51. Overview of Silicone Rubber. MatWeb, Material Property Data. 9 Jan. 2010. <http://www.matweb.com/search/DataSheet.aspx?MatGUID=cbe7a469897a47eda563816c86a73520>

APPENDIX A

Raw Data and Calculations

Table A.1: Bulk factor calculation for 8HS and PW laminates

Laminate number	Material	t_{i1}	t_{i2}	t_{i3}	t_{i7}	t_{i8}	t_{i9}	$t_{avgflange\ i}$	$t_{avgflange}$	c_1
								Eq. (14)	Table A.2, Table A.3	Eq. (15)
		(mm)						(mm)		
16	8HS	9.14	9.24	9.11	9.26	9.39	9.30	9.24	7.63	1.21
									c_1 average:	**1.21**
25	PW	7.18	7.07	7.20	7.07	7.10	7.08	7.12	5.92	1.20
26	PW	7.67	7.84	7.72	7.76	7.78	7.79	7.76	6.53	1.19
29	PW	4.83	4.87	4.92	4.99	4.95	4.84	4.90	3.99	1.23
30	PW	5.73	5.75	5.84	5.85	5.86	5.83	5.81	4.78	1.21
31	PW	2.58	2.60	2.54	2.71	2.65	2.61	2.62	1.98	1.32
32	PW	4.00	3.95	3.97	3.92	3.98	4.03	3.98	3.22	1.24
33	PW	5.28	5.25	5.25	5.13	5.32	5.31	5.26	4.37	1.20
34	PW	6.57	6.56	6.53	6.52	6.50	6.50	6.53	5.34	1.22
36	PW	8.95	8.97	9.13	9.09	9.00	8.93	9.01	7.50	1.20
39	PW	7.07	7.09	7.11	7.04	7.15	7.22	7.11	5.95	1.20
40	PW	7.49	7.53	7.59	8.14	8.04	8.01	7.80	6.53	1.19
									c_1 average:	**1.22**

Table A.2: Thickness measurements (mm) for Cytec 5320 8HS laminates and calculation of the thickness variation (mm)

Laminate number	R/t	Surface of cut 01									Surface of cut 02									$t_{avgflange}$	t_c	Δt	error
		t_1	t_2	t_3	t_4	t_5	t_6	t_7	t_8	t_9	t_{10}	t_{11}	t_{12}	t_{13}	t_{14}	t_{15}	t_{16}	t_{17}	t_{18}	Eq. (4), (5)	Eq. (6), (7)	Eq. (8), (9)	Eq. (10)
		(mm)									(mm)									(mm)			
1	5.14	1.94	1.94	1.89	2.00	2.19	2.04	1.89	1.98	1.94	1.89	1.96	1.96	2.06	2.25	2.00	1.96	2.00	2.00	1.95	2.22	0.27	0.01
2	4.28	2.25	2.25	2.29	2.34	2.59	2.25	2.29	2.23	2.25	2.25	2.29	2.27	2.36	2.53	2.48	2.25	2.29	2.23	2.26	2.56	0.30	0.03
3	2.85	3.43	3.43	3.45	3.66	3.78	3.64	3.47	3.37	3.43	3.43	3.43	3.37	3.66	3.92	3.71	3.41	3.45	3.49	3.43	3.85	0.42	0.07
4	2.14	4.59	4.57	4.53	5.05	5.45	5.20	4.51	4.59	4.59	4.61	4.59	4.61	5.07	5.40	5.12	4.63	4.63	4.67	4.59	5.43	0.83	0.05
5	1.61	6.06	6.00	5.96	6.65	7.15	6.51	6.00	6.04	6.11	6.00	6.06	6.02	6.61	7.01	6.59	6.08	6.06	6.11	6.04	7.08	1.04	0.08
6	1.43	6.86	6.80	6.76	8.25	8.41	8.13	6.78	6.82	6.91	6.88	6.78	6.78	7.89	8.25	7.77	6.86	6.86	6.86	6.83	8.33	1.50	0.09
7	6.85	1.87	1.87	1.89	1.92	2.07	1.94	1.87	1.89	1.87	1.89	1.96	1.87	1.94	2.10	1.94	1.79	1.94	1.89	1.89	2.08	0.20	0.01
8	4.28	3.07	3.07	3.03	3.20	3.42	3.20	3.05	3.09	3.07	3.05	3.01	3.05	3.28	3.39	3.16	3.07	3.14	3.09	3.07	3.41	0.34	0.02
9	3.42	3.79	3.81	3.79	4.04	4.08	4.02	3.75	3.73	3.77	3.77	3.83	3.77	3.87	4.05	4.04	3.73	3.75	3.79	3.77	4.06	0.29	0.02
10	2.85	4.61	4.63	4.61	4.78	4.97	4.72	4.59	4.59	4.65	4.55	4.61	4.59	4.84	5.00	4.86	4.61	4.59	4.59	4.60	4.99	0.39	0.03
11	3.42	1.92	1.98	1.96	1.94	2.22	2.04	1.94	1.92	1.92	1.92	1.89	1.87	1.96	2.19	2.00	1.98	1.94	1.87	1.92	2.20	0.28	0.00
12	2.14	3.05	3.12	3.09	3.07	3.38	3.16	3.05	3.05	3.07	3.01	3.08	3.05	3.20	3.41	3.16	3.05	3.05	3.07	3.06	3.39	0.33	0.02
13	1.43	4.59	4.53	4.51	4.67	5.00	4.67	4.61	4.61	4.55	4.57	4.57	4.61	4.72	5.00	4.78	4.63	4.59	4.59	4.58	5.00	0.42	0.01
14	1.22	5.26	5.28	5.22	5.45	5.99	5.54	5.35	5.31	5.35	5.33	5.33	5.26	5.47	5.85	5.47	5.31	5.31	5.31	5.30	5.92	0.62	0.07
15	1.07	6.23	6.19	6.17	6.19	6.70	6.34	6.17	6.19	6.17	6.23	6.23	6.29	6.25	6.71	6.27	6.25	6.32	6.17	6.22	6.71	0.49	0.02
16	0.86	7.66	7.56	7.64	7.89	8.25	7.83	7.68	7.64	7.71	7.60	7.60	7.64	7.83	8.26	7.96	7.58	7.66	7.58	7.63	8.25	0.62	0.03
17	2.85	3.33	3.37	3.37	3.49	3.63	3.47	3.43	3.43	3.35	3.37	3.37	3.35	3.45	3.69	3.58	3.31	3.33	3.41	3.37	3.66	0.30	0.04
18	2.14	4.55	4.46	4.46	4.65	4.94	4.61	4.48	4.59	4.51	4.46	4.53	4.51	4.63	4.85	4.57	4.48	4.51	4.51	4.50	4.90	0.39	0.04
19	1.61	6.02	6.03	6.04	6.19	6.40	6.15	6.07	6.07	5.98	6.11	6.04	6.06	6.25	6.34	6.11	6.08	6.06	6.06	6.05	6.37	0.32	0.05
20	1.43	6.87	6.80	6.85	6.95	7.27	6.97	6.87	6.89	6.87	6.84	6.82	6.82	6.91	7.20	6.99	6.84	6.84	6.82	6.84	7.23	0.39	0.02

Table A.3: Thickness measurements (mm) for Cytec 5320 PW laminates and calculation of the thickness variation (mm)

Laminate number	R/t	Surface of cut 01									Surface of cut 02									$t_{avgflange}$	t_c	Δt	error
		t_1	t_2	t_3	t_4	t_5	t_6	t_7	t_8	t_9	t_{10}	t_{11}	t_{12}	t_{13}	t_{14}	t_{15}	t_{16}	t_{17}	t_{18}	Eq. (4), (5)	Eq. (6), (7)	Eq. (8), (9)	Eq. (10)
		(mm)									(mm)									(mm)			
21	6.96	1.39	1.41	1.41	1.45	1.55	1.47	1.37	1.43	1.43	1.41	1.41	1.41	1.47	1.53	1.39	1.41	1.45	1.41	1.41	1.54	0.13	0.01
22	4.06	2.46	2.46	2.48	2.48	2.64	2.57	2.42	2.42	2.44	2.42	2.42	2.46	2.44	2.56	2.46	2.34	2.40	2.34	2.42	2.60	0.18	0.01
23	2.71	3.62	3.60	3.60	3.71	3.96	3.79	3.58	3.64	3.62	3.60	3.58	3.60	3.75	3.89	3.79	3.66	3.62	3.60	3.61	3.92	0.31	0.04
24	2.03	4.78	4.82	4.76	5.09	5.33	5.05	4.78	4.82	4.82	4.76	4.76	4.72	5.03	5.23	5.03	4.78	4.80	4.80	4.78	5.28	0.49	0.04
25	1.62	5.89	5.94	5.94	6.19	6.31	6.15	5.94	5.89	5.87	5.92	5.92	5.81	6.19	6.42	6.19	5.98	5.98	5.98	5.92	6.36	0.44	0.04
26	1.48	6.55	6.55	6.51	6.97	7.19	6.86	6.53	6.48	6.55	6.55	6.57	6.55	6.95	7.24	6.91	6.48	6.55	6.51	6.53	7.21	0.68	0.02
27	5.41	2.46	2.44	2.40	2.51	2.53	2.40	2.40	2.36	2.40	2.44	2.38	2.46	2.48	2.55	2.51	2.40	2.40	2.34	2.41	2.54	0.13	0.01
28	4.06	3.16	3.26	3.24	3.26	3.41	3.39	3.18	3.26	3.28	3.16	3.16	3.18	3.26	3.32	3.26	3.20	3.22	3.24	3.21	3.36	0.15	0.02
29	3.25	4.02	4.08	4.04	4.15	4.29	4.13	3.94	3.94	4.00	3.96	3.94	4.00	4.13	4.24	4.06	4.00	3.96	4.02	3.99	4.26	0.27	0.01
30	2.71	4.86	4.82	4.82	4.93	5.06	4.93	4.80	4.76	4.82	4.76	4.76	4.78	4.86	5.02	4.93	4.80	4.74	4.69	4.78	5.04	0.25	0.01
31	3.25	1.98	2.02	2.00	2.02	2.14	2.17	1.98	1.94	1.96	1.94	1.96	2.02	2.19	2.08	1.96	2.02	1.96	1.98	1.98	2.11	0.13	0.03
32	2.03	3.24	3.26	3.18	3.33	3.45	3.31	3.20	3.20	3.26	3.20	3.22	3.24	3.31	3.48	3.31	3.22	3.20	3.16	3.22	3.47	0.25	0.02
33	1.48	4.36	4.38	4.42	4.53	4.76	4.42	4.34	4.38	4.38	4.38	4.38	4.34	4.46	4.79	4.40	4.38	4.40	4.32	4.37	4.78	0.41	0.02
34	1.20	5.37	5.35	5.28	5.39	5.73	5.41	5.33	5.37	5.41	5.28	5.33	5.35	5.41	5.88	5.39	5.31	5.35	5.35	5.34	5.81	0.47	0.09
35	1.08	6.06	5.96	6.00	6.00	6.33	6.13	5.98	6.02	6.00	5.94	5.89	5.89	6.04	6.39	6.00	5.98	5.89	5.92	5.96	6.36	0.40	0.07
36	0.85	7.41	7.47	7.47	7.71	8.04	7.62	7.56	7.54	7.54	7.45	7.49	7.54	7.62	8.04	7.62	7.52	7.60	7.43	7.50	8.04	0.54	0.00
37	2.71	3.58	3.58	3.60	3.68	3.81	3.62	3.58	3.62	3.56	3.54	3.60	3.60	3.66	3.81	3.60	3.58	3.62	3.60	3.59	3.81	0.22	0.00
38	2.03	4.76	4.74	4.80	4.88	5.00	4.84	4.76	4.74	4.76	4.74	4.80	4.80	4.82	5.11	4.80	4.72	4.78	4.80	4.77	5.05	0.29	0.05
39	1.62	5.96	6.00	5.98	6.00	6.24	6.04	5.94	5.96	5.92	5.94	5.96	5.92	6.06	6.19	6.00	5.94	5.94	5.94	5.95	6.22	0.27	0.01
40	1.48	6.51	6.57	6.53	6.61	6.77	6.63	6.55	6.53	6.51	6.53	6.57	6.53	6.53	6.88	6.55	6.51	6.51	6.53	6.53	6.83	0.30	0.05

Table A.4: Thickness measurements (mm) for Parts A to G and relative thickness calculations

Part name	Surface of cut 01									Surface of cut 02									$t_{avgflange}$	t_{rel1}	t_{rel2}	t_{rel3}	t_{rel4}	t_{rel5}	t_{rel6}	t_{rel7}	t_{rel8}	t_{rel9}
	t_1	t_2	t_3	t_4	t_5	t_6	t_7	t_8	t_9	t_{10}	t_{11}	t_{12}	t_{13}	t_{14}	t_{15}	t_{16}	t_{17}	t_{18}	Eq. (4), (5)	Eq. (11), (13)									
	(mm)									(mm)									(mm)	(mm)									
A	3.22	3.27	3.31	3.26	3.59	3.12	3.20	3.26	3.18	3.39	3.31	3.35	3.35	3.13	3.20	3.20	3.24	3.22	3.26	1.03	1.02	1.04	1.03	1.04	0.98	1.00	1.01	1.00
B	3.20	3.33	3.35	3.26	3.35	3.22	3.18	3.20	3.28	3.24	3.33	3.26	3.28	3.32	3.20	3.26	3.28	3.28	3.27	1.00	1.04	1.03	1.02	1.04	1.00	1.00	1.01	1.02
C	3.12	3.09	3.12	4.04	5.08	4.17	3.22	3.05	3.14	3.14	3.03	3.07	4.40	4.81	4.53	3.07	3.03	3.05	3.09	0.97	0.95	0.96	1.31	1.54	1.35	0.98	0.95	0.96
D	3.20	3.24	3.28	3.39	3.87	3.41	3.20	3.29	3.31	3.24	3.27	3.24	3.45	3.72	3.43	3.22	3.22	3.20	3.24	1.00	1.01	1.02	1.06	1.18	1.06	1.00	1.01	1.01
E	3.29	3.35	3.12	3.52	3.93	3.58	3.20	3.27	3.20	3.27	3.24	3.18	3.67	4.08	3.27	3.07	3.24	3.24	3.22	1.02	1.03	0.98	1.12	1.25	1.07	0.98	1.01	1.00
F	3.18	3.24	3.16	3.56	3.65	3.41	3.22	3.20	3.22	3.20	3.16	3.20	3.37	3.56	3.58	3.24	3.22	3.18	3.20	0.99	1.00	0.99	1.08	1.12	1.09	1.01	1.00	1.00
F_E	3.24	3.24	3.12	3.41	4.00	3.66	3.18	3.20	3.28	3.18	3.18	3.05	3.66	3.92	3.39	3.28	3.07	3.18	3.18	1.00	1.00	0.96	1.10	1.23	1.10	1.01	0.98	1.01
G	3.16	3.31	3.33	3.43	3.56	3.41	3.52	3.16	3.16	3.12	3.16	3.35	3.49	3.56	3.41	3.18	3.26	3.12	3.23	0.98	1.01	1.04	1.08	1.11	1.06	1.04	1.00	0.98
																		t_{avg} Eq. (12):	3.21									